ISSN 1949-8470 (online)

World Journal of *Radiology*

World J Radiol 2011 March 28; 3(3): 55-84

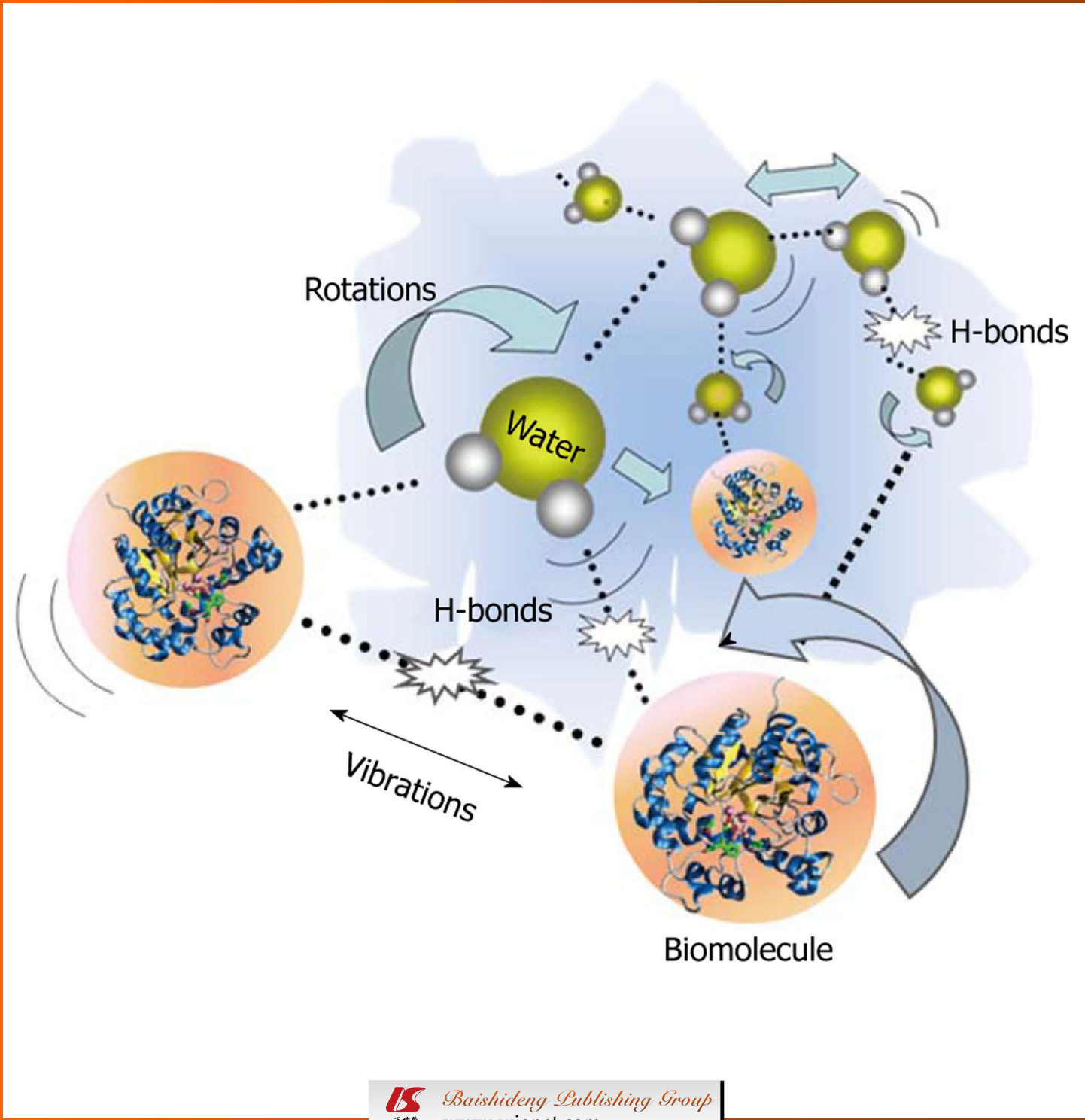

Baishideng Publishing Group
www.wjgnet.com

WJR World Journal of Radiology

A peer-reviewed, online, open-access journal of Radiology

Editorial Board

2009-2013

The *World Journal of Radiology* Editorial Board consists of 319 members, representing a team of worldwide experts in radiology. They are from 40 countries, including Australia (3), Austria (4), Belgium (5), Brazil (3), Canada (9), Chile (1), China (25), Czech (1), Denmark (1), Egypt (4), Estonia (1), Finland (1), France (6), Germany (17), Greece (8), Hungary (1), India (9), Iran (5), Ireland (1), Israel (4), Italy (28), Japan (14), Lebanon (1), Libya (1), Malaysia (2), Mexico (1), Netherlands (4), New Zealand (1), Norway (1), Saudi Arabia (3), Serbia (1), Singapore (2), Slovakia (1), South Korea (16), Spain (8), Switzerland (5), Thailand (1), Turkey (20), United Kingdom (16), and United States (82).

Spain

Eduardo J Aguilar, *Valencia*
Miguel Alcaraz, *Murcia*
Juan Luis Alcazar, *Pamplona*
Gorka Bastarrika, *Pamplona*
Rafael Martínez-Monge, *Pamplona*
Alberto Muñoz, *Madrid*
Joan C Vilanova, *Girona*

Switzerland

Nicolau Beckmann, *Basel*
Silke Grabherr, *Lausanne*
Karl-Olof Lövblad, *Geneva*
Tilo Niemann, *Basel*
Martin A Walter, *Basel*

Thailand

Sudsriluk Sampatchalit, *Bangkok*

Turkey

Olus Api, *Istanbul*
Kubilay Aydin, *İstanbul*
Işıl Bilgen, *Izmir*
Zulkif Bozgeyik, *Elazig*
Barbaros E Çil, *Ankara*
Gulgun Engin, *Istanbul*
M Fatih Evcimik, *Malatya*
Ahmet Kaan Gündüz, *Ankara*
Tayfun Hakan, *Istanbul*
Adnan Kabaalioglu, *Antalya*
Fehmi Kaçmaz, *Ankara*
Musturay Karcaaltincaba, *Ankara*
Osman Kizilkilic, *Istanbul*
Zafer Koc, *Adana*
Cem Onal, *Adana*
Yahya Paksoy, *Konya*
Bunyamin Sahin, *Samsun*
Ercument Unlu, *Edirne*
Ahmet Tuncay Turgut, *Ankara*
Ender Uysal, *Istanbul*

United Kingdom

K Faulkner, *Wallsend*
Peter Gaines, *Sheffield*
Balaji Ganeshan, *Brighton*
Nagy Habib, *London*
Alan Jackson, *Manchester*
Pradesh Kumar, *Portsmouth*
Tarik F Massoud, *Cambridge*
Igor Meglinski, *Bedfordshire*
Robert Morgan, *London*
Ian Negus, *Bristol*
Georgios A Plataniotis, *Aberdeen*
N J Raine-Fenning, *Nottingham*
Manuchehr Soleimani, *Bath*
MY Tseng, *Nottingham*
Edwin JR van Beek, *Edinburgh*
Feng Wu, *Oxford*

United States

Athanassios Argiris, *Pittsburgh*
Stephen R Baker, *Newark*
Lia Bartella, *New York*
Charles Bellows, *New Orleans*
Walter L Biffl, *Denver*
Homer S Black, *Houston*
Wessam Bou-Assaly, *Ann Arbor*
Owen Carmichael, *Davis*
Shelton D Caruthers, *St Louis*
Yuhchyau Chen, *Rochester*
Melvin E Clouse, *Boston*
Ezra Eddy Wyssam Cohen, *Chicago*
Aaron Cohen-Gadol, *Indianapolis*
Patrick M Colletti, *Los Angeles*
Kassa Darge, *Philadelphia*
Abhijit P Datir, *Miami*
Delia C DeBuc, *Miami*
Russell L Deter, *Houston*
Adam P Dicker, *Phil*
Khaled M Elsayes, *Ann Arbor*
Steven Feigenberg, *Baltimore*
Christopher G Filippi, *Burlington*
Victor Frenkel, *Bethesda*
Thomas J George Jr, *Gainesville*
Patrick K Ha, *Baltimore*
Robert I Haddad, *Boston*
Walter A Hall, *Syracuse*
Mary S Hammes, *Chicago*
John Hart Jr, *Dallas*
Randall T Higashida, *San Francisco*
Juebin Huang, *Jackson*
Andrei Iagaru, *Stanford*
Craig Johnson, *Milwaukee*
Ella F Jones, *San Francisco*
Csaba Juhasz, *Detroit*
Riyad Karmy-Jones, *Vancouver*
Daniel J Kelley, *Madison*
Amir Khan, *Longview*
Euishin Edmund Kim, *Houston*
Vikas Kundra, *Houston*
Kennith F Layton, *Dallas*
Rui Liao, *Princeton*
CM Charlie Ma, *Philadelphia*
Nina A Mayr, *Columbus*
Thomas J Meade, *Evanston*
Steven R Messé, *Philadelphia*
Nathan Olivier Mewton, *Baltimore*
Feroze B Mohamed, *Philadelphia*
Koenraad J Mortele, *Boston*
Mohan Natarajan, *San Antonio*
John L Nosher, *New Brunswick*
Chong-Xian Pan, *Sacramento*
Dipanjan Pan, *St Louis*
Martin R Prince, *New York*
Reza Rahbar, *Boston*
Carlos S Restrepo, *San Antonio*
Veronica Rooks, *Honolulu*
Maythem Saeed, *San Francisco*
Edgar A Samaniego, *Palo Alto*
Kohkan Shamsi, *Doylestown*
Jason P Sheehan, *Charlottesville*
William P Sheehan, *Willmar*
Charles Jeffrey Smith, *Columbia*
Monvadi B Srichai-Parsia, *New York*
Dan Stoianovici, *Baltimore*
Janio Szklaruk, *Houston*
Dian Wang, *Milwaukee*
Jian Z Wang, *Columbus*
Liang Wang, *New York*
Shougang Wang, *Santa Clara*
Wenbao Wang, *New York*
Aaron H Wolfson, *Miami*
Gayle E Woloschak, *Chicago*
Ying Xiao, *Philadelphia*
Juan Xu, *Pittsburgh*
Benjamin M Yeh, *San Francisco*
Terry T Yoshizumi, *Durham*
Jinxing Yu, *Richmond*
Jianhui Zhong, *Rochester*

WJR World Journal of Radiology

Contents

Monthly Volume 3 Number 3 March 28, 2011

World Journal of Radiology
Volume 3 Number 3 March 28, 2011

Contents

NAME OF JOURNAL
World Journal of Radiology

LAUNCH DATE
December 31, 2009

SPONSOR
Beijing Baishideng BioMed Scientific Co., Ltd.,
Room 903, Building D, Ocean International Center,
No. 62 Dongsihuan Zhonglu, Chaoyang District,
Beijing 100025, China
Telephone: +86-10-8538-1892
Fax: +86-10-8538-1893
E-mail: baishideng@wjgnet.com
http://www.wjgnet.com

EDITING
Editorial Board of *World Journal of Radiology*,
Room 903, Building D, Ocean International Center,
No. 62 Dongsihuan Zhonglu, Chaoyang District,
Beijing 100025, China
Telephone: +86-10-8538-1892
Fax: +86-10-8538-1893
E-mail: wjr@wjgnet.com
http://www.wjgnet.com

PUBLISHING
Baishideng Publishing Group Co., Limited,
Room 1701, 17/F, Henan Building,
No.90 Jaffe Road, Wanchai, Hong Kong, China
Fax: +852-3115-8812
Telephone: 00852-5804-2046
E-mail: baishideng@wjgnet.com
http://www.wjgnet.com

SUBSCRIPTION
Beijing Baishideng BioMed Scientific Co., Ltd.,
Room 903, Building D, Ocean International Center,
No. 62 Dongsihuan Zhonglu, Chaoyang District,
Beijing 100025, China
Telephone: +86-10-8538-1892
Fax: +86-10-8538-1893
E-mail: baishideng@wjgnet.com
http://www.wjgnet.com

PUBLICATION DATE
March 28, 2011

SERIAL PUBLICATION NUMBER
ISSN 1949-8470 (online)

EDITORIAL OFFICE
Na Ma, Director
World Journal of Radiology
Room 903, Building D, Ocean International Center,
No. 62 Dongsihuan Zhonglu, Chaoyang District,
Beijing 100025, China
Telephone: +86-10-8538-1892
Fax: +86-10-8538-1893
E-mail: wjr@wjgnet.com
http://www.wjgnet.com

INSTRUCTIONS TO AUTHORS
Full instructions are available online at http://www.wjgnet.com/1949-8470/g_info_20100316162358.htm.

ONLINE SUBMISSION
http://www.wjgnet.com/1949-8470office

World Journal of Radiology

Online Submissions: http://www.wjgnet.com/1949-8470office
wjr@wjgnet.com
doi:10.4329/wjr.v3.i3.55

World J Radiol 2011 March 28; 3(3): 55-65
ISSN 1949-8470 (online)

EDITORIAL

A promising diagnostic method: Terahertz pulsed imaging and spectroscopy

Yiwen Sun, Ming Yiu Sy, Yi-Xiang J Wang, Anil T Ahuja, Yuan-Ting Zhang, Emma Pickwell-MacPherson

Yiwen Sun, Ming Yiu Sy, Yuan-ting Zhang, Department of Electronic Engineering, The Chinese University of Hong Kong, Hong Kong, China
Yi-Xiang J Wang, Anil T Ahuja, Department of Imaging and Interventional Radiology, The Chinese University of Hong Kong, Hong Kong, China
Yuan-ting Zhang, The Institute of Biomedical and Health Engineering, Shenzhen Instituted of Advanced Technology, Chinese Academy of Sciences, Shenzhen 518000, Guangdong Province, China
Yuan-Tng Zhang, Key Laboratory for Biomedical Informatics and Health Engineering, Chinese Academy of Sciences, Shenzhen 518000, Guangdong Province, China
Emma Pickwell-MacPherson, Department of Electronic and Computer Engineering, Hong Kong University of Science and Technology, Hong Kong, China
Author contributions: Wang YXJ gave the idea of the paper was given; Sun Y, Sy MY and Pickwell-MacPherson E collected the data presented; all authors were involved in writing and editing the paper.
Supported by in part for this work from the Research Grants Council of the Hong Kong Government and the Shun Hing Institute of Advanced Engineering, Hong Kong
Correspondence to: Dr. Emma Pickwell-MacPherson, Department of Electronic and Computer Engineering, Hong Kong University of Science and Technology, Hong Kong, China. eeemma@ust.hk
Telephone: +852-23585034 Fax: +852-23581485
Received: November 18, 2010 Revised: January 19, 2010
Accepted: January 26, 2010
Published online: March 28, 2011

Abstract

The terahertz band lies between the microwave and infrared regions of the electromagnetic spectrum. This radiation has very low photon energy and thus it does not pose any ionization hazard for biological tissues. It is strongly attenuated by water and very sensitive to water content. Unique absorption spectra due to intermolecular vibrations in this region have been found in different biological materials. These unique features make terahertz imaging very attractive for medical applications in order to provide complimentary information to existing imaging techniques. There has been an increasing interest in terahertz imaging and spectroscopy of biologically related applications within the last few years and more and more terahertz spectra are being reported. This paper introduces terahertz technology and provides a short review of recent advances in terahertz imaging and spectroscopy techniques, and a number of applications such as molecular spectroscopy, tissue characterization and skin imaging are discussed.

Key words: Biomedical; Imaging; Spectroscopy; Terahertz

Peer reviewer: Yicheng Ni, MD, PhD, Professor, Biomedical Imaging, Interventional Therapy and Contrast Media Research, Department of Radiology, University Hospitals, K.U. Leuven, Herestraat 49, B-3000, Leuven, Belgium

Sun Y, Sy MY, Wang YXJ, Ahuja AT, Zhang YT, Pickwell-MacPherson E. A promising diagnostic method: Terahertz pulsed imaging and spectroscopy. *World J Radiol* 2011; 3(3): 55-65 Available from: URL: http://www.wjgnet.com/1949-8470/full/v3/i3/55.htm DOI: http://dx.doi.org/10.4329/wjr.v3.i3.55

INTRODUCTION

Terahertz (THz, 1 THz = 10^{12} Hz) radiation, also known as THz waves, THz light, or T-rays, is situated in the frequency regime between optical and electronic techniques. This regime is typically defined as 0.1-10 THz and has become a new area for research in physics, chemistry, biology, materials science and medicine. Experiments with THz radiation date back to measurements of black body radiation using a bolometer in the 1890s[1,2]. However, for a long time, this region remained unexplored due to a lack of good sources and detectors, and it was commonly

referred to as the "THz gap". In 1975, David Auston at AT&T Bell Laboratories developed a photoconductive emitter gated with an optical pulse that led towards bridging this gap - the 'Auston switch' emitted broadband THz radiation up to 1 mW. A coherent method to detect THz pulses in the time domain was also proposed[3]. This became the foundation of THz time-domain spectroscopy (THz-TDS)[4], since then many improvements in the generation and detection of coherent THz radiation enabled THz-TDS and imaging techniques to be pioneered for applications in various fields such as biomedical engineering, physics, astronomy, security screening, communications, genetic engineering, pharmaceutical quality control and medical imaging[5]. In this paper, THz technology is introduced and some emerging applications in biology and medicine including molecular spectroscopy, tissue characterization and skin imaging are presented.

The aim of this article is to review the potential of THz pulsed imaging and spectroscopy as a promising diagnostic method. Several unique features make THz very suitable for medical applications. (1) THz radiation has very low photon energy, which is insufficient to cause chemical damage to molecules, or knock particles out of atoms. Thus, it will not cause harmful ionization in biological tissues; this makes it very attractive for medical applications; (2) THz radiation is very sensitive to polar substances, such as water and hydration state. For this reason, THz waves can provide a better contrast for soft tissues than X-rays; (3) THz-TDS techniques use coherent detection to record the THz wave's temporal electric fields, which means both the amplitude and phase of the THz wave can be obtained simultaneously. The temporal waveforms can be further Fourier transformed to give the spectra. This allows precise measurements of the refractive index and absorption coefficient of samples without resorting to the Kramers-Kronig relations; and (4) The energy of rotational and vibrational transitions of molecules lies in the THz region and intermolecular vibrations such as hydrogen bonds exhibit different spectral characteristics in the THz range. These unique spectral features can be used to distinguish between different materials or even isomers.

PRINCIPLES OF THZ PULSED IMAGING AND SPECTROSCOPY

THz systems

Over the past two decades, technology for generating and detecting THz radiation has advanced considerably. Several commercialized systems are now available[6-10] and THz systems have been set up by many groups all over the world. According to the laser source used, THz systems can be divided into two general classes: continuous wave (CW) and pulsed.

A typical CW system can produce a single fixed frequency or several discrete frequency outputs. Some of them can be tunable. Generation of CW THz radiation can be achieved by approaches such as photomixing[11], free-electron lasers[12] and quantum cascade lasers[13]. Figure 1 illustrates a CW THz system which photomixes two CW lasers in a photoconductor as an example[14]. The mixing of two above-bandgap (visible or near-infrared) wavelengths produces beating, which can modulate the conductance of a photoconductive switch at the THz difference frequency. The photomixing device is labeled "emitter" in Figure 1. Since the source spectrum of the CW system is narrow and sometimes only the intensity information is of interest, the data structures and post-processing are relatively simple. It is possible now to drive a whole CW system by laser diodes and thus it can be made compact and inexpensive. However, due to the limited information that CW systems provide, they are sometimes confined to those applications where only features at some specific frequencies are of interest.

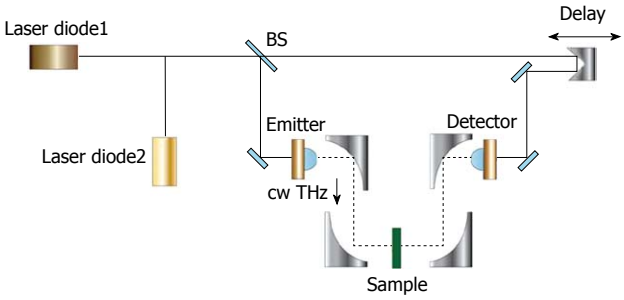

Figure 1 Schematic illustration of a continuous wave THz imaging system in transmission geometry.

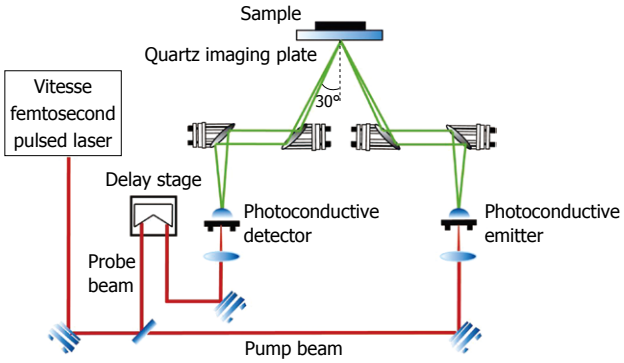

Figure 2 Schematic illustration of a pulsed THz imaging system with reflection geometry.

In pulsed systems, broadband emission up to several THz can be achieved. Currently, there are a number of ways to generate and detect pulsed THz radiation, such as ultrafast switching of photoconductive antennas[3], rectification of optical pulses in crystals[15], rapid screening of the surface field *via* photoexcitation of dense electron hole plasma in semiconductors[16] and carrier tunneling in coupled double quantum well structures[17]. Among them, the most established approaches based on photoconductive antennas, where an expensive femtosecond laser is required and configured as shown in Figure 2. Unlike CW THz imaging system, coherent detection in pulsed THz imaging techniques can record THz waves in the time do-

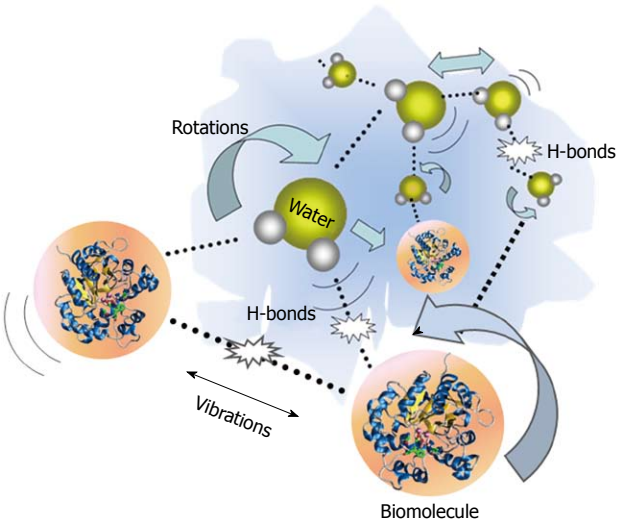

Figure 3 Schematic representation of H-bond interactions between water and biomolecules.

main, including both the intensity and phase information, which can be further used to obtain more details of the target such as spectral and depth information[18]. This key advantage lends coherent THz imaging to a wider range of applications.

Molecular interactions in the THz regime

There has been an increased interest in understanding the interactions between molecules and THz radiation. Many of the intricate interactions on a molecular level rely on changes in biomolecular conformation of the basic units of proteins such as α helices and β sheets. In recent years, dynamic signatures of the THz frequency vibrations in RNA and DNA strands have been characterized[19,20]. Furthermore, studies of water molecule interactions with proteins have attracted significant research interest[21]. In a protein-water network, the protein's structure and dynamics are affected by the surrounding water which is called biological water, or hydration water. As illustrated in Figure 3, hydrogen bonds, which are weak attractive forces, form between the hydrated water molecules and the side chains of protein. These affect the dynamic relaxation properties of protein and enable distinction between the hydration water layer and bulk water. The remarkable effects of the hydrogen bonds associated with the intermolecular information are able to be detected using THz spectroscopy. THz spectra contain information about intermolecular modes as well as intra-molecular bonds and thus usually carry more structural information than vibrations in the mid-infrared spectral region which tend to be dominated by intra-molecular vibrations.

Unique advantages and challenges for biomedical applications

The energy level of 1 THz is only about 4.14 meV (which is much less than the energy of X-rays 0.12 to 120 keV), it therefore does not pose an ionization hazard as in X-ray radiation. Research into safe levels of exposure has also been carried out through studies on keratinocytes[22] and blood leukocytes[23,24], neither of which has revealed any detectable alterations. This non-ionizing nature is a crucial property that lends THz techniques to medical applications.

The fundamental period of THz-frequency electromagnetic radiation is around 1ps, and so it is uniquely suited to investigate biological systems with mechanisms at picosecond timescales. The energy levels of THz light are very low, therefore damage to cells or tissue should be limited to generalized thermal effects, i.e. strong resonant absorption seems unlikely. From a spectroscopy standpoint, biologically important collective modes of proteins vibrate at THz frequencies, in addition, frustrated rotations and collective modes cause polar liquids (such as water) to absorb at THz frequencies. Many organic substances have characteristic absorption spectra in this frequency range[25,26] enabling research into THz spectroscopy for biomedical applications.

THz wavelengths have a diffraction limited spot size consistent with the resolution of a 1990's vintage laser printer ($1.22\lambda_0$ = 170 μm at 2.160 THz or 150 dots/in). At 1 THz, the resolution could be as good as a decent computer monitor (70 dots/in). Submillimeter-wavelength means that THz signals pass through tissue with only Mie or Tyndall scattering (proportional to f^2) rather than much stronger Rayleigh scattering (proportional to f^4) that dominates in the IR and optical since cell size is less than the wavelength.

Since most tissues are immersed in, dominated by, or preserved in polar liquids, the exceptionally high absorption losses at THz frequencies make penetration through biological materials of any substantial thickness infeasible. However, the same high absorption coefficient that limits penetration in tissue also promotes extreme contrast between substances with lesser or higher degrees of water content which can help to show distinctive contrast in medical imaging.

IMAGING *VS* SPECTROSCOPY

THz pulsed imaging

Early applications of THz technology were confined mostly to space science[27] and molecular spectroscopy[28,29], but interest in biomedical applications has been increasing since the first introduction of THz pulsed imaging (TPI) in 1995 by Hu and Nuss[30]. Their THz images of porcine tissue demonstrated a contrast between muscle and fats. This initial study promoted later research on the application of THz imaging to other biological samples. THz pulsed imaging actually can be viewed as an extension of the THz-TDS method. In addition to providing valuable spectral information, 2D images can be obtained with THz-TDS by spatial scanning of either the THz beam or the object itself. In this way, geometrical images of the sample can be produced to reveal its inner structures[31]. Thus, it is possible to obtain three-dimensional views of a layered structure.

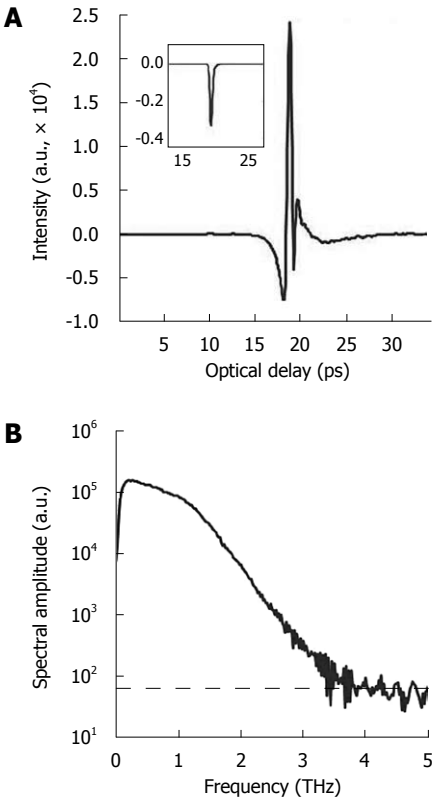

Figure 4 Typical terahertz pulse and corresponding spectrum. A: Temporal waveform of a sample (drawn by raw data with the inset representing its corresponding processed data after deconvolution with a reference measurement); B: The corresponding spectrum of the raw data with the noise floor (indicated by dashed line).

When a THz pulse is incident on such a target, a train of pulses will be reflected back from the various interfaces. For each individual pulse in the detected signal, the amplitude and timing are different and can be measured precisely. The principle of time of flight technique is to estimate the depth information of the internal dielectric profiles of the target through the time that is required to travel over a certain distance. This permits looking into the inside of optically opaque material and it has been used for THz 3D imaging. Among the earliest demonstrations of THz 3D imaging, Mittleman *et al*[31] imaged a conventional floppy disk. In their work the various parts inside the disk were identified and the discontinuous refractive index profile was derived. This method was further extended into THz reflection computed tomography[32,33], where the target was rotated to provide back reflection from different angles. In a similar way to X-ray CT imaging, the filtered back projection algorithm was applied to reconstruct the edge map of the target's cross-section. With advances in interactive publishing, Wallace *et al*[34] highlighted the ability of 3-D THz imaging in a number of niche applications. For example they were able to resolve two layers of drugs beneath the protective coating of a pharmaceutical tablet.

THz spectroscopy

THz spectroscopy is typically done with a single point measurement (with transmission geometry in most cases) of a homogenous sample and the resulting THz electric field can be recorded as a function of time. Thus, it can be Fourier transformed to offer meaningful spectroscopic information due to the broadband nature of pulsed THz radiation, shown in Figure 4. Although the spectral resolution is not as good as that with narrowband techniques, coherent detection of THz-TDS can provide both high sensitivity and time-resolved phase information[35]. This spectroscopic technique is primarily used to probe material properties and it is helpful to see where it lies in the electromagnetic spectrum in relation to atomic and molecular transitions.

THz spectroscopy is complementary to THz imaging and is primarily used to determine optical properties in the frequency domain. Since THz pulses are created and detected using short pulsed visible lasers with pulse widths varying from approximately 200 fs down to approximately 10 fs, it is now possible to make time resolved far-infrared studies with sub-picosecond temporal resolution[36]. This was not achievable with conventional far-infrared studies. An important aspect of THz time-domain spectroscopy is that both the phase and amplitude of the spectral components of the pulse are determined. The amplitude and phase are directly related to the absorption coefficient and refractive index of a sample and thus the complex permittivity is obtained without requiring Kramers-Kronig analysis. Furthermore, another advantage of THz spectroscopy is that it is able to non-destructively detect differences because it uses radiation of sufficiently long wavelength and low energy that does not induce any phase changes or photochemical reactions to living organisms.

BIOLOGICAL APPLICATIONS

Pharmaceuticals

There has been a strong drive in the pharmaceutical industry for comprehensive quality assurance monitoring. This motivates development of new tools providing useful analysis of tablet formulations. The ability of THz technology to determine both spectral and structural information has fuelled interest in the pharmaceutical applications of this technique[37]. For example THz spectroscopy has been employed for polymorph identification and quantification[38], phase transition monitoring[39], and distinguishing between behaviors of hydrated forms[40]. THz radiation can penetrate through plastic packaging materials. To illustrate this we give an example using Maalox PlusTM - an over the counter medicine for stomach upsets. Each tablet has "Rorer" engraved on one side and "Maalox Plus" on the other side. Figure 5A contains a photo of a tablet in its packaging as well as a THz image taken after removing it from the packaging - the engraved lettering is clearly seen in the THz image. Figure 5C is a THz image of the tablet taken through the packaging - we can still see the lettering on the surface of the tablet. The cross-section of the tablet is better conveyed by an image of the depth profile. THz pulses are reflected first off the

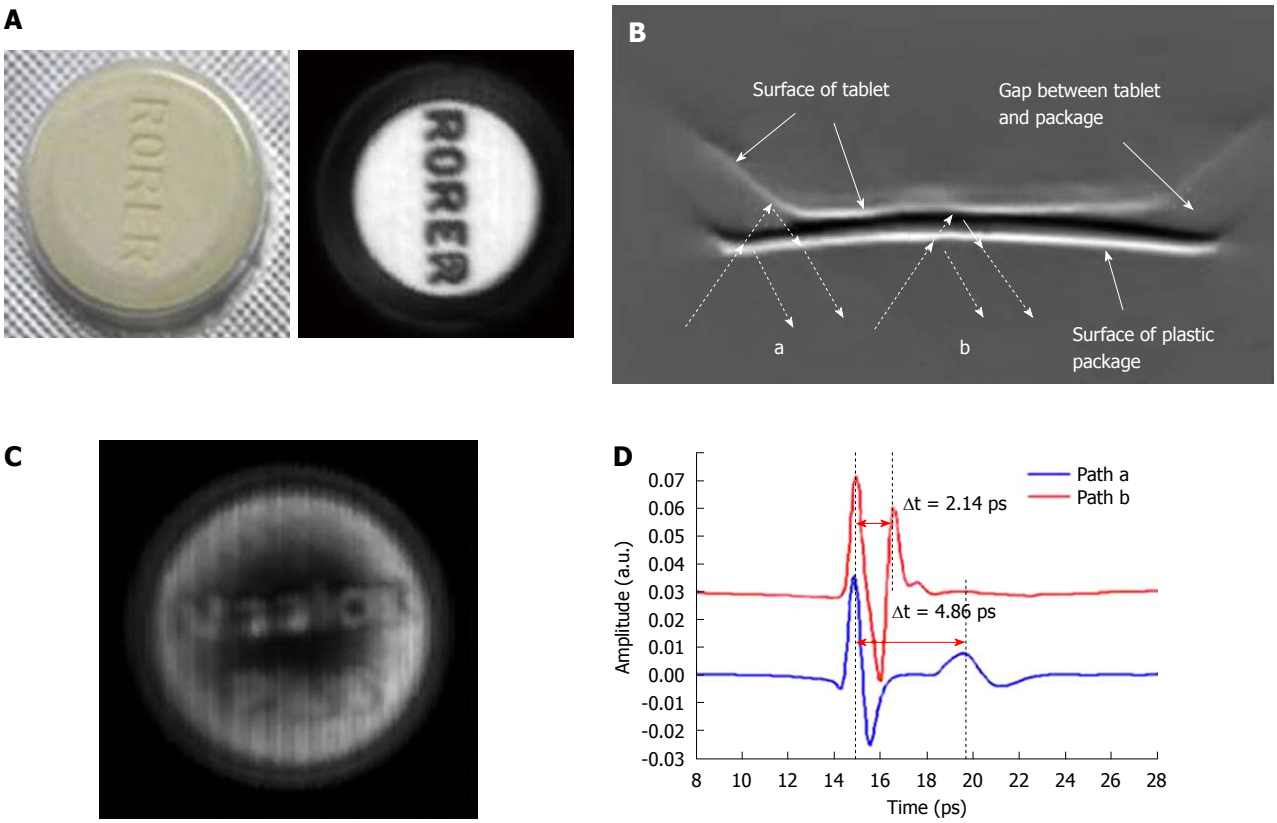

Figure 5 Terahertz imaging of the tablet. A: Photograph of the tablet in the plastic package and THz C-Scan section imaging without the packaging; B: THz B-Scan image shows the structure of the cross-section of the tablet and the THz light paths at the edge of the tablet (path a) and the centre (path b); C: THz C-Scan image shows the tablet face inside the plastic package; D: THz deconvolved waveforms in the time-domain reflected from the paths a and b in Figure 5B.

front surface of the package and then from any subsurface structure within it resulting in multiple pulses returning to the detector. The dashed arrows in Figure 5B mark out the THz light paths at the edge of the tablet (path A) and the center (path B). In path A the beveled edge means that there is an air gap between the packaging and the tablet and this corresponds to a greater optical delay between the reflected peaks in the waveforms illustrated in Figure 5D. Thus, THz imaging has non-destructively revealed the structure of the tablet through the packaging.

Protein spectroscopy

Towards the higher frequency end of the THz range (from about 1 THz and above) there are vibrational modes corresponding to protein tertiary structural motion; such intermolecular interactions are present in many biomolecules. Other molecular properties that can be probed in the THz range include bulk dielectric relaxation modes[41] and phonon modes[42] these can be difficult to probe using other techniques. For instance nuclear magnetic resonance (NMR) spectroscopy can determine the presence of various carbon bonds, but it cannot be used to distinguish between molecules with the same molecular formula, but with different structural forms (isomers)[10]. THz spectroscopy is able to distinguish between isomers and polymorphs[43] and is therefore emerging as an important and highly sensitive tool to determine biomolecular structure and dynamics[44,45]. Indeed THz spectroscopy can distinguish between two types of artificial RNA strands when measured in dehydrated form[46]. Furthermore, Fischer *et al*[47] demonstrated that even when the molecular structure differs only in the orientation of a single hydroxyl group with respect to the ring plane, a pronounced difference in the THz spectra is observed. Intermolecular interactions are present in all biomolecules, and since biomolecules are the fundamental components of biological samples, they can be used to provide a natural source of image contrast in biomedical THz imaging[48].

Biomolecules, especially proteins, which play an essential structural and catalytic role in cells and tissues, often require an aqueous phase in order to be transported to their target sites. In the protein-water system, the characteristic water structure induced near the surfaces of proteins arises not only through hydrogen bonding of the water molecules to available proton donor and proton acceptor sites, but also through electrostatic forces associated with the water molecule that arise from its large electric dipole moment. If an electric field is applied to such a system of protein-associated water, there will be a torque exerted on each water dipole moment inducing them to attempt to align along the direction of the field vector. The dielectric spectrum has been widely used to describe the interaction between protein and its solvent molecule in THz frequency[49]. A dielectric orientational relaxation time τ can then be defined as the time required for $1/e$ of the field-oriented water molecules to become randomly reoriented on removing

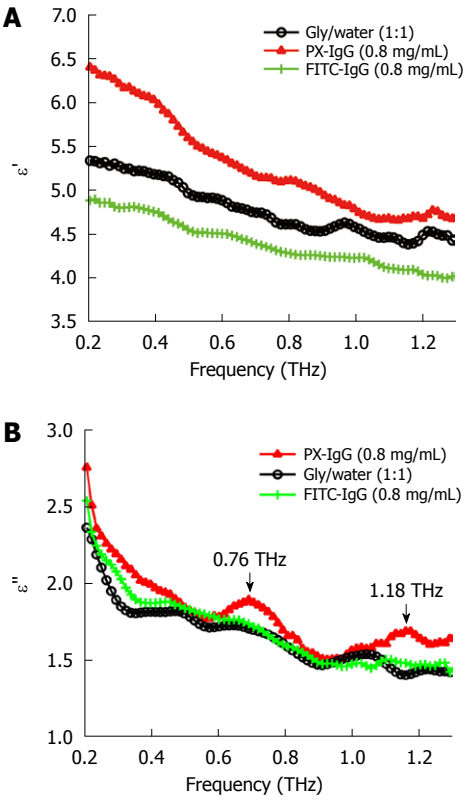

Figure 6 Dielectric constant spectra (A) and dielectric loss spectra (B) of water/ glycerol mix (black line with circles), peroxidase conjugated IgG (red line with triangles) and the fluorescein conjugated IgG (green line with crosses) dissolved in the water/glycerol solution at the concentration of 0.8 mg/mL in the frequency range of 0.1-1.3 THz. PX: Peroxidase conjugated; FITC: Fluorescein conjugated.

the applied field. Measurements may be analyzed in terms of the complex dielectric constant ε(ω) (where ω denotes angular frequency) or the complex refractive index $n(\omega)$. The degree of orientational polarization and the rate of reorientational relaxation depend on how the water dipoles are influenced by local electrostatic forces and the extent to which the breaking and/or reforming of local hydrogen bonds is required to accommodate the changes in orientation. Relaxations of polar side-groups, vibrations of the polypeptide backbone, and fluctuating proton transfer between ionized side-groups of the protein also contribute to the overall polarizability of the protein-water system. If dielectric measurements are made on protein solutions, then orientational relaxations of the protein molecule itself will also be observed[50]. Figure 6 shows that the vibration mode of two types of labeled antibodies (peroxidase conjugated IgG and the fluorescein conjugated IgG) can be distinguished at 0.76 and 1.18 THz using the THz dielectric spectrum. By investigating the concentration dependence of the spectra it is also possible to obtain an estimate of the hydration shell thickness around the protein molecules[51].

MEDICAL APPLICATIONS

Tissue characterization

There is also interest in tissue contrast for *in vivo and ex vivo* identification of abnormalities, hydration, and subdermal probing. Only a small number of measurements have been made to date, and systematic investigations to catalogue absorption coefficients, refractive indices and contrast mechanisms are just beginning to accumulate. Measurements on the absorption and refractive index of biological materials in the THz region go back at least to 1976[52]. Several research groups have investigated excised and fixed tissue samples, either alcohol perfused[8], formalin fixed[53-57], or freeze dried and wax mounted[58] looking for inherent contrast to define unique modalities. One of the first applications on human *ex vivo* wet tissue involved imaging of excised basal cell carcinoma[59,60]. *In vivo* work has focused on the skin[61] and accessible external surfaces of the body for measuring hydration[62] and tumor infiltration[60]. A catalogue of unfixed tissue properties (including blood constituents) was compiled by the University of Leeds, UK[54] for frequencies between 500-1500 GHz using a pulsed time-domain system. Difficulties in extrapolating measurements on excised tissue to *in vivo* results are numerous and include for example uptake of saline from the sample storage environment, changes in hydration level during measurement, temperature-dependent loss, measurement chamber interactions, and scattering effects. In our previous work[63], we performed reflection geometry spectroscopy to investigate the properties of several types of healthy organ tissues, including liver, kidney, heart muscle, leg muscle, pancreas and abdominal fat tissues using THz pulsed imaging. The frequency dependent refractive index and the absorption coefficient of the tissues are shown in Figure 7. All the results are the mean values of the ten samples and error bars represent the 95% confidence intervals. We found clear differences between the tissue properties, particularly the absorption coefficient. Since fatty tissue largely consists of hydrocarbon chains and relatively few polar molecules, the absorption coefficient and refractive index of the fatty tissue are much lower that those of the kidney and liver tissues.

We have also investigated the optical properties of fresh and formalin fixed samples in the THz frequency range using THz reflection spectroscopy[64]. As seen in Figure 8A, when the fixing time increased the waveform amplitude of the adipose tissue also increased. This was primarily because the refractive index of the adipose tissue was decreasing over the majority of the bandwidth (due to the fixing) and this meant there was a greater difference between the refractive index of the quartz (n approximately 2.1) and that of the adipose tissue (e.g. 1.5 at 1 THz when fixed compared to 1.6 when it was fresh). From Fresnel theory, this increased difference in refractive indices resulted in a greater reflected amplitude. As the fixing time increased for the muscle, three main changes were apparent. A small peak started to appear preceding the trough and the width and magnitude of the trough decreased (Figure 8B). These changes can also be explained by considering the effects of the formalin on the refractive index and absorption coefficient of the muscle. For the muscle, the formalin significantly reduced both

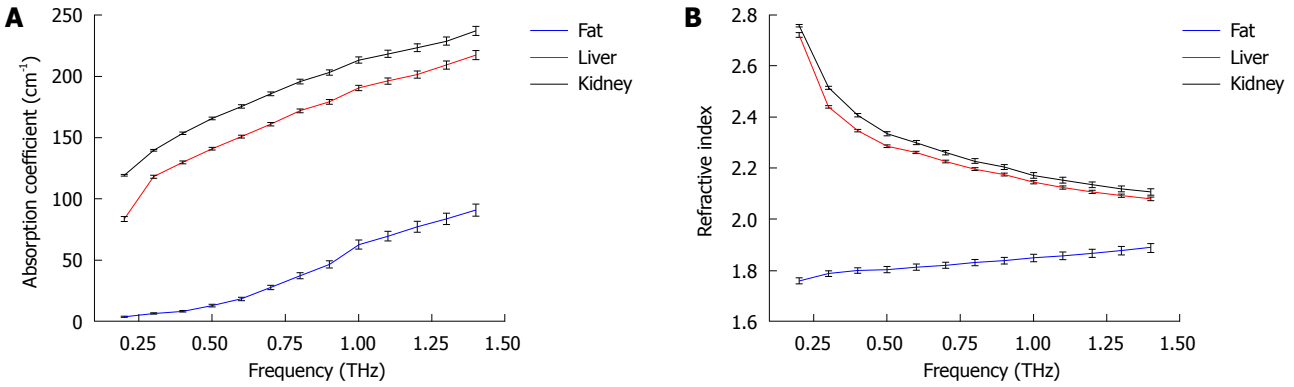

Figure 7 Tissue characterization using THz spectroscopy. A: Mean absorption coefficients of kidney, liver and abdominal fat; B: Mean refractive indices of all the tissue samples. Error bars represent 95% confidence intervals.

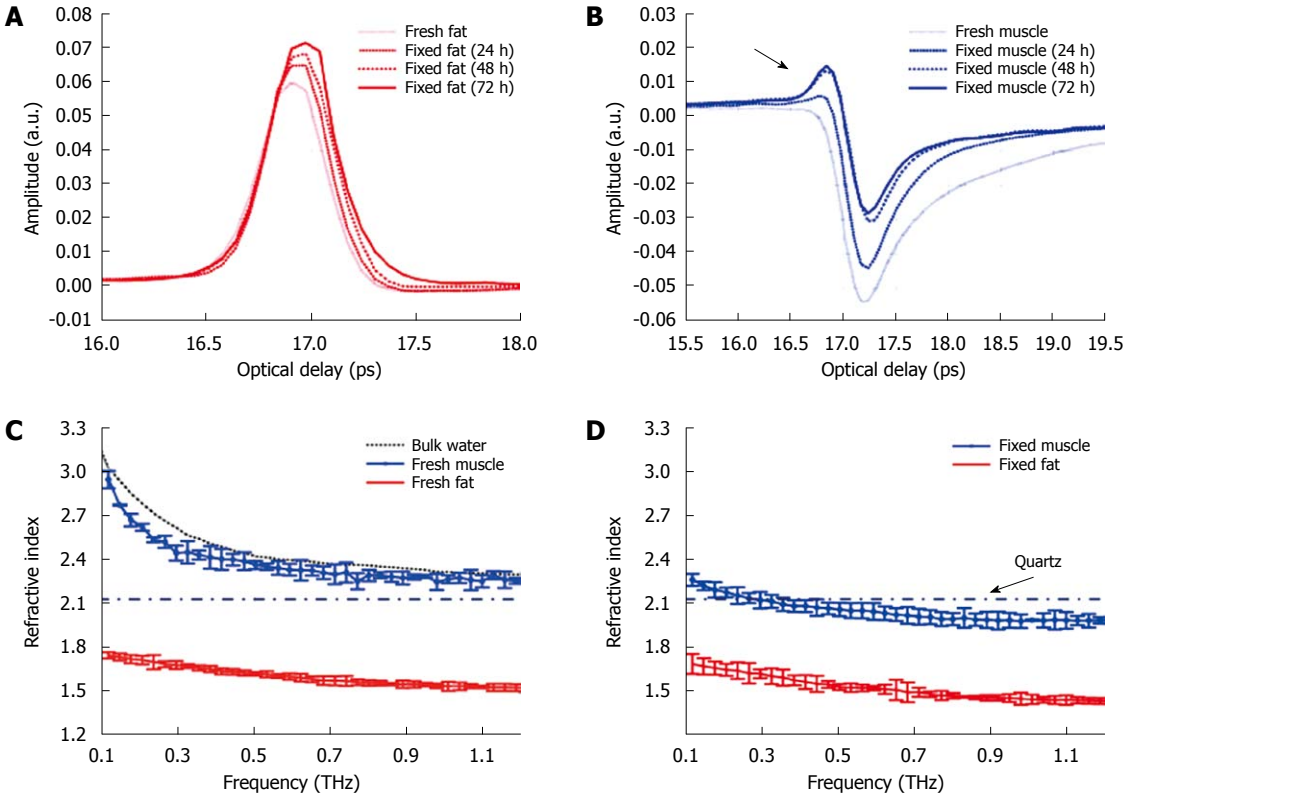

Figure 8 The deconvolved mean waveforms for adipose tissue (A) and skeletal muscle (B) as the fixing time progressed and the mean refractive index for fresh (C) and fixed samples (D) of adipose tissue and skeletal muscle. The dot-dash line indicates the refractive index of the quartz window on which the sample was measured. Error bars represent 95% CI. The water data were acquired in transmission and the error bars are too small to be seen on this graph.

the refractive index and the absorption coefficient. Before fixing, the refractive index of the fresh muscle was greater than that of quartz over the whole of the frequency range measured (Figure 8C). The fixing reduced the refractive index so much that the refractive index became lower than that of quartz at higher frequencies (Figure 8D) and this was the cause for the small peak which appeared (arrow in Figure 8B) and increased as the fixing time was increased.

Skin cancer, breast tumors and dental caries

Due to the low penetration depth of THz in biological tissues, THz biomedical applications investigated to date have been limited to easily accessible parts of the body, such as skin and teeth, or those that would benefit from intra-operative imaging such as breast cancer. Figure 9 is a photograph of the reflection geometry THz probe from TeraView Ltd. which we use in Hong Kong.

One potential application of THz imaging is the diagnosis of skin cancer. Work by Woodward *et al*[60] has demonstrated the potential to use THz imaging to determine regions of skin cancer non-invasively using a reflection geometry imaging system. The first *ex vivo* measurements on skin cancer revealing the ability of TPI to differentiate basal cell carcinoma (BCC) from normal skin were pro-

Figure 9 Photograph of the THz hand-held probe.

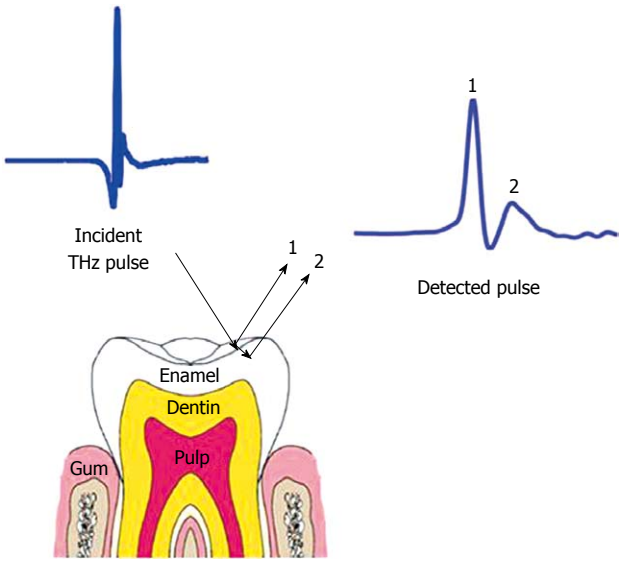

Figure 10 Schematic representation of the THz reflections from enamel. Reflection 1 is the reflection from the surface of the enamel and reflection 2 is the reflection from within the enamel due to tooth decay causing mineral loss.

duced by Woodward *et al*[59].

Breast-conserving surgery is also an area of medicine which may benefit from THz imaging. Fitzgerald *et al*[65] conducted *ex vivo* studies of breast cancer to investigate the potential of THz imaging to aid the removal of breast cancer intra-operatively. In particular, they studied the feasibility of THz pulsed imaging to map the tumor margins on freshly excised human breast tissue. Good correlation was found for the area and shape of tumor in the THz images compared with that of histology. They also performed a spectroscopy study comparing the THz optical properties (absorption coefficient and refractive index) of the excised normal breast tissue and breast tumor. Both the absorption coefficient and refractive index were higher for tissue that contained tumor and this is a very positive indication that THz imaging could be used to detect margins of tumor and provide complementary information to techniques such as infrared and optical imaging, thermography, electrical impedance, and magnetic resonance imaging[66,67].

Since *in vivo* THz imaging is currently limited to surface features, another potential application of THz imaging is the diagnosis of dental caries[68,69]. Figure 10 is a schematic diagram of a THz reflection from the outer layer of enamel. Caries are a result of mineral loss from enamel, and this causes a change in refractive index within the enamel. The change in refractive index means that small lesions, smaller than those detected by the naked eye, can be detected[70]. However, in practice THz imaging systems are large and cumbersome - even structures as obvious as teeth can make a challenging target. In this respect THz imaging is still some way off offering a non-ionizing alternative to X-rays in dentistry.

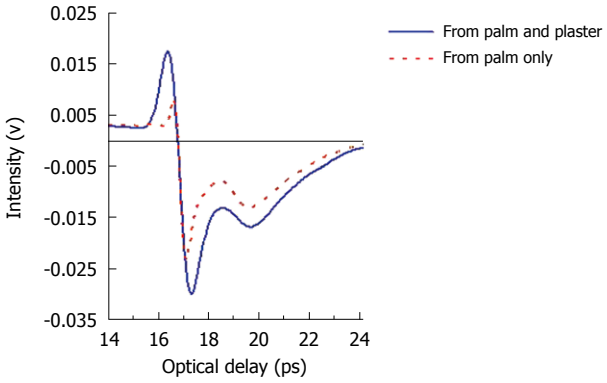

Figure 11 Measured pulses from the palm. The blue line is the measurement of the palm through a tegaderm plaster and the red dotted line is the measurement of the palm alone. In both cases, two troughs are seen - they are the reflections from the top and bottom surfaces of the stratum corneum.

Burn depth diagnosis

Since THz waves can penetrate several hundreds of microns into the skin and most burn injuries are superficial, this opens up the possibility of employing THz techniques for burn assessment[71]. The waveforms and optical parameters of the burn wounds were investigated and THz images have shown contrast between burn-damaged tissue and healthy tissue. Their results indicate that THz imaging may be promising in evaluating skin burn severity, especially for characterizing burn areas. Moreover, the time of flight technique is able to reveal the depth profile thus could be used to evaluate burn depth.

The potential of THz imaging as a burn diagnostic has been demonstrated using chicken breast[6]. It is also conceivable that THz imaging could be of use in monitoring treatment of skin conditions (like psoriasis), since THz imaging is cheaper than MRI and does not require a coupling gel like ultrasound[72].

THz light can penetrate many materials: we have investigated whether it can resolve skin layers beneath a Tegaderm® plaster as this would also be of benefit in monitoring burn wounds. Normal skin comprises three different layers: the stratum corneum, epidermis, and dermis. The stratum corneum on the palm of the hand is 100-200 μm thick and thus has been resolved in previous *in vivo* skin studies. We placed the plaster on the palm of the hand and the resulting THz reflected waveform

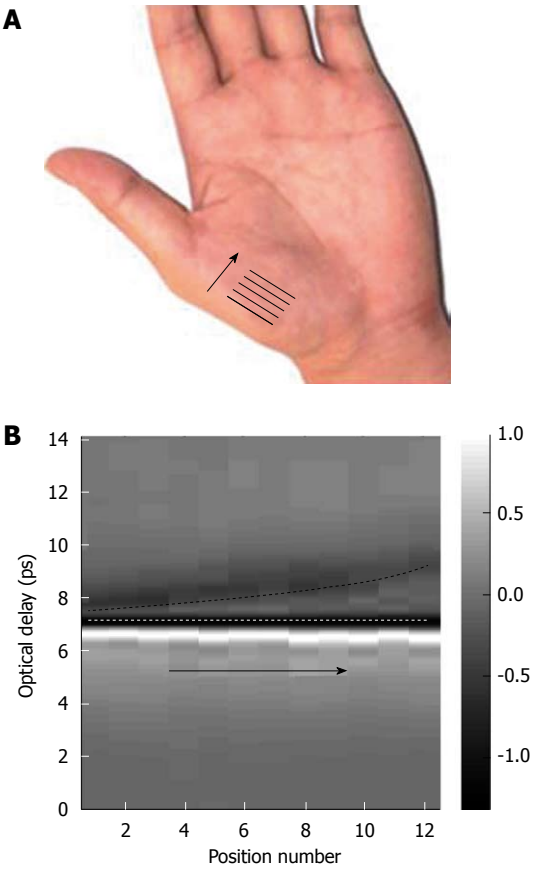

Figure 12 *In vivo* measurement of the variation in stratum corneum thickness of the palm. A: Photograph of the palm, indicating where the THz measurements were taken; B: A b-scan image showing the variation in stratum corneum thickness with palm position. The white dashed line indicates the interface between the quartz window and the stratum corneum; and the black dashed line indicates the interface between the stratum corneum and the epidermis. The grey bar represents the ratio of the electric field at a given optical delay, t, over the maximum electric field [E(t)/Emax].

is shown in Figure 11. For comparison the measurement of the palm alone is also plotted. In the figure, there are 2 troughs, which correspond to the top and bottom surface of the stratum corneum. The optical delay between them can be used to calculate the thickness of this layer. These results show that THz light is able to penetrate through wound dressings with only slight attenuation to reveal the skin depth information. This therefore indicates that THz imaging is likely to be able to detect and measure changes to the stratum corneum and epidermis which could for example, be caused by burns. To illustrate how sensitive THz imaging is to the stratum corneum, we have also imaged the side of a healthy hand. As the position of the measurement changes, as indicated by the arrow in Figure 12A, the optical delay between the reflections from the top and bottom of the stratum corneum increases. This is because the stratum corneum is thicker at the tip of the arrow than at the arrow foot. By plotting the reflected amplitude intensity against position we obtain the depth profile image of the palm in Figure 12B. By using frequency and wavelet domain deconvolution we are able to resolve thinner layers of skin than if basic deconvolution is used[73].

COMPARISON WITH OTHER TECHNOLOGIES

Numerous groups have investigated direct transmission or reflection THz imaging as a means of distinguishing tissue types[30,55,74] and recognizing diseases including tumors penetrating below the surface layers of skin or into organs[56,58,75]. Although progress is being made, the competition from other more developed imaging modalities is fierce. Optical coherence tomography, ultrasound, near-IR, and Raman spectroscopy, MRI, positron emission tomography, *in situ* confocal microscopy, and X-ray techniques have all received much more attention and currently offer enhanced resolution, greater penetration, higher acquisition speeds, and specifically targeted contrast mechanisms. This does not preclude THz imaging from finding a niche in this barrage of already favorable modalities. There is still no technique that can readily distinguish benign from malignant lesions macroscopically at the surface or subdermally. The sensitivity of THz signals to skin moisture, which is often a key indictor, is very high, and competing techniques such as high-resolution MRI are less convenient and more costly.

The resolution of ordinary THz imaging is diffraction limited, however, its high sensitivity to water content and great surface imaging capability provide motivation for further development and sub-wavelength resolution has been achieved in near-field studies[76]. Indeed shallow subsurface images can be very revealing and the first few hundred micrometers are hard to image with other modalities. The high sensitivity of THz radiation to fluid composition and the variable conductivity in tissue[77] is likely to lead to statistically significant differences between nominally identical samples taken at different locations in the body at different times or from different subjects. This may ultimately prove advantageous; however, in the short term, it will tend to mask sought for differences that are indicative of diseases.

CONCLUSION

THz imaging is still in its early stage of development, but as this paper has shown, has great potential to be a valuable imaging technique in the future. In the past decade, THz imaging applications in biomedical fields have drawn extensive interest and advancements in imaging methods and theoretical analysis continue to enable further applications to be investigated.

REFERENCES

1 **Nichols EF**. A method for energy measurements in the infra-red spectrum and the properties of the ordinary ray in quartz for waves of great wave length. *Phys Rev* (Series I) 1897; **4**: 297-313
2 **Rubens H**, Nichols EF. Heat rays of great wave length. *Phys Rev* (Series I) 1897; **4**: 314-323
3 **Auston DH**. Picosecond optoelectronic switching and gating in silicon. *Appl Phys Lett* 1975; **26**: 101-103
4 **Grischkowsky D**, Keiding S, van Exter M, Fattinger C. Far-

infrared time-domain spectroscopy with terahertz beams of dielectrics and semiconductors. *J Opt Soc Am B* 1990; **7**: 2006-2015
5 **Wallace VP**, Arnone DA, Woodward RM, Pye RJ. Biomedical applications of terahertz pulse imaging. Houston, TX: Engineering in Medicine and Biology, 2002. 24th Annual Conference and the Annual Fall Meeting of the Biomedical Engineering Society. Proceedings of the Second Joint EMBS/BMES Conference, 2002: 2333-2334
6 **Mittleman DM**, Gupta M, Neelamani R, Baraniuk RG, Rudd JV, Koch M. Recent advances in terahertz imaging. *Applied Physics B* 1999; **68**: 1085-1094
7 **Zhang XC**. Terahertz wave imaging: horizons and hurdles. *Phys Med Biol* 2002; **47**: 3667-3677
8 **Siegel PH**. Terahertz technology in biology and medicine. *IEEE T Micro Theory* 2004; **52**: 2438-2447
9 **Wallace VP**, Taday PF, Fitzgerald AJ, Woodward RM, Cluff J, Pye RJ, Arnone DD. Terahertz pulsed imaging and spectroscopy for biomedical and pharmaceutical applications. *Faraday Discuss* 2004; **126**: 255-263; discussion 303-311
10 **Withayachumnankul W**, Png GM, Yin X, Atakaramians S, Jones I, Lin H, Ung SY, Balakrishnan J, Ng BWH, Ferguson B, Mickan SP, Fischer BM, Abbott D. T-ray sensing and imaging. *Proc IEEE* 2007; **95**: 1528-1558
11 **Brown ER**, McIntosh KA, Nichols KB, Dennis CL. Photomixing up to 3.8 THz in low-temperature-grown GaAs. *Appl Phys Lett* 1995; **66**: 285-287
12 **Jeong YU**, Lee BC, Kim SK, Cho SO, Cha BH, Lee J, Kazakevitch GM, Vobly PD, Gavrilov NG, Kubarev VV, Kulipanov GN. First lasing of the KAERI compact far-infrared free-electron laser driven by a magnetron-based microtron. *Nucl Instr Meth* 2001; **475**: 47-50
13 **Smet JH**, Fonstad CG, Hu Q. Intrawell and interwell intersubband transitions in multiple quantum wells for far-infrared sources. *J Appl Phys* 1996; **79**: 9305-9320
14 **Baker C**, Gregory IS, Tribe WR, Evans MJ, Missous M, Linfield EH. Continuous-Wave Terahertz Photomixing in Low-Temperature InGaAs. Conference Digest of the 2004 Joint 29th International Conference on Infrared and Millimeter Waves, 2004 and 12th International Conference on Terahertz Electronics, 2004: 367-368
15 **Zhang XC**, Ma XF, Jin Y, Lu TM, Boden EP, Phelps PD, Stewart KR, Yakymyshyn CP. Terahertz optical rectification from a nonlinear organic crystal. *Appl Phys Lett* 1992; **61**: 3080-3082
16 **Huber R**, Tauser F, Brodschelm A, Bichler M, Abstreiter G, Leitenstorfer A. How many-particle interactions develop after ultrafast excitation of an electron-hole plasma. *Nature* 2001; **414**: 286-289
17 **Roskos HG**, Nuss MC, Shah J, Leo K, Miller DA, Fox AM, Schmitt-Rink S, Köhler K. Coherent submillimeter-wave emission from charge oscillations in a double-well potential. *Phys Rev Lett* 1992; **68**: 2216-2219
18 **McClatchey K**, Reiten MT, Cheville RA. Time resolved synthetic aperture terahertz impulse imaging. *Appl Phys Lett* 2001; **79**: 4485-4487
19 **Woolard DL**, Globus TR, Gelmont BL, Bykhovskaia M, Samuels AC, Cookmeyer D, Hesler JL, Crowe TW, Jensen JO, Jensen JL, Loerop WR. Submillimeter-wave phonon modes in DNA macromolecules. *Phys Rev E* 2002; **65**: 051903
20 **Globus T**, Bykhovskaia M, Woolard D, Gelmont B. Sub-millimetre wave absorption spectra of artificial RNA molecules. *J Phys D* 2003; **36**: 1314
21 **Pal SK**, Peon J, Zewail AH. Biological water at the protein surface: Dynamical solvation probed directly with femtosecond resolution. *Proc Natl Acad Sci USA* 2002; **99**: 1763-1768
22 **Bourne N**, Clothier RH, D'Arienzo M, Harrison P. The effects of terahertz radiation on human keratinocyte primary cultures and neural cell cultures. *Altern Lab Anim* 2008; **36**: 667-684
23 **Berry E**, Walker GC, Fitzgerald AJ, Zinov'ev NN, Chamberlain M, Smye SW, Miles RE, Smith MA. Do in vivo terahertz imaging systems comply with safety guidelines? *J Laser Appl* 2003; **15**: 192-198
24 **Zeni O**, Gallerano GP, Perrotta A, Romanò M, Sannino A, Sarti M, D'Arienzo M, Doria A, Giovenale E, Lai A, Messina G, Scarfì MR. Cytogenetic observations in human peripheral blood leukocytes following in vitro exposure to THz radiation: a pilot study. *Health Phys* 2007; **92**: 349-357
25 **Kawase K**, Ogawa Y, Watanabe Y, Inoue H. Non-destructive terahertz imaging of illicit drugs using spectral fingerprints. *Opt Express* 2003; **11**: 2549-2554
26 **Ning L**, Shen J, Jinhai S, Laishun L, Xu X, Lu M, Yan J. Study on the THz spectrum of methamphetamine. *Opt Express* 2005; **13**: 6750-6755
27 **Walker CK**, Kulesa CA. Terahertz Astronomy From The Coldest Place on Earth. The Joint 30th International Conference, 2005: 3-4
28 **Møller U**, Cooke DG, Tanaka K, Jepsen PU. Terahertz reflection spectroscopy of Debye relaxation in polar liquids. *J Opt Soc Am B* 2009; **26**: A113-A125
29 **Davies A**, Linfield E. Molecular and organic interactions. In: Miles RE, Zhang XC, Eisele H, Krotkus A, editors. Terahertz frequency detection and identification of materials and objects. The Netherlands: Springer, 2007: 91-106
30 **Hu BB**, Nuss MC. Imaging with terahertz waves. *Opt Lett* 1995; **20**: 1716
31 **Mittleman DM**, Hunsche S, Boivin L, Nuss MC. T-ray tomography. *Opt Lett* 1997; **22**: 904-906
32 **Pearce J**, Choi H, Mittleman DM, White J, Zimdars D. T-ray reflection computed tomography. *Opt Lett* 2005; **30**: 1653-1655
33 **Pearce J**, Choi H, Mittleman DM, White J, Zimdars D. Terahertz wide aperture reflection tomography. *Opt Lett* 2005; **30**: 1653-1655
34 **Wallace VP**, Macpherson E, Zeitler JA, Reid C. Three-dimensional imaging of optically opaque materials using nonionizing terahertz radiation. *J Opt Soc Am A Opt Image Sci Vis* 2008; **25**: 3120-3133
35 **Ferguson B**, Zhang XC. Materials for terahertz science and technology. *Nat Mater* 2002; **1**: 26-33
36 **Beard MC**, Turner GM, Schmuttenmaer CA. Subpicosecond carrier dynamics in low-temperature grown. GaAs as measured by time-resolved terahertz spectroscopy. *J Appl Phys* 2001; 90: 5915-5923
37 **Ho L**, Müller R, Römer M, Gordon KC, Heinämäki J, Kleinebudde P, Pepper M, Rades T, Shen YC, Strachan CJ, Taday PF, Zeitler JA. Analysis of sustained-release tablet film coats using terahertz pulsed imaging. *J Control Release* 2007; **119**: 253-261
38 **Strachan CJ**, Rades T, Newnham DA, Gordon KC, Pepper M, Taday PF. Using terahertz pulsed spectroscopy to study crystallinity of pharmaceutical materials. *Chem Phys Lett* 2004; **390**: 20-24
39 **Zeitler JA**, Newnham DA, Taday PF, Strachan CJ, Pepper M, Gordon KC, Rades T. Temperature dependent Terahertz Pulsed Spectroscopy of carbamazepine. *Thermochimica Acta* 2005; **436**: 71-77
40 **Zeitler JA**, Kogermann K, Rantanen J, Rades T, Taday PF, Pepper M, Aaltonen J, Strachan CJ. Drug hydrate systems and dehydration processes studied by terahertz pulsed spectroscopy. *Int J Pharm* 2007; **334**: 78-84
41 **Kindt JT**, Schmuttenmaer CA. Far-infrared dielectric properties of polar liquids probed by femtosecond terahertz pulse spectroscopy. *J Phys chem* 1996; **100**: 10373-10379
42 **Tielrooij KJ**, Timmer RL, Bakker HJ, Bonn M. Structure dynamics of the proton in liquid water probed with terahertz time-domain spectroscopy. *Phys Rev Lett* 2009; **102**: 198303
43 **Strachan CJ**, Taday PF, Newnham DA, Gordon KC, Zeitler JA, Pepper M, Rades T. Using terahertz pulsed spectroscopy to quantify pharmaceutical polymorphism and crystallinity. *J*

Pharm Sci 2005; **94**: 837-846
44 **Mittleman DM**, Nuss MC, Colvin VL. Terahertz spectroscopy of water in inverse micelles. *Chem Phys Lett* 1997; **275**: 332-338
45 **Walther M**, Fischer B, Schall M, Helm H, Jepsen PU. Far-infrared vibrational spectra of all-trans, 9-cis and 13-cis retinal measured by THz time-domain spectroscopy. *Chem Phys Lett* 2000; **332**: 389-395
46 **Fischer B**, Hoffmann M, Helm H, Wilk R, Rutz F, Kleine-Ostmann T, Koch M, Jepsen P. Terahertz time-domain spectroscopy and imaging of artificial RNA. *Opt Express* 2005; **13**: 5205-5215
47 **Fischer BM**, Helm H, Jepsen PU. Chemical recognition with broadband THz spectroscopy. *Proc IEEE* 2007; **95**: 1592-1604
48 **Woodward RM**, Wallace VP, Arnone DD, Linfield EH, Pepper M. Terahertz pulsed imaging of skin cancer in the time and frequency domain. *J Bio Phys* 2003; **29**: 257-259
49 **Grant EH**, Sheppard RJ, South GP. Dielectric behaviour of biological molecules in solution. Oxford: Clarendon Press, 1978
50 **Pethig R**. Protein-water interactions determined by dielectric methods. *Annu Rev Phys Chem* 1992; **43**: 177-205
51 **Sun Y**, Zhang Y, Pickwell-Macpherson E. Investigating antibody interactions with a polar liquid using terahertz pulsed spectroscopy. *Biophys J* 2011; **100**: 225-231
52 **Hartwick TS**, Hodges DT, Barker DH, Foote FB. Far infrared imagery. *Appl Opt* 1976; **15**: 1919-1922
53 **Siebert KJ**, Löffler T, Quast H, Thomson M, Bauer T, Leonhardt R, Czasch S, Roskos HG. All-optoelectronic continuous wave THz imaging for biomedical applications. *Phys Med Biol* 2002; **47**: 3743-3748
54 **Fitzgerald AJ**, Berry E, Zinov'ev NN, Homer-Vanniasinkam S, Miles RE, Chamberlain JM, Smith MA. Catalogue of human tissue optical properties at terahertz frequencies. *J Biol Phys* 2003; **29**: 123-128
55 **Löffler T**, Siebert K, Czasch S, Bauer T, Roskos HG. Visualization and classification in biomedical terahertz pulsed imaging. *Phys Med Biol* 2002; **47**: 3847
56 **Löffler T**, Bauer T, Siebert K, Roskos H, Fitzgerald A, Czasch S. Terahertz dark-field imaging of biomedical tissue. *Opt Express* 2001; **9**: 616-621
57 **Kan WC**, Lee WS, Cheung WH, Wallace VP, Pickwell-Macpherson E. Terahertz pulsed imaging of knee cartilage. *Biomed Opt Express* 2010; **1**: 967-974
58 **Knobloch P**, Schmalstieg K, Koch M, Rehberg E, Vauti F, Donhuijsen K. THz imaging of histo-pathological samples. *Proc SPIE* 2001; **4434**: 239-245
59 **Woodward RM**, Wallace VP, Pye RJ, Cole BE, Arnone DD, Linfield EH, Pepper M. Terahertz pulse imaging of ex vivo basal cell carcinoma. *J Invest Dermatol* 2003; **120**: 72-78
60 **Woodward RM**, Cole BE, Wallace VP, Pye RJ, Arnone DD, Linfield EH, Pepper M. Terahertz pulse imaging in reflection geometry of human skin cancer and skin tissue. *Phys Med Biol* 2002; **47**: 3853-3863
61 **Pickwell E**, Cole BE, Fitzgerald AJ, Pepper M, Wallace VP. In vivo study of human skin using pulsed terahertz radiation. *Phys Med Biol* 2004; **49**: 1595-1607
62 **Cole BE**, Woodward RM, Crawley D, Wallace VP, Arnone DD, Pepper M. Terahertz imaging and spectroscopy of human skin, in vivo. *Proc SPIE* 2001; **4276**: 1-10
63 **Huang SY**, Wang YX, Yeung DK, Ahuja AT, Zhang YT, Pickwell-Macpherson E. Tissue characterization using terahertz pulsed imaging in reflection geometry. *Phys Med Biol* 2009; **54**: 149-160
64 **Sun Y**, Fischer BM, Pickwell-MacPherson E. Effects of formalin fixing on the terahertz properties of biological tissues. *J Biomed Opt* 2009; **14**: 064017
65 **Fitzgerald AJ**, Wallace VP, Jimenez-Linan M, Bobrow L, Pye RJ, Purushotham AD, Arnone DD. Terahertz pulsed imaging of human breast tumors. *Radiology* 2006; **239**: 533-540
66 **Bolan PJ**, Meisamy S, Baker EH, Lin J, Emory T, Nelson M, Everson LI, Yee D, Garwood M. In vivo quantification of choline compounds in the breast with 1H MR spectroscopy. *Magn Reson Med* 2003; **50**: 1134-1143
67 **Boppart SA**, Luo W, Marks DL, Singletary KW. Optical coherence tomography: feasibility for basic research and image-guided surgery of breast cancer. *Breast Cancer Res Treat* 2004; **84**: 85-97
68 **Knobloch P**, Schildknecht C, Kleine-Ostmann T, Koch M, Hoffmann S, Hofmann M, Rehberg E, Sperling M, Donhuijsen K, Hein G, Pierz K. Medical THz imaging: an investigation of histo-pathological samples. *Phys Med Biol* 2002; **47**: 3875-3884
69 **Pickwell E**, Wallace VP, Cole BE, Ali S, Longbottom C, Lynch RJ, Pepper M. Using terahertz pulsed imaging to measure enamel demineralisation in teeth. Shanghai: Joint 31st International Conference on Infrared Millimeter Waves and 14th International Conference on Teraherz Electronics, 2006: 578
70 **MacPherson EP**. Biological applications of terahertz pulsed imaging and spectroscopy. Cambridge: Cambridge University Press, 2005
71 **Huang SY**, Macpherson E, Zhang YT. A feasibility study of burn wound depth assessment using terahertz pulsed imaging. Cambridge: 4th IEEE/EMBS International Summer School and Symposium on Medical Devices and Biosensors, 2007: 132-135
72 **Fitzgerald AJ**, Berry E, Zinovev NN, Walker GC, Smith MA, Chamberlain JM. An introduction to medical imaging with coherent terahertz frequency radiation. *Phys Med Biol* 2002; **47**: R67-R84
73 **Chen Y**, Huang S, Pickwell-MacPherson E. Frequency-Wavelet Domain Deconvolution for terahertz reflection imaging and spectroscopy. *Opt Express* 2010; **18**: 1177-1190
74 **Ferguson B**, Wang S, Gray D, Abbott D, Zhang XC. Towards functional 3D T-ray imaging. *Phys Med Biol* 2002; **47**: 3735-3742
75 **Woodward RM**, Wallace VP, Cole BE, Pye RJ, Arnone DD, Linfield EH, Pepper M. Terahertz pulse imaging in reflection geometry of skin tissue using time-domain analysis techniques. In: Cohn GE, Editor. Clinical Diagnostic Systems: Technologies and Instrumentation. San Jose, CA: SPIE, 2002: 160-169
76 **Chen HT**, Kersting R, Cho GC. Terahertz imaging with nanometer resolution. *Appl Phys Lett* 2003; **83**: 3009-3011
77 **Ülgen Y**, Sezdi M. Electrical parameters of human blood. Hong Kong: Proceedings of the IEEE/EMBS 20th Annual International Conference, 1998: 2983-2986

S- Editor Cheng JX **L- Editor** Webster JR **E- Editor** Zheng XM

World Journal of Radiology

Online Submissions: http://www.wjgnet.com/1949-8470office
wjr@wjgnet.com
doi:10.4329/wjr.v3.i3.66

World J Radiol 2011 March 28; 3(3): 66-69
ISSN 1949-8470 (online)

REVIEW

Applications of new irradiation modalities in patients with lymphoma: Promises and uncertainties

Youlia M Kirova, Cyrus Chargari

Youlia M Kirova, Cyrus Chargari, Department of Radiation Oncology, Institut Curie 26, rue d'Ulm, 75248 Paris, Cedex 05, France
Author contributions: Kirova YM designed the study; Kirova YM and Chargari C wrote the paper.
Correspondence to: Youlia M Kirova, MD, Department of Radiation Oncology, Institut Curie 26, rue d'Ulm, 75248 Paris, Cedex 05, France. youlia.kirova@curie.net
Telephone: +33-1-44324193 Fax: +33-1-53102653
Received: January 15, 2011 Revised: March 2, 2011
Accepted: March 9, 2011
Published online: March 28, 2011

Abstract

New highly conformal irradiation modalities have emerged for treatment of Hodgkin lymphoma. Helical Tomotherapy offers both intensity-modulated irradiation and accurate patient positioning and was shown to significantly decrease radiation doses to the critical organs. Here we review some of the most promising applications of helical tomotherapy in Hodgkin disease. By decreasing doses to the heart or the breast, helical tomotherapy might decrease the risk of long-term cardiac toxicity or secondary breast cancers, which are major concerns in patients receiving chest radiotherapy. Other strategies, such as debulking radiotherapy prior to stem cell transplantation or total lymphoid irradiation may be clinically relevant. However, helical tomotherapy may also increase the volume of tissues that receive lower doses, which has been implicated in the carcinogenesis process. Prospective assessments of these new irradiation modalities of helical tomotherapy are required to confirm the potential benefits of highly conformal therapies applied to hematological malignancies.

Key words: Hodgkin lymphoma; Helical tomotherapy; Cardiac toxicity; Secondary cancers

Peer reviewer: Ying Xiao, PhD, Professor, Director, Medical Physics, Department of Radiation Oncology, Thomas Jefferson University Hospital, Philadelphia, PA 19107-5097, United States

Kirova YM, Chargari C. Applications of new irradiation modalities in patients with lymphoma: Promises and uncertainties. *World J Radiol* 2011; 3(3): 66-69 Available from: URL: http://www.wjgnet.com/1949-8470/full/v3/i3/66.htm DOI: http://dx.doi.org/10.4329/wjr.v3.i3.66

INTRODUCTION

Radiation therapy still plays a major role in the management of hematological malignancies. Its place and modalities for treatment of lymphoma have evolved over recent decades. First, randomized studies supported reduction of field size and dose radiation in treatment programs for Hodgkin disease[1]. These developments were encouraged by reports that mediastinal radiotherapy was associated with cardiac toxicity and second malignancies, particularly when chemotherapy agents were used concomitantly or sequentially. Second, sophisticated imaging technologies and new radiation delivery techniques have become available[2]. With the recent advances in irradiation devices, new intensity modulated irradiation modalities have emerged. Those offer both increased target dose conformality and improved normal tissue avoidance. Helical tomotherapy combines inversely planned intensity modulated radiotherapy (IMRT) with on-board megavoltage imaging devices[3]. In this way, it has become possible to tailor very sharp dose distributions around the target volumes, close to critical organs[4]. It has emerged as one of the most promising techniques for IMRT delivery.

Here we summarize some of the most promising applications of helical tomotherapy in patients with hematological malignancies.

CLINICAL APPLICATIONS

For lymphoma irradiation, it is now the standard of care

to use involved-field radiotherapy rather than the extended radiation fields of the past[5]. In this setting of volume reduction, implementation of new strategies aimed at further improving target coverage is promising. Helical tomotherapy combines inversely planned IMRT with on-board megavoltage imaging devices[3]. In this way, it has become possible to tailor very sharp dose distributions around the target volumes, close to critical organs. Improving dose conformality around the volumes has become an important end-point for radiation oncologists. Dosimetric results from planning studies of helical tomotherapy have demonstrated its ability in better sparing critical organs from irradiation, in comparison with more conventional irradiation modalities. Helical tomotherapy was shown to provide similar target coverage, and to improve both dose conformality and dose homogeneity within the target volume. This modern irradiation device allows accurate repositioning and critical organs visualization. Tomita *et al*[6] compared radiation treatment plans that used IMRT with helical tomotherapy or three-dimensional conformal radiation therapy for nasal natural killer/T-cell lymphoma. Authors found that IMRT achieved significantly better coverage of the planning target volume (PTV), with more than 99% of the PTV receiving 90% of the prescribed dose, whereas 3D-CRT could not provide adequate coverage of the PTV, with only 90.0% receiving 90% ($P < 0.0001$). These results and others demonstrated that helical tomotherapy could significantly improve target coverage when the PTV was close to critical organs.

Prospective data with long-term follow-up evidenced that heart dose exposure may cause cardiac disease and adversely affect quality of life, particularly in young patients with mediastinal radiotherapy for Hodgkin lymphoma. Hudson *et al*[7] assessed the impact of treatment toxicity on long-term survival in pediatric Hodgkin's disease, and reported an excess mortality from cardiac disease in survivors of pediatric Hodgkin's disease (22, 95% CI: 8-48), compared with age- and sex-matched control populations. Cardiac irradiation contributes to this excess of risk[8]. Recent data reported that helical tomotherapy could decrease radiation dose exposure for breasts, lung, heart and thyroid gland in patients treated for advanced Hodgkin's disease[9].

Since radiation-induced cardiovascular pathology is a major concern in patients undergoing therapeutic chest irradiation, helical tomotherapy has been logically investigated for improving heart avoidance. The physiopathology and manifestations of radiation-induced heart disease may considerably vary according to the dose, volume and technique of irradiation, and every effort should be made to avoid irradiating cardiac structures[10]. In this way, it will be possible to substantially decrease the risk of death from ischemic heart disease associated with radiation, which is particularly significant in patients receiving other cardiotoxic agents, such as anthracyclines. Actually, helical tomotherapy also allows treatments that would be difficult for conventional radiotherapy machines to deliver, such as treating mediastinal lymph nodes[11]. Figure 1 shows the distribution dose during radiotherapy of a patient who was diagnosed with multiple pleural and mediastinal locations from lymphoma. Dose-volumes histograms evidence accurate sparing of some organs at risk, with the possibility to treat multiple targets simultaneously.

Several other promising applications for helical tomotherapy have emerged. These strategies include treatment of patients who are at high risk of radiation-induced toxicity because of individual susceptibility, such as patients with acquired immunodeficiency[12]. Helical tomotherapy could also be used for decreasing the doses to critical structures in patients treated with concurrent targeted agents, which might potentially increase the risk of side effects[13]. Moreover, it permits re-irradiation of relapsed disease, a setting that considerably increases the risk of consequent delayed toxicity. Introducing helical tomotherapy to the field of lymphoma may also provide safer and more accurate radiotherapy to selected patients with bulky residual disease[1]. We previously reported the feasibility of helical tomotherapy to decrease the acute toxicity of debulking irradiation before allograft in patients with refractory lymphoma. In other malignancies, our retrospective data in patients with solitary plasmocytoma demonstrated that doses to critical organs, including the heart, lungs, or kidneys could be decreased[14]. This may be clinically relevant in heavily pretreated patients who are at risk for subsequent treatment-related cardiac toxicity. High response rates were also reported and encouraged further prospective assessment, and most patients experienced a complete response prior to stem cell allograft.

An increased risk of secondary malignancies has been reported after radiotherapy for lymphoma. In particular, young patients have a high risk of developing breast cancer in their life after mediastinal radiotherapy for a lymphoma[15]. The improved outcome among patients with Hodgkin's lymphoma has been associated with increased incidence of second malignancies. This risk becomes significantly elevated 5 to 10 years after irradiation for Hodgkin lymphoma[16,17] and the incidence of breast cancer has been reported to increase by a factor of 4.3 (95% CI: 2.0-8.4) for patients treated with mantle irradiation[18]. Koh *et al*[19] quantified the reduction in radiation dose to normal tissues and modeled the reduction in secondary breast cancer risk, and suggested significant relative risk reduction for second cancers with involved field radiotherapy. While the dose response for radiation dose above 10 Gy remains uncertain, carcinogenesis after radiation is exacerbated by the large dose gradient across the breast and treatment field position[20]. Although helical tomotherapy might significantly decrease high doses delivered to the breast, it increases the volume that receives lower doses, which has also been implicated in the carcinogenesis process. For that reason, intensity-modulated irradiation should not be delivered in children outside of a clinical trial.

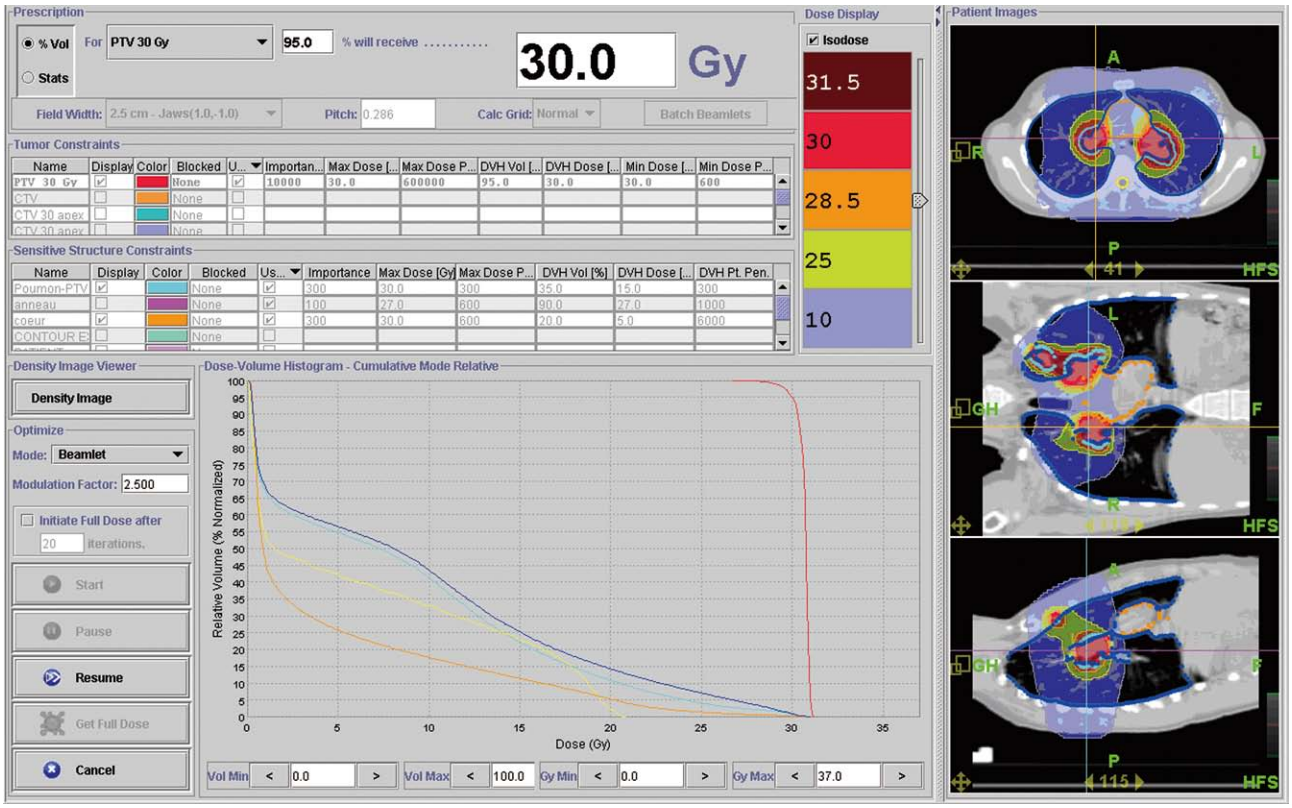

Figure 1 This figure shows the dose distribution during radiotherapy for the first patient who was diagnosed with multiple pleural and mediastinal tumors and also the dose-volumes histograms showing the sparing of some organs at risk (for example heart in orange with 5 Gy received by 20% of heart volume, in red planning target volume (planning treatment volume with homogeneous dose distribution and adequate coverage). Since irradiation to the bilateral hilum increases the risk of radiation pneumonitis, every effort was made to decrease the doses to the lung. Helical tomotherapy could be particularly useful in this setting. In this example, no more than 10% of the volume defined as the [lung - PTV] received 20 Gy.

Finally, preliminary results suggested that helical tomotherapy could be employed for total lymphoid irradiation in the preparative regimens for allogeneic bone marrow and chronic graft-versus-host disease. When using conventional irradiation devices, extended source-to-skin patient setup and/or field matching are required, and all critical organs are within the beam coverage. Treatment planning with helical tomotherapy for total lymphoid irradiation in adults demonstrated that the dose to the spinal cord, kidneys, intestinal compartment, and lungs could be decreased[21,22].

ALTERNATIVE IRRADIATION MODALITIES

We have pointed out the potential of helical tomotherapy in the light of our institutional experience. Actually, helical tomotherapy is not the only solution to improve both dose conformality and dose homogeneity within the target volume, and its availability remains rather limited (low number of helical tomotherapy devices). Other IMRT techniques could also be applied for delivering highly conformal irradiation. In 2005, Goodman *et al*[23] assessed the feasibility and potential advantages of linear accelerator based IMRT in the treatment of lymphoma involving large mediastinal disease volumes or requiring reirradiation. Compared to conventional parallel-opposed plans and conformal radiotherapy plans, IMRT could decrease the dose delivered to the lung by 12% and 14%, respectively. The PTV coverage was also improved, compared with conventional RT[23]. Recent dosimetric data demonstrated that the forward planned IMRT technique could be easily used for improving PTV conformity while sparing normal tissue in Hodgkin's lymphoma[24].

Volumetric modulated arc therapy (VMAT) has also demonstrated its ability in tailoring accurate dose distributions around the target volumes. Weber *et al*[25] compared VMAT to conventional fixed beam IMRT in ten patients with early Hodgkin disease. They found no difference in levels of dose homogeneity. However, for involved node radiotherapy, doses to the PTV and OAR were higher and lower with VMAT when compared to IMRT, respectively.

Finally, the dosimetric advantages of proton therapy could also be used for reducing the risk of late radiation-induced toxicity related to low-to-moderate doses in critical organs. Chera *et al*[26] compared the dose distribution in Hodgkin's lymphoma patients using conventional radiotherapy, IMRT, and 3D proton therapy in Hodgkin's lymphoma patients with stage II disease. Authors found that 3D proton therapy could reduce the dose to the breast, lung, and total body. However, the availability of

proton therapy is very low and only a few patients could benefit from this highly conformal irradiation modality.

CONCLUSION

There is growing dosimetric evidence that highly conformal irradiation modalities may improve critical organs sparing, with clinically relevant consequences. Prospective clinical evaluation of helical tomotherapy modalities is required to confirm the potential benefits of highly conformal therapies applied to hematological malignancies.

REFERENCES

1 **Yahalom J**. Transformation in the use of radiation therapy of Hodgkin lymphoma: new concepts and indications lead to modern field design and are assisted by PET imaging and intensity modulated radiation therapy (IMRT). *Eur J Haematol Suppl* 2005; 90-97
2 **Girinsky T**, Ghalibafian M. Radiotherapy of hodgkin lymphoma: indications, new fields, and techniques. *Semin Radiat Oncol* 2007; **17**: 206-222
3 **Welsh JS**, Patel RR, Ritter MA, Harari PM, Mackie TR, Mehta MP. Helical tomotherapy: an innovative technology and approach to radiation therapy. *Technol Cancer Res Treat* 2002; **1**: 311-316
4 **Beavis AW**. Is tomotherapy the future of IMRT? *Br J Radiol* 2004; **77**: 285-295
5 **Fermé C**, Eghbali H, Meerwaldt JH, Rieux C, Bosq J, Berger F, Girinsky T, Brice P, van't Veer MB, Walewski JA, Lederlin P, Tirelli U, Carde P, Van den Neste E, Gyan E, Monconduit M, Diviné M, Raemaekers JM, Salles G, Noordijk EM, Creemers GJ, Gabarre J, Hagenbeek A, Reman O, Blanc M, Thomas J, Vié B, Kluin-Nelemans JC, Viseu F, Baars JW, Poortmans P, Lugtenburg PJ, Carrie C, Jaubert J, Henry-Amar M. Chemotherapy plus involved-field radiation in early-stage Hodgkin's disease. *N Engl J Med* 2007; **357**: 1916-1927
6 **Tomita N**, Kodaira T, Tachibana H, Nakamura T, Nakahara R, Inokuchi H, Mizoguchi N, Takada A. A comparison of radiation treatment plans using IMRT with helical tomotherapy and 3D conformal radiotherapy for nasal natural killer/T-cell lymphoma. *Br J Radiol* 2009; **82**: 756-763
7 **Hudson MM**, Poquette CA, Lee J, Greenwald CA, Shah A, Luo X, Thompson EI, Wilimas JA, Kun LE, Crist WM. Increased mortality after successful treatment for Hodgkin's disease. *J Clin Oncol* 1998; **16**: 3592-3600
8 **Prosnitz RG**, Chen YH, Marks LB. Cardiac toxicity following thoracic radiation. *Semin Oncol* 2005; **32**: S71-S80
9 **Vlachaki MT**, Kumar S. Helical tomotherapy in the radiotherapy treatment of Hodgkin's disease - a feasibility study. *J Appl Clin Med Phys* 2010; **11**: 3042
10 **Gagliardi G**, Constine LS, Moiseenko V, Correa C, Pierce LJ, Allen AM, Marks LB. Radiation dose-volume effects in the heart. *Int J Radiat Oncol Biol Phys* 2010; **76**: S77-S85
11 **Chargari C**, Vernant JP, Tamburini J, Zefkili S, Fayolle M, Campana F, Fourquet A, Kirova YM. Feasibility of Helical Tomotherapy for Debulking Irradiation Before Stem Cell Transplantation in Malignant Lymphoma. *Int J Radiat Oncol Biol Phys* 2010; Epub ahead of print
12 **Chargari C**, Zefkili S, Kirova YM. Potential of helical tomotherapy for sparing critical organs in a patient with AIDS who was treated for Hodgkin lymphoma. *Clin Infect Dis* 2009; **48**: 687-689
13 **Kirova YM**, Chargari C, Amessis M, Vernant JP, Dhedin N. Concurrent involved field radiation therapy and temsirolimus in refractory mantle cell lymphoma (MCL). *Am J Hematol* 2010; **85**: 892
14 **Chargari C**, Kirova YM, Zefkili S, Caussa L, Amessis M, Dendale R, Campana F, Fourquet A. Solitary plasmocytoma: improvement in critical organs sparing by means of helical tomotherapy. *Eur J Haematol* 2009; **83**: 66-71
15 **Henderson TO**, Amsterdam A, Bhatia S, Hudson MM, Meadows AT, Neglia JP, Diller LR, Constine LS, Smith RA, Mahoney MC, Morris EA, Montgomery LL, Landier W, Smith SM, Robison LL, Oeffinger KC. Systematic review: surveillance for breast cancer in women treated with chest radiation for childhood, adolescent, or young adult cancer. *Ann Intern Med* 2010; **152**: 444-455; W144-W154
16 **Alm El-Din MA**, El-Badawy SA, Taghian AG. Breast cancer after treatment of Hodgkin's lymphoma: general review. *Int J Radiat Oncol Biol Phys* 2008; **72**: 1291-1297
17 **Metayer C**, Lynch CF, Clarke EA, Glimelius B, Storm H, Pukkala E, Joensuu T, van Leeuwen FE, van't Veer MB, Curtis RE, Holowaty EJ, Andersson M, Wiklund T, Gospodarowicz M, Travis LB. Second cancers among long-term survivors of Hodgkin's disease diagnosed in childhood and adolescence. *J Clin Oncol* 2000; **18**: 2435-2443
18 **Zellmer DL**, Wilson JF, Janjan NA. Dosimetry of the breast for determining carcinogenic risk in mantle irradiation. *Int J Radiat Oncol Biol Phys* 1991; **21**: 1343-1351
19 **Koh ES**, Tran TH, Heydarian M, Sachs RK, Tsang RW, Brenner DJ, Pintilie M, Xu T, Chung J, Paul N, Hodgson DC. A comparison of mantle versus involved-field radiotherapy for Hodgkin's lymphoma: reduction in normal tissue dose and second cancer risk. *Radiat Oncol* 2007; **2**: 13
20 **Hodgson DC**, Koh ES, Tran TH, Heydarian M, Tsang R, Pintilie M, Xu T, Huang L, Sachs RK, Brenner DJ. Individualized estimates of second cancer risks after contemporary radiation therapy for Hodgkin lymphoma. *Cancer* 2007; **110**: 2576-2586
21 **McCutchen KW**, Watkins JM, Eberts P, Terwilliger LE, Ashenafi MS, Jenrette JM 3rd. Helical tomotherapy for total lymphoid irradiation. *Radiat Med* 2008; **26**: 622-626
22 **Wong JY**, Liu A, Schultheiss T, Popplewell L, Stein A, Rosenthal J, Essensten M, Forman S, Somlo G. Targeted total marrow irradiation using three-dimensional image-guided tomographic intensity-modulated radiation therapy: an alternative to standard total body irradiation. *Biol Blood Marrow Transplant* 2006; **12**: 306-315
23 **Goodman KA**, Toner S, Hunt M, Wu EJ, Yahalom J. Intensity-modulated radiotherapy for lymphoma involving the mediastinum. *Int J Radiat Oncol Biol Phys* 2005; **62**: 198-206
24 **Cella L**, Liuzzi R, Magliulo M, Conson M, Camera L, Salvatore M, Pacelli R. Radiotherapy of large target volumes in Hodgkin's lymphoma: normal tissue sparing capability of forward IMRT versus conventional techniques. *Radiat Oncol* 2010; **5**: 33
25 **Weber DC**, Peguret N, Dipasquale G, Cozzi L. Involved-node and involved-field volumetric modulated arc vs. fixed beam intensity-modulated radiotherapy for female patients with early-stage supra-diaphragmatic Hodgkin lymphoma: a comparative planning study. *Int J Radiat Oncol Biol Phys* 2009; **75**: 1578-1586
26 **Chera BS**, Rodriguez C, Morris CG, Louis D, Yeung D, Li Z, Mendenhall NP. Dosimetric comparison of three different involved nodal irradiation techniques for stage II Hodgkin's lymphoma patients: conventional radiotherapy, intensity-modulated radiotherapy, and three-dimensional proton radiotherapy. *Int J Radiat Oncol Biol Phys* 2009; **75**: 1173-1180

S- Editor Cheng JX **L- Editor** O'Neill M **E- Editor** Zheng XM

World Journal of Radiology

Online Submissions: http://www.wjgnet.com/1949-8470office
wjr@wjgnet.com
doi:10.4329/wjr.v3.i3.70

World J Radiol 2011 March 28; 3(3): 70-81
ISSN 1949-8470 (online)

ORIGINAL ARTICLE

Estimation of intra-operator variability in perfusion parameter measurements using DCE-US

Marianne Gauthier, Ingrid Leguerney, Jessie Thalmensi, Mohamed Chebil, Sarah Parisot, Pierre Peronneau, Alain Roche, Nathalie Lassau

Marianne Gauthier, Ingrid Leguerney, Jessie Thalmensi, Sarah Parisot, Pierre Peronneau, Alain Roche, Nathalie Lassau, IR4M, UMR 8081, CNRS, Paris-Sud 11 Univ, Gustave Roussy Institute, Villejuif 94805, France
Mohamed Chebil, Nathalie Lassau, Department of Imaging, Ultrasonography Unit, Gustave Roussy Institute, Villejuif 94805, France
Author contributions: Gauthier M performed the majority of experiments, designed the study and wrote the manuscript; Leguerney I was involved in analyzing results and editing the manuscript; Thalmensi J, Parisot S and Peronneau P provided substantial contributions to conception and design, acquisition of data, analysis, and interpretation of the data; Chebil M was involved in the design of the study; Roche A supervised the project; Lassau N managed each step of the study, provided contribution to data analyses and was involved in editing the manuscript.
Correspondence to: Marianne Gauthier, MSc, IR4M, UMR 8081, CNRS, Paris-Sud 11 Univ, Gustave Roussy Institute, Villejuif 94805, France. marianne.gauthier@igr.fr
Telephone: +33-1-42116215 Fax: +33-1-42115495
Received: December 24, 2010 Revised: March 2, 2011
Accepted: March 9, 2011
Published online: March 28, 2011

Abstract

AIM: To investigate intra-operator variability of semi-quantitative perfusion parameters using dynamic contrast-enhanced ultrasonography (DCE-US), following bolus injections of SonoVue®.

METHODS: The *in vitro* experiments were conducted using three in-house sets up based on pumping a fluid through a phantom placed in a water tank. In the *in vivo* experiments, B16F10 melanoma cells were xenografted to five nude mice. Both *in vitro* and *in vivo*, images were acquired following bolus injections of the ultrasound contrast agent SonoVue® (Bracco, Milan, Italy) and using a Toshiba Aplio® ultrasound scanner connected to a 2.9-5.8 MHz linear transducer (PZT, PLT 604AT probe) (Toshiba, Japan) allowing harmonic imaging ("Vascular Recognition Imaging") involving linear raw data. A mathematical model based on the dye-dilution theory was developed by the Gustave Roussy Institute, Villejuif, France and used to evaluate seven perfusion parameters from time-intensity curves. Intra-operator variability analyses were based on determining perfusion parameter coefficients of variation (CV).

RESULTS: *In vitro*, different volumes of SonoVue® were tested with the three phantoms: intra-operator variability was found to range from 2.33% to 23.72%. *In vivo*, experiments were performed on tumor tissues and perfusion parameters exhibited values ranging from 1.48% to 29.97%. In addition, the area under the curve (AUC) and the area under the wash-out (AUWO) were two of the parameters of great interest since throughout *in vitro* and *in vivo* experiments their variability was lower than 15.79%.

CONCLUSION: AUC and AUWO appear to be the most reliable parameters for assessing tumor perfusion using DCE-US as they exhibited the lowest CV values.

Key words: Dynamic contrast-enhanced ultrasonography; Intra-operator variability; Functional imaging; Semi-quantitative perfusion parameters; Linear raw data; Quantification

Peer reviewers: Chan Kyo Kim, MD, Assistant Professor, Department of Radiology, Samsung Medical Center, Sungkyunkwan University School of Medicine, 50 Ilwon-dong, Kangnam-gu, Seoul 135-710, South Korea; Sergio Casciaro, PhD, Institute of Clinical Physiology - National Research Council,Campus Universitario Ecotekne, Via Monteroni, 73100 Lecce, Italy

Gauthier M, Leguerney I, Thalmensi J, Chebil M, Parisot S, Peronneau P, Roche A, Lassau N. Estimation of intra-operator variability in perfusion parameter measurements using DCE-

US. *World J Radiol* 2011; 3(3): 70-81 Available from: URL: http://www.wjgnet.com/1949-8470/full/v3/i3/70.htm DOI: http://dx.doi.org/10.4329/wjr.v3.i3.70

INTRODUCTION

Tumor angiogenesis is a process involving the proliferation of new blood vessels which penetrate tumors supplying them with nutrients and oxygen[1,2]. Nowadays, research is focused on the development of anti-angiogenic treatments whose aim is to destroy neoblood vessels which often occur initially without any morphological changes[3,4].

Until now, treatment evaluation has been based on Response Evaluation Criteria in Solid Tumors (RECIST)[5]. Even though RECIST criteria were recently revised, they still only concern morphological information[6]. It is commonly recognized that this criterion is no longer optimal for the early assessment of anti-angiogenic treatments which primarily target microvascularization. Functional imaging is currently establishing itself as the best modality for evaluating such therapies, by determining a series of semi-quantitative perfusion parameters related to tumor perfusion. These were defined as semi-quantitative as they only provided a relative evaluation of the physiological parameters such as blood flow or blood volume based on the dye dilution theory.

Nowadays, dynamic contrast-enhanced ultrasonography (DCE-US) is becoming increasingly widespread[7,8] as it allows functional imaging[9,10]. However, one of its major drawbacks is its intra-operator variability which could have a major impact on measurements, leading to erroneous interpretations. A small difference in perfusion could be interpreted as a functional change but might simply be due to operator variability.

Until now, information on intra-operator variability has been lacking. Consequently, the purpose of our study was to evaluate the intra-operator variability of semi-quantitative perfusion parameter measurements using DCE-US, both *in vitro* and *in vivo*, following bolus injections of SonoVue® (Bracco, Milan, Italy).

MATERIALS AND METHODS

Contrast agents

DCE-US studies were performed using bolus injections of SonoVue®, a second generation contrast agent, consisting of microbubbles of sulphur hexafluoride (SF_6) stabilized by a shell of amphiphilic phospholipids[11,12]. The SF_6 gas does not interact with any other molecules found in the body as it is a very inert gas. The size of the microbubbles, ranging from 1 to 10 μm[12], allows them to circulate through the whole blood volume. In addition, SonoVue® is a purely intravascular contrast agent which makes it ideal for the evaluation of perfusion[12]. Insonated at low acoustic power, SonoVue®, whose nonlinear harmonic response is high[13], provides continuous real-time ultrasonographic (US) imaging without destroying the microbubbles[14].

Before any US exam, the contrast agent was reconstituted by introducing 5 mL of 0.9% sodium chloride into the vial, containing a pyrogen-free lyophilized product, followed by manual shaking for at least 20 s. One experiment involved several injections of SonoVue®. As the microbubbles tended to accumulate at the upper surface because of buoyancy, the preparation was systematically manually checked before each injection in order to recover the required homogeneous solution. Each experiment lasted less than 2 h on account of the stability of SonoVue® over time which is 6 h after its reconstitution[11].

Time-intensity method

The time intensity method is essentially based on the dye dilution theory: after the injection of the indicators, contrast agent concentration is monitored as a function of time, generating a time intensity curve (TIC) from which a series of semi-quantitative perfusion parameters is extracted and analyzed[15,16]. To be valid, a series of assumptions must be verified[17]: (1) Flow has to be constant so that the amount of microbubbles injected has no effect on the flux; (2) Blood and contrast agent must be adequately mixed to obtain a homogeneous concentration; (3) Recirculation should not interfere with the first pass; and (4) The mixing of the contrast agent must exhibit linearity and a stable condition[18]. Linearity refers to the linear relationship between bubble concentration and signal intensity and was previously confirmed for low doses by Greis[12] as well as by Lampaskis *et al*[19] in the context of bolus injection.

In our study, conditions were assumed to be satisfied. The semi-quantitative perfusion parameters that we analyzed were therefore directly extracted from the TIC.

In vitro studies

US protocol: SonoVue® bolus injections were performed through a 1-mL syringe (Terumo®, Belgium) and a "26Gx1/2" needle (Terumo®, Belgium). The injection site was marked so that the same site was used for all the *in vitro* studies. It was positioned at a distance of 30 cm from the input of the phantom.

According to the Guidelines for Evaluating and Expressing the Uncertainty of NIST (National Institute of Standards and Technology) Measurements Results, intra-operator variability studies must be performed under the following conditions: (1) The same measurement procedure; (2) The same observer; (3) The same measuring instrument, used under the same conditions; (4) The same location; and (5) Repetition over a short period of time.

Thus, all the experimental conditions as well as the operators injecting the SonoVue® and manipulating the ultrasound scanner were the same for all acquisitions.

To minimize errors which might have been due to possible SonoVue® residues in the injection materials, a new syringe and a new needle were used for each injection. In addition, the circuit was entirely emptied, rinsed

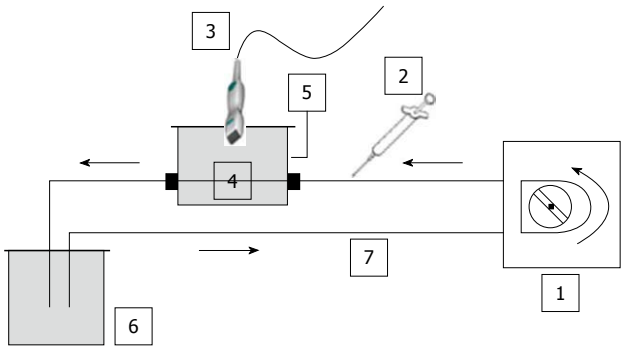

Figure 1 Schematic diagram of the closed-circuit. No contact with ambient air was possible. In addition, as water was degassed, no significant amount of gas was trapped in the circuit. Based on the same set-up, three phantoms were used throughout the *in vitro* experiments: (a) a single straight pipe phantom; (b) a three intertwined pipe phantom; (c) a dialyzer. The Gustave Roussy Institute (IGR) ratio was tested throughout the *in vitro* experiments as it corresponded to the ratio (4.8 mL per patient) previously validated and routinely used at the IGR. 1: Peristaltic pump; 2: Syringe; 3: PZT, PLT 604AT probe; 4: Phantom; 5: Custom-made water tank; 6: Reservoir; 7: Tubing (silicone pipe; internal diameter: 2 mm; wall thickness: 1 mm).

and reset with degassed water between each acquisition. Thus, no contrast agent residues were present in the circuit so that the initial conditions were exactly the same for all the experiments.

The three phantoms consisted of a closed-circuit flow model as no contact with ambient air was possible. Consequently, as the water was degassed and the circuit was closed, no significant amount of gas was trapped in the set-up (Figure 1).

Images were acquired using a Toshiba Aplio® ultrasound scanner (Toshiba, Japan) version 6, release 5, connected to a 2.9-5.8 MHz linear transducer (PZT, PLT 604AT probe). Harmonic imaging was performed using the "Vascular Recognition Imaging" (VRI) mode combining: (1) Fundamental B mode imaging, which allows simultaneous but independent grey scale visualization of morphological structures; (2) Doppler imaging, which provides vascular information; and (3) Harmonic imaging, based on the pulse inversion mode, which consists of summing echoes resulting from two waves which are inverted copies of each other. As microbubbles exhibit non-linear responses, the resulting sum of the echoes will be different from 0 implying a non-null signal[20].

Acquisitions lasting 50 s were obtained at a low mechanical index (MI = 0.1) and at a rate of 5 frames per second (fps).

Single straight pipe phantom: The first assembly consisted of a single straight silicone pipe phantom, immersed in a custom-made water tank which was connected to a peristaltic pump (SP vario/PD 5101, Heidolph®, Germany) providing a defined water flow rate of 42.4 mL/min. This phantom was used to mimic blood flow. Tubing was made of a 1 mm thick silicone pipe with a 2 mm internal diameter. A custom-made probe holder was used to keep the probe still throughout the experiments.

A region of interest (ROI) was set in the upper part

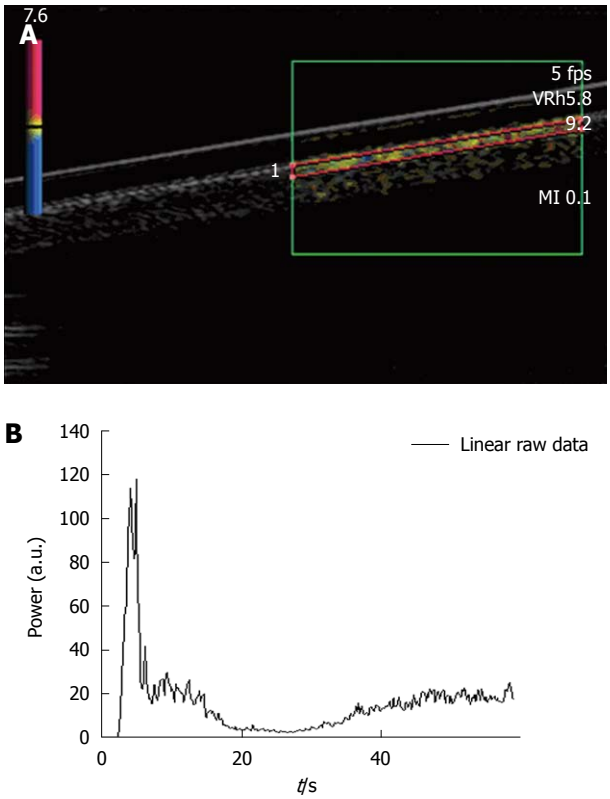

Figure 2 Single straight pipe phantom. A: Image extracted from an acquisition obtained after the bolus injection of SonoVue®. Harmonic imaging was done based on the Vascular Recognition Imaging mode. The region of interest was set in the upper part of the pipe. Each acquisition involved a new manually drawn region of interest. Once the region of interest was selected, the ultrasound scanner directly allowed access to the time intensity curve associated with the selected region of interest. The linear raw data to be modeled were converted through text files generated by the ultrasound scanner and extracted to obtain a graph using Excel®; B: The graph displays the Excel® curve to be fitted and analyzed in order to obtain the perfusion parameters.

of the pipe (Figure 2A). Each injection involved a new ROI and its associated TIC (Figure 2B). Three volumes of SonoVue® were tested. The first experiment involved five 0.02 mL bolus injections of contrast agent for a total amount of water set at 50 mL in the closed-circuit. This ratio respected that granted by marketing approval ("Autorisation de Mise sur le Marché": AMM) (2.4 mL of SonoVue® for 5 L of blood). The second experiment was performed by injecting five times a 0.05 mL bolus of SonoVue®. This volume involved a ratio routinely used for clinical exams (4.8 mL of SonoVue® for 5 L of blood) and particularly in four studies performed at the Gustave Roussy Institute (IGR), involving 117 patients and 823 DCE-US exams[21,22] as well as a national project supported by the "Institut National du Cancer" (French National Cancer Institute)[23]. The last experiment involved five 0.08 mL bolus injections of SonoVue®. As the phantom became more complex, we focused on the IGR ratio previously validated in IGR studies.

Three intertwined pipe phantom: A second phantom consisted of three intertwined silicone pipes immersed in a custom-made water tank. Two of the three tubes were

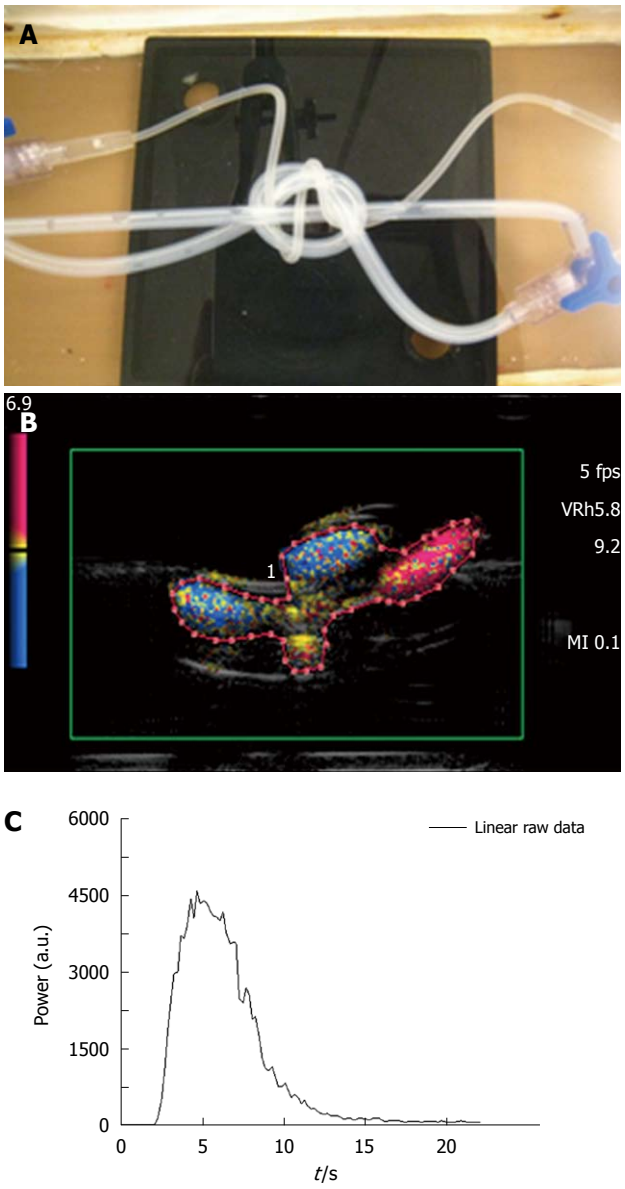

Figure 3 Three intertwined pipe phantom. A: Picture of the phantom: three pipes (2 pipes with a 2 mm internal diameter and a 1 mm thick wall, 1 pipe with a 1 mm internal diameter and a 0.5 mm thick wall) were intertwined to mimic a complex structure akin to that of vessels in the microvascularization; B: Image extracted from an acquisition obtained after a bolus injection of SonoVue®. As in the case of the first phantom, harmonic imaging was based on the Vascular Recognition Imaging mode. The region of interest contained both pipes and water and was manually drawn for each of the five injections; C: Based on the selected region of interest, the ultrasound scanner provided the time intensity curve converted through text files. These were used to display the associated Excel® curve to be analyzed.

in silicone with an internal diameter of 2 mm and a 1 mm thick wall as in the case of the previous phantom. The third one, originating from a catheter (Surflo® winged infusion set, Terumo®, Belgium), had a 1 mm internal diameter and a 0.5 mm thick wall. The input and the output of the phantom were composed of three-way taps (Discofix®, B. Braun, Melsungen, Germany) allowing linkage between the three pipes (Figure 3A). The phantom was connected to the same pump as previously described, providing a defined water flow rate set at 42.4 mL/min. Such an assembly was designed to mimic a complex structure akin to that of vessels in tumors.

A new ROI containing both pipes and water spaces (Figure 3B), was drawn for each injection and the associated TIC was obtained (Figure 3C). The total amount of water in the circuit was set at 60 mL. Two series of acquisitions were obtained involving, respectively, five 0.03 mL (AMM ratio) and 0.06 mL (IGR ratio) bolus injections of contrast agent.

Dialyzer: The third assembly was composed of a dialyzer (FX PAED, Fresenius Medical Care, France). The dialysis cartridge, consisting of about 1550 capillaries with an internal diameter of 220 μm, was connected to the peristaltic pump providing a water flow rate of 42.4 mL/min and was immersed in water. To minimize attenuation due to the original plastic case of the dialyzer, a rectangular part of it was removed and replaced by a cellophane sheet to maintain the circuit closed[24]. The advantage of such a phantom was that the capillaries of the dialyzer were comparable in dimension to that of one type of vessel found in the microvascularization (arteriole diameter < 300 μm). In addition, as the size of SonoVue® microbubbles ranged from 1 to 10 μm[12], they were about a thousand-fold the dimensions of capillary pores (2.4 nm), thus ensuring the intravascular property of the ultrasound contrast agent.

As shown in Figure 4A, attenuation occurs in the lower part of the dialyzer: it is characterized by a strong decrease in amplitude and a loss of the contrast signal. An ROI was drawn for each of the repeated measurements and only contained the upper part of the dialyzer so that the acquisition was not prone to attenuation phenomena[25]. Based on the selected ROI, the associated time intensity curve was obtained for the analysis (Figure 4B). The total amount of water was 100 mL and a volume of 0.10 mL of SonoVue® was tested five times (IGR ratio).

In vivo studies

Animals and tumor model: Experiments were conducted with nude female mice aged from 6 to 8 wk with the approval of the European Convention for the Protection of Vertebrate Animals used for experimental and other scientific purposes (Strasbourg, 18.III.1986; text amended according to the provisions of protocol ETS No. 170 as of its entry into force on 2nd December 2005).

The selected tumor model was the B16F10 (CRL-6475, ATCC, American Type Culture Collection) melanoma cell line which is a murine skin cancer. The tumor cells were cultured in DMEM (Dulbecco minimum essential medium) (Gibco Life Technologies, France) combined with 10% fetal bovine serum, 1% penicillin/streptomycin and glutamate (Invitrogen Life Technologies, Inc., France) to avoid bacterial contamination of the solution. While growing, cells were maintained in an incubator at 37℃. Tumors were xenografted onto the right flank of five mice (Figure 5A) through a subcutaneous injection of 2 × 10^6 melanoma cells in 0.2 mL of Phosphate Buffered Saline (PBS). DCE-US exams were performed following three 0.02 mL, 0.05 mL or 0.1 mL retro-orbital bolus

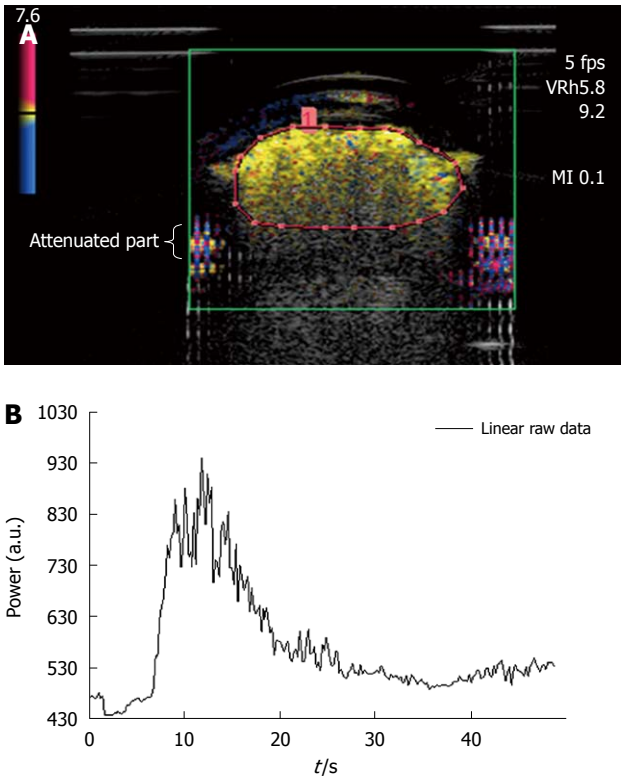

Figure 4 Dialyzer. A: Image extracted from an acquisition obtained after a bolus injection of SonoVue®. As in the case of the first two phantoms, harmonic imaging was based on the Vascular Recognition Imaging mode. The region of interest contained the upper part of the dialyzer to avoid attenuation phenomena in the lower parts. This was manually drawn for each injection; B: To determine perfusion parameters from the time intensity curve obtained following the selection of the region of interest, this was converted through text files so that the analysis could be performed using the Solver program in Excel®.

injections of SonoVue® according to the methodology used in our lab.

Settings: During the experiments, mice were placed on the left flank and maintained at a constant temperature through a warming pad (TEM, Bordeaux, France) connected to a Gaymar T/Pump® (Gaymar Industries, Inc., USA). The temperature was regulated with the adjustable thermostat of the pump and was set at 40°C (internal mouse temperature: 39°C). Each mouse was weighed and the tumor volume was determined before each DCE-US exam. The ROI was set to exclusively include the tumor (Figure 5B-C). An ROI was drawn for each of the repeated measurements and once it was selected, the ultrasound scanner directly allowed access to the time intensity curve associated with the selected ROI. The linear raw data to be modeled were converted through text files and extracted to obtain a graph using Excel® (Figure 5D).

A break of at least 15 min was observed between each injection in addition to 3 min of insonation at a high mechanical index (MI = 1.4), so that contrast agent could be eliminated. Mice were kept asleep no more than 2 h. This duration included the time required for the mice to obtain a stationary heart rate after the administration of anesthesia, acquisition time and the duration of the break between each injection. Three injections per mouse were considered for the data analysis. Mice underwent either chemical or gaseous anesthesia.

Chemical anesthesia: The amount of chemical anesthesia was determined based upon mouse body weight. Once weighed, the required amount of anesthesia was prepared and injected intraperitoneally using the 1-mL syringe and a "30Gx1/2" needle (Microlance™, Ireland). The solution consisted of ketamine (10 mg/mL, Ketalar®, Parapharm, France) and xylazine (2%, Rompun®, Bayer, France). To ensure that the mice remained asleep throughout the experiment, 150 μL/g per mouse were systematically injected.

Gaseous anesthesia: Mice were anaesthetized through a 2 L/min inhalation of O_2 combined with 2.5% of isoflurane. It was possible to modify the flow rate during the experiment so that mice could be maintained asleep without being endangered throughout the experiment.

US protocol: Preliminary fundamental B-mode imaging using a 14 MHz PLT 1204AT (Toshiba, Japan) probe was performed to determine the tumor volume prior to the SonoVue® injection (Figure 5B). The largest longitudinal and transversal sections allowed us to determine the tumor volume by measuring the three perpendicular tumor diameters[26] according to the following formula: $V = 1/2 \times (\text{depth} \times \text{width} \times \text{length})$.

Harmonic imaging was performed in the same way as for the *in vitro* experiments with a mechanical index set at 0.1 and a rate of 5 fps. Acquisitions lasting 3 min were recorded allowing visualization of both the wash-in and wash-out parts of the TICs.

Data analysis

As already described in the literature, linear raw data (uncompressed linear data obtained before standard video-visualization) have the advantage of exhibiting a linear dynamic range which is the essential part of the evaluation of semi-quantitative perfusion parameters from TICs[27]. Acquisitions involved recording harmonic images after the SonoVue® injection, using dedicated software, CHI-Q®, on the Toshiba Aplio® ultrasound scanner. In a manually outlined ROI, the mean US signal intensity induced by contrast uptake was obtained and expressed in arbitrary units. This was linearly linked to the number and size of microbubbles in the ROI (Aplio® procedure)[28,29]. Then, the corresponding TIC to be modeled was converted through text files generated by the ultrasound scanner and extracted to obtain a graph using Excel®. Seven semi-quantitative perfusion parameters were extracted from this curve: the peak intensity (PI) was the difference between V_{max} [maximal intensity value: $V(T_{max})$] and V_0 [Initial intensity value: $V(T_0)$] and represented the highest intensity value attained by the TIC for the defined ROI. The time to peak intensity (T_{PI}), corresponding to Time to Peak Intensity, was the time required for the contrast agent to arrive in the tumor and reach the PI. It

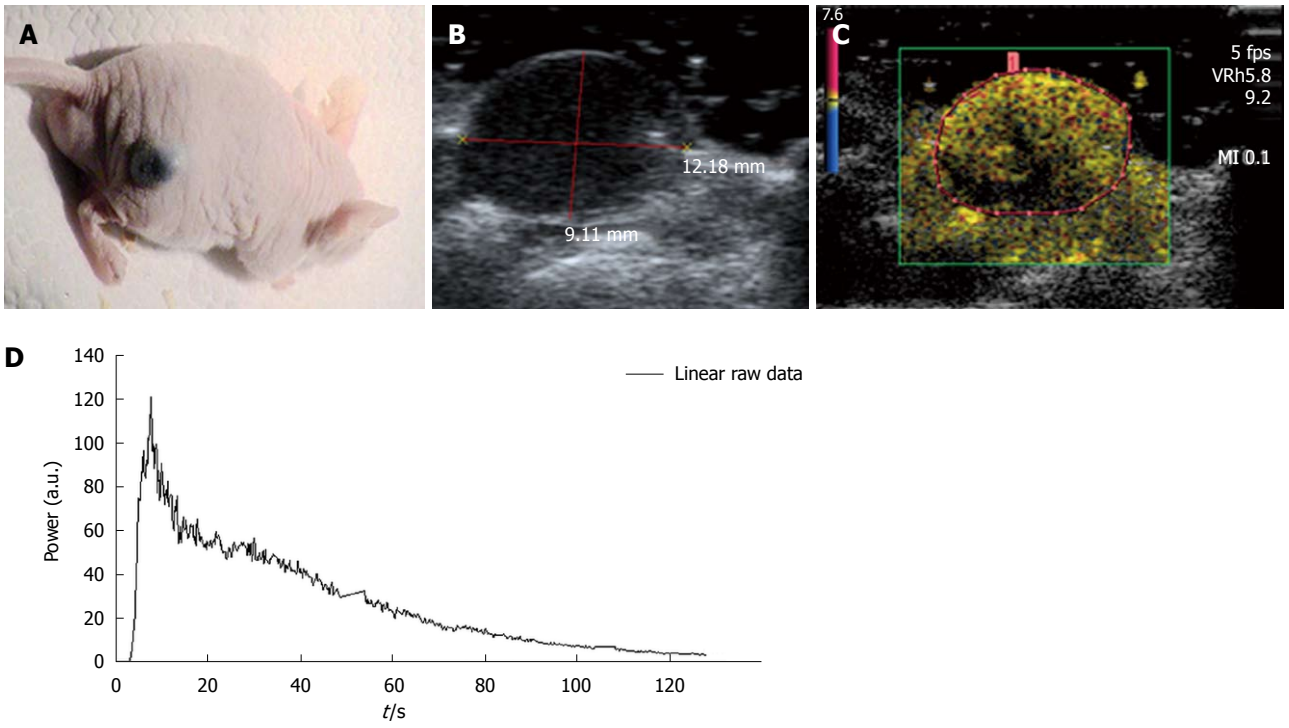

Figure 5 ***In vivo.*** A: Experiments were conducted with nude female mice aged from 6 to 8 wk. The selected tumor model was the B16F10 melanoma cell line which is a murine skin cancer; B, C: The region of interest contained only the tumor and was drawn for each injection performed. If the image was not well defined using the harmonic mode, the B-mode image was used to correctly define the region of interest; D: As in the case of the *in vitro* experiments, the ultrasound scanner displayed the associated time intensity curve. This was extracted and converted through an Excel® file so that the analysis could be performed to obtain the required perfusion parameters.

corresponded to the difference between the latency time (T_L), defined as the time between the injection of the product and the beginning of contrast uptake, and T_{max}. From a mathematical point of view, T_L corresponded to the time at the intersection between $y=V_0$ and the tangent at $T_{max}/2$. The AUC, AUWI and AUWO corresponded to the area under the curve, the area under the wash-in (from T_0 to T_{max}) and the area under the wash-out (from T_{max} to T_{end} corresponding to the end of the acquisition) of the TIC. The area calculations were based on the trapezoidal rule: the region under the graph of the fitted curve was approximated by trapezoids whose areas were calculated to provide approximations of the areas under the curve, the wash-in or the wash-out. An additional operation of subtracting the offset on the y-axis was performed so that the total area under the curve was independent of it. The limits of integration were defined as follows:

$$X \in [T_0, T_{end}]$$

Where T_0 is the initial time. The slope coefficient of the wash-in (WI) was literally defined as the slope of the tangent of the wash-in at half maximum. Finally, the full-width at half maximum (FWHM) was defined as the time interval during which the value of the intensity was higher than $V_{max}/2$. This parameter is commonly considered as a first approximation of the mean transit time (MTT) (Figure 6)[8,26,30]. However, as the linear raw data provided by the ultrasound scanner were too noisy, extraction was performed after TIC fitting. This was based on the mathematical model developed at the IGR (Patent: WO/2008/053268 entitled "Method and system for quantification of tumoral vascularization").

$$I(t) = a_0 + (a_1 - a_0) * \left(\frac{A + \left(\frac{t}{a_2} \right)^p}{B + \left(\frac{t}{a_2} \right)^q} \right)$$

where $I(t)$ describes the variation in the intensity of contrast uptake as a function of time; a_0 is the intensity before the arrival of the contrast agent; a_1 is linked to the maximum value of contrast uptake; a_2 is linked to the rise time to the peak intensity; p is a coefficient related to the increase in intensity; q is a coefficient related to the decrease in intensity; A and B are arbitrary parameters.

The fitted curve was obtained by adjusting all the coefficients of the equation (called the IGR equation) to obtain a sum of the least-squares differences between the linear raw data and the modeled values as close to 0 as possible. Equation parameters were derived through the mathematical model so that asymptotic values were properly defined. This fitting was performed using the Solver program in Excel®. Through this modeling step, it was possible to avoid recirculation so that the conditions required to apply the time intensity method were fulfilled. Indeed, the IGR equation was used to perfectly fit the wash-in part of the curve while the wash-out part was

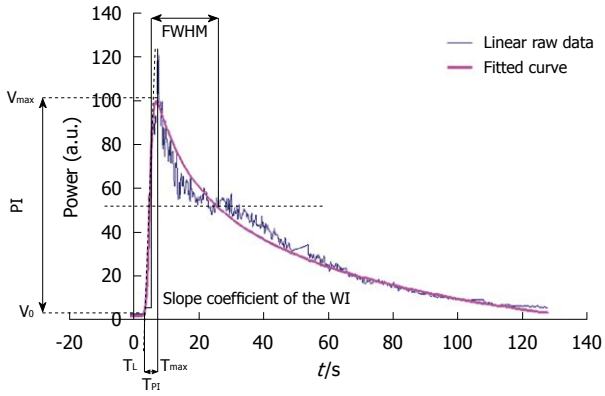

Figure 6 The graph displays an example of a time intensity curve with 4 of its 7 associated perfusion parameters: the peak intensity or peak intensity (difference between V_{max} and V_0), the time to peak intensity or time to peak intensity (the difference between T_{max} and T_L), the slope coefficient of the wash-in (the slope of the tangent of the wash-in at half maximum) and the full width at half maximum or FWHM (corresponding to a first approximation of the mean transit time). The three other perfusion parameters extracted from the time intensity curve were the area under the curve, the area under the wash-in and the area under the wash-out. PI: Peak intensity; T_{PI}: Time to peak intensity.

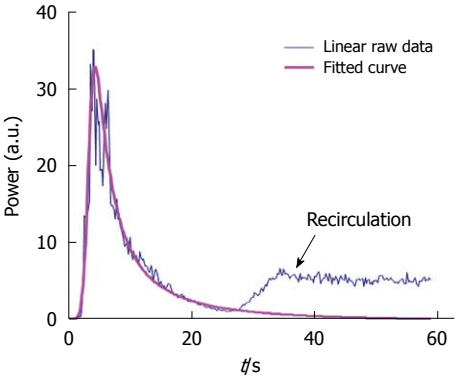

Figure 7 This graph displays both a time intensity curve and its associated fitted curve. Recirculation is avoided through the modeling process so that the conditions required to apply the time intensity method are fulfilled: the Gustave Roussy Institute equation perfectly fits the wash-in part of the curve while the wash-out part is adjusted so that recirculation is not taken into account in the final fitted curve.

adjusted so that recirculation was not taken into account in the final fitted curve (Figure 7). This adjustment is often performed[31] to ensure that the conditions required for the time intensity method are adequately verified. Once the fitted curve was determined, the semi-quantitative perfusion parameters were derived according to their previously described definitions.

Statistical analysis

Intra-operator variability was measured as the coefficient of variation (CV) which is the ratio of the SD of a specific parameter to its mean. CV = SD/mean.

For each set of experiments, the CV was evaluated and recorded for each of the seven semi-quantitative perfusion parameters. An overall range of variation was additionally provided in the "Results" part.

Table 1 Single straight pipe phantom: intra-operator variability of semi-quantitative perfusion parameters following five 0.02/0.05/0.08 mL bolus injections of SonoVue®

	PI	T_{PI}	Slope of the WI	FWHM	AUC	AUWI	AUWO
0.02 mL/ CV (%)	6.03	9.78	9.57	6.43	9.40	9.97	11.11
0.05 mL/ CV (%)	9.27	10.14	8.28	13.24	5.23	12.76	6.84
0.08 mL/ CV (%)	20.87	10.10	23.52	17.43	5.87	23.72	2.94

CV: Coefficient of variation; PI: Peak intensity; T_{PI}: Time to peak intensity; FWHM: Full width at half maximum; AUC: Area under the curve; AUWI: Area under the wash-in; AUWO: Area under the wash-out.

RESULTS

In vitro experiments

Three different phantoms were tested. Acquisitions were obtained after five injections of SonoVue®.

1st phantom - Single straight pipe phantom results: Three volumes of SonoVue® were tested: 0.02, 0.05 and 0.08 mL. For each volume, five fitted TICs were obtained following the five contrast agent injections. Data analysis was performed according to the protocol detailed in the "Materials and Methods" part: semi-quantitative perfusion parameters were extracted directly from the fitted TICs and their associated CV values were evaluated. The 0.02, 0.05 and 0.08 mL five injections respectively led to CV values ranging from 6.03% to 11.11%, from 5.23% to 13.24% and from 2.94% to 23.72%. Table 1 shows perfusion parameter CV values obtained following each set of experiments.

2nd phantom - Three intertwined pipe phantom results: The five fitted TICs resulting from the series of 0.03 and 0.06 mL bolus injections of SonoVue® were analyzed using the IGR model. Intra-operator variability values were found to respectively range from 2.33% to 9.65% and from 6.12% to 11.62%. CV values associated with each perfusion parameter are shown in Table 2.

For both these phantoms, maximum CV values were found in correspondence with the highest injected dose of SonoVue®. This observation might impact on the linear assumption. However, as previously mentioned in the "Time Intensity Method" part, to transfer *in vitro* results into clinical context, the concentration of interest is the IGR one which remains in the linear range.

3rd phantom - Dialyzer results: Data analysis was performed following five 0.10 mL bolus injections of SonoVue®. This series of experiments led to intra-operator variability values ranging from 8.11% to 19.11%. Table 3 provides more detailed results associated with each evaluated semi-quantitative perfusion parameter.

In vivo experiments

Intra-operator variability studies were performed on five

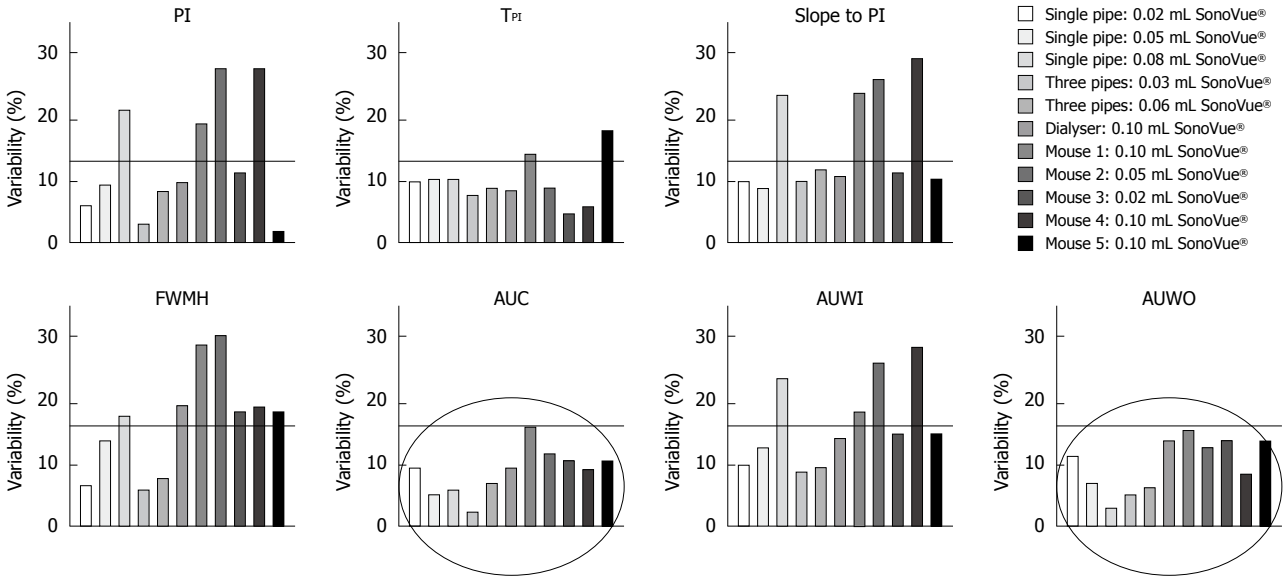

Figure 8 This graph shows the variability of perfusion parameters involved in both the *in vitro* and *in vivo* experiments. Five injections were recorded for each of the three phantoms and three for each mouse. The results demonstrated less than 30% overall variability, whatever the perfusion parameter. CV: Coefficient of variation; PI: Peak intensity; TPI: Time to peak intensity; FWHM: Full width at half maximum; AUC: Area under the curve; AUWI: Area under the wash-in; AUWO: Area under the wash-out.

Table 2 Three intertwined pipe phantom: intra-operator variability of semi-quantitative perfusion parameters following five 0.03/0.06 mL bolus injections of SonoVue®

	PI	TPI	Slope of the WI	FWHM	AUC	AUWI	AUWO
0.03 mL/ CV (%)	3.16	7.69	9.65	5.56	2.33	8.55	5.32
0.06 mL/ CV (%)	7.85	8.60	11.62	7.53	6.73	9.52	6.12

CV: Coefficient of variation; PI: Peak intensity; TPI: Time to peak intensity; FWHM: Full width at half maximum; AUC: Area under the curve; AUWI: Area under the wash-in; AUWO: Area under the wash-out.

Table 3 Dialyzer: intra-operator variability of semi-quantitative perfusion parameters following five 0.10 mL bolus injections of SonoVue®

	PI	TPI	Slope of the WI	FWHM	AUC	AUWI	AUWO
0.10 mL/ CV (%)	9.66	8.11	10.27	19.11	9.31	13.89	13.36

CV: Coefficient of variation; PI: Peak intensity; TPI: Time to peak intensity; FWHM: Full width at half maximum; AUC: Area under the curve; AUWI: Area under the wash-in; AUWO: Area under the wash-out.

mice following three 0.02 mL, 0.05 mL or 0.1 mL bolus injections of SonoVue®. Experiments were performed over 5 d.

Chemical anesthesia: Four mice underwent chemical anesthesia. The body weight was found to be 23.5 g (min: 22.6 g; max: 25 g) throughout the experiments. As experiments lasted over 5 d and due to the rapid doubling time of melanoma cells[32-34], tumor volume ranged from 93.8 to 599.7 mm^3 with a mean tumor value of 339.39 mm^3. We calculated the semi-quantitative perfusion parameters directly from the TICs using the IGR mathematical model. CV values ranged from 1.48% to 29.97%. Table 4 shows variability values associated with each perfusion parameter for each mouse.

Gaseous anesthesia: One mouse underwent gaseous anesthesia. It weighed 24.6 g. The tumor volume was 503.56 mm^3. CV values were determined based on the fitted TICs and ranged from 1.90% to 24.96%. More detailed results are provided in Table 4.

DISCUSSION

In this study, intra-operator variability was assessed through the determination of the coefficients of variation of semi-quantitative perfusion parameters using three distinct phantoms as well as *in vivo*. Throughout the experiments, CV values were consistently lower than 30% (Figure 8). The area under the curve and the area under the wash-out exhibited CV values below 15.79% both *in vitro* and *in vivo*.

Sources of variability

For each set of experiments, conditions such as the probe, the phantom, the whole circuit and the settings of the ultrasound scanner were maintained unchanged so that the assembly remained identical throughout the acquisitions.

The first source of variation could come from the ultrasound contrast agent itself. Indeed, before each injection, SonoVue® was reconstituted by manual agitation. Consequently, the solution may not have been identically homogeneous throughout the experiments. In addition, the precision of the syringe used to administer SonoVue® (within 0.01 mL) was low compared to the injected doses. Consequently, variations may have occurred even prior to any acquisition.

Table 4 ***In vivo*** **studies: intra-operator variability of semi-quantitative perfusion parameters following three 0.02/0.05/0.1 mL bolus injections of SonoVue®**

		Mouse	PI	TPI	Slope of the WI	FWHM	AUC	AUWI	AUWO
0.02 mL/	Chemical anaesthesia	1	18.99	14.04	23.85	28.87	15.79	18.43	15.46
0.05 mL/		2	27.60	8.33	25.75	18.90	9.06	28.39	8.12
0.1 mL/		3	11.39	4.41	1.48	18.44	10.76	14.73	13.58
CV (%)		4	27.88	5.68	28.82	29.97	11.21	26.22	12.42
	Gaseous anaesthesia	5	1.90	17.63	10.09	24.96	12.32	12.43	12.79

CV: Coefficient of variation; PI: Peak intensity; T_{PI}: Time to peak intensity; FWHM: Full width at half maximum; AUC: Area under the curve; AUWI: Area under the wash-in; AUWO: Area under the wash-out.

Table 5 Acoustic properties of different media

	Density (kg/m^3)	Velocity (m/s)	Attenuation coefficient (dB/cm at 1 MHz)	Impedance (MRayl)
Blood	1057	1575	0.18	1.61
Water	1000	1480	0.0022[1]	1.51 (50℃)

[1]Quadratic frequency dependence of this attenuation coefficient. Sources: Hedrick *et al*[36], Gupta *et al*[35], Goldstein *et al*[37].

The second source of variation could come from the injection step. Manual injections were performed by the same operator and a mark was drawn on the injection site so that the same site was used throughout the experiment. A new syringe was used for each injection. However, even if the mark allowed us to maintain the same injection site, it did not provide information concerning the exact position of the syringe within the pipe. In addition, even though the injection was administered by the same operator, variations could have occurred as it was performed manually (rate or angle of the injection). Other errors may have affected the data analysis part. A region of interest had to be selected to compute the TICs. It had to be the same for all TICs. However, as a new ROI was manually drawn for each injection, results may have been tarnished because of mistakes. Additional sources of variation can occur *in vivo*. Indeed, even if mice were maintained asleep, their physiological parameters were not entirely monitorable and variations may have occurred during the experiments.

The next step concerned TIC fitting. To ensure that no variations could come from the solver itself, a series of ten fittings were performed on the same TIC. The parameters provided by the IGR mathematical model were exactly the same for all the curves which allowed us to conclude that only the first three steps mentioned above may have induced variations in the results.

Study limitations

First, *in vitro*, the fluid used was water at ambient temperature which did not exhibit the same ultrasound properties as blood[35-37] (Table 5). In addition, none of the phantoms contained tissue-mimicking material[38,39]: the first two were composed of silicone pipes leading to the same remark as with the fluid: the ultrasound properties of the silicone are different from those of vessels. The properties of the third phantom were more similar to those of the microvascularization due to its dimensions. However, the parallelism with the capillaries did not reflect the complex and irregular structure of tumor microvascularization. Consequently, the three increasingly complex phantoms we worked with were mainly used for intra-operator variability evaluations and their properties tend to mimic only some *in vivo* properties which might induce difficulties in transferring *in vitro* results to *in vivo* ones. Moreover, *in vivo*, variability measures were based on three injections. Having more injections to interpret might have provided us with a better statistical analysis: this last limitation was offset by the number of mice we worked on. Another limitation might concern the stability of the ultrasound contrast agent. Indeed, each experiment duration was less than 2 h on account of the stability of SonoVue® over time which is 6 h after its reconstitution as described by Schneider[11]. However, recent studies reported a significant incidence of spontaneous gas diffusion phenomena on temporal evolution of contrast microbubble size[40-42]. In the following study, gas diffusion phenomena occurring for 2 h from initial formation of contrast agent was neglected: this assumption might impact the results. Finally, as previously mentioned, the precision of the syringe was a source of variability and the absence of any measurements performed to accurately evaluate microbubble concentration at the injection time might be a limitation.

Intra-operator variability studies using MRI, CT, PET and US

Several intra-operator variability studies using MRI, CT and PET have been described in the literature. These reported an overall intra-observer variability ranging from 3% to 30%[43-50]. The ranges of the semi-quantitative perfusion parameters we evaluated were consistent with those reported in the literature. Evelhoch *et al*[45] analyzed CV for the initial area under the gadolinium diethylenetriaminepentaacetate uptake *vs* time curve (IAUC) in 19 patients examined with two scans. The CV was found to be 18%. Wells *et al*[47] evaluated regional flow and the volume of tissue distribution of the contrast agent in tumor and normal tissue in 5 patients who underwent two PET-CT using inhaled $C^{15}O_2$ 1 wk apart. They obtained CV values ranging from 9% to 14% (11% in the tumor) for the flow and from 3% to 13% (6% in the tumor) for the volume

distribution. Myocardial perfusion values using CT imaging were determined by Groves *et al*[49] using two different approaches: the maximum-slope method and the peak method. CV values ranging from 12.6% to 23.7% for intra-observer agreement were observed. No published studies on intra-operator variability using DCE-US were found in the literature. Our results are concordant with these previous findings since the overall intra-operator variability of the semi-quantitative parameters observed both *in vivo* and *in vitro* ranged from 1.48% to 29.97%.

Anti-angiogenesis therapies and DCE-US imaging

Anti-angiogenic treatments inhibit the formation of neoblood vessels in tumors obstructing their dissemination because of the lack of a blood supply. Such drugs exert activity primarily on the microvascularization: they may be effective even if no obvious change in tumor shape is observed after their administration. In order for functional imaging to be efficient in assessing such treatments, the variability of any semi-quantitative perfusion parameters should be lower than any reduction in perfusion. Thomas *et al*[51] found a decrease of 40% in AUC values, using DCE-MRI, at day 28 in 43 patients suffering from advanced cancers (24 colorectal, 1 breast, 2 mesothelioma, 6 neuroendocrine, 2 renal and 8 others) and who received single-agent PTK/ZK. Other studies demonstrated that reductions in perfusion following anti-angiogenesis treatments, using MRI, CT, PET or US, range from 30% to greater than 90%[26,52-55]. For example, Lavisse *et al*[26] studied the evolution of the peak intensity (PI), the T_{PI} and the FWHM after the administration of AVE8062. They found that 6 h after the injection, the PI value represented 7% of the initial PI, T_{PI} was three-fold higher than the initial T_{PI} and FHWM was twice the initial FWHM.

In the light of these data, the CV values found in the current DCE-US study justified its use as an imaging method for assessing anti-angiogenic treatments.

In addition, in this study, the AUC and AUWO exhibited both *in vitro* and *in vivo* CV values below 15.79%. This is a major result considering the previous findings reported by Lassau *et al*[22,56,57] in different types of tumors such as GIST or RCC: among the seven semi-quantitative perfusion parameters evaluated, the two parameters which always correlated with the RECIST response and overall survival were the AUC and the AUWO. These two complementary observations highlight the reliability of such parameters in assessing anti-angiogenic treatments: AUC and AUWO are associated to a good correlation to RECIST response as well as to low intra-operator variability values. The T_{PI} may also be considered a parameter of interest as it exhibited CV values in a range noticeably similar to AUC and AUWO: it ranged from 4.41% to 17.63%.

Dynamic T1-weighted MRI and CT are commonly used in assessing tumor angiogenesis as DCE-US suffers from some limitations. One of its major drawbacks is its operator dependence. In addition, CV values might depend on the organ as some can be more challenging to image such as the liver suffering from respiration artifacts. There is also a limited depth penetration making imaging of deepest regions difficult[50,58]. Finally, some anti-angiogenic treatments mainly involve change in tumor vasculature permeability without tumor flow. Consequently, as ultrasound contrast agents are purely intravascular, DCE-US can only provide tumor blood flow information: no information concerning tumor permeability can be determined[50].

On the other hand, further studies involving intra-operator variability might support DCE-US as the imaging method of choice for the early evaluation of anti-angiogenic drugs because it also has many additional specific advantages. Contrast agents used in DCE-MRI are extracellular ones and no linear relationship exists, whatever the dose between the measured signal and the concentration of the MRI contrast agents[50]. DCE-US involves working with purely intravascular contrast agents. In addition, within a certain range, the measured intensity exhibits a linear relationship with microbubble concentration making it possible to assess perfusion parameters. In spite of the advantage of a linear relationship between the change in CT intensity and the concentration of the contrast agent as well as a high spatial resolution, DCE-CT has a low sensitivity and high concentrations of contrast agent can be toxic[50]. PET and SPECT modalities are highly sensitive to very low tracer concentrations but exhibit a poor resolution[50] compared to that of DCE-US. In addition DCE-US has advantages linked to ultrasound imaging: it is non-invasive, easy to use, not expensive, rapid and widely available.

Further studies

In this study, intra-operator variability measurements were based on semi-quantitative parameters, i.e. parameters extracted from the measured TIC within phantoms or tumors. Such parameters are often determined to estimate physiological parameters but do not take into account variations linked to physiological effects[31]. Blood flow and blood volume could be determined using methods that take into account patient hemodynamic conditions as well as the way the contrast agent is injected[31] which are elements included in the arterial input function. Consequently, further studies including the arterial input function will have to be performed to determine its influence on the DCE-US technique.

This work performed using *in vitro* and *in vivo* models demonstrated that among the seven semi-quantitative perfusion parameters, two (the AUC and the AUWO) linked to the blood volume and blood flow[9,10] exhibited an intra-operator variability value below 15.79% and could be the most reliable for early evaluation of anti-angiogenic treatments.

ACKNOWLEDGMENTS

The authors thank Lorna Saint Ange for editing.

COMMENTS

Background

Early functional imaging of anti-angiogenesis treatments in oncology is of major importance. Dynamic contrast-enhanced ultrasonography (DCE-US) is now

commonly recognized as a functional imaging technique able to evaluate such therapies as it is a sensitive and highly available modality allowing early prediction of tumor response to treatments based on changes in vascularity before any morphological ones occur.

Research frontiers

Microbubble contrast agents for DCE-US have developed during the past 10 years and are currently approved in Europe, Asia and Canada. Nowadays, ultrasound provides an ideal imaging modality for angiogenesis: it is widely available, not ionizing, low cost and provides real time imaging. However, until now, information on intra-operator variability in perfusion parameter measurements performed using DCE-US is lacking. In this study, the authors evaluated such variability and highlighted values similar to previous findings using other imaging modalities.

Innovations and breakthroughs

DCE-US is supported by the French National Cancer Institute which is currently studying the technique in several pathologies to establish the optimal perfusion parameters and timing for quantitative anticancer efficacy assessments: currently 400 patients with 1096 DCE-US demonstrated that the area under the curve quantified at 1 mo could be a robust parameter to predict response at 6 mo. The following study is the first one analyzing intra-operator variability in perfusion parameter measurements performed using DCE-US. Our study would suggest that DCE-US technique has comparable intra-operator variability than other functional imaging modalities that are currently used in routine.

Applications

By evaluating intra-operator variability in perfusion parameter measurements performed using DCE-US, this study may confirm the interest of dynamic contrast enhanced-ultrasonography as functional imaging in anti-angiogenic therapy evaluations.

Terminology

DCE-US involves the use of microbubble contrast agents and specialized imaging techniques to evaluate blood flow and tissue perfusion. Intra-operator variability studies aim to determine the variation in measurements performed by a single operator and instrument on the same item and under the same conditions.

Peer review

This is an interesting study and may draw the readers' attention because the authors evaluated the feasibility and reproducibility of DCE-US through in vitro and in vivo. Moreover, I think that this study would guide the readers about the methods of basic research in the areas of radiology. Unfortunately, strength of reported findings is limited by some experimental constraints and manuscript presentation needs several improvements before publication.

REFERENCES

1 **Lanza GM**, Caruthers SD, Winter PM, Hughes MS, Schmieder AH, Hu G, Wickline SA. Angiogenesis imaging with vascular-constrained particles: the why and how. *Eur J Nucl Med Mol Imaging* 2010; **37** Suppl 1: S114-S126

2 **Eisenbrey JR**, Forsberg F. Contrast-enhanced ultrasound for molecular imaging of angiogenesis. *Eur J Nucl Med Mol Imaging* 2010; **37** Suppl 1: S138-S146

3 **Kalva SP**, Namasivayam S, Vasuedo Sahani D. Imaging Angiogenesis. In: Teicher BA, Ellis LM, editors. Cancer Drug Discovery and Development: Antiangiogenic Agents in Cancer Therapy. Totowa, NJ: Humana Press, 2008: 189-203

4 **Lassau N**, Chami L, Péronneau P. Imagerie de contraste ultrasonore pour l'évaluation précoce des thérapeutiques ciblées. In: Tranquart F, Correas JM, Bouakaz A, editors. Echographie de contraste. Paris: Springer, 2007: 81-86

5 **Therasse P**, Arbuck SG, Eisenhauer EA, Wanders J, Kaplan RS, Rubinstein L, Verweij J, Van Glabbeke M, van Oosterom AT, Christian MC, Gwyther SG. New guidelines to evaluate the response to treatment in solid tumors. European Organization for Research and Treatment of Cancer, National Cancer Institute of the United States, National Cancer Institute of Canada. *J Natl Cancer Inst* 2000; **92**: 205-216

6 **Eisenhauer EA**, Therasse P, Bogaerts J, Schwartz LH, Sargent D, Ford R, Dancey J, Arbuck S, Gwyther S, Mooney M, Rubinstein L, Shankar L, Dodd L, Kaplan R, Lacombe D, Verweij J. New response evaluation criteria in solid tumours: revised RECIST guideline (version 1.1). *Eur J Cancer* 2009; **45**: 228-247

7 **Quaia E**. Microbubble ultrasound contrast agents: an update. *Eur Radiol* 2007; **17**: 1995-2008

8 **Ignee A**, Jedrejczyk M, Schuessler G, Jakubowski W, Dietrich CF. Quantitative contrast enhanced ultrasound of the liver for time intensity curves-Reliability and potential sources of errors. *Eur J Radiol* 2010; **73**: 153-158

9 **Claassen L**, Seidel G, Algermissen C. Quantification of flow rates using harmonic grey-scale imaging and an ultrasound contrast agent: an in vitro and in vivo study. *Ultrasound Med Biol* 2001; **27**: 83-88

10 **Schwarz KQ**, Bezante GP, Chen X, Mottley JG, Schlief R. Volumetric arterial flow quantification using echo contrast. An in vitro comparison of three ultrasonic intensity methods: radio frequency, video and Doppler. *Ultrasound Med Biol* 1993; **19**: 447-460

11 **Schneider M**. Characteristics of SonoVuetrade mark. *Echocardiography* 1999; **16**: 743-746

12 **Greis C**. Technology overview: SonoVue (Bracco, Milan). *Eur Radiol* 2004; **14** Suppl 8: P11-P15

13 **Quaia E**, Calliada F, Bertolotto M, Rossi S, Garioni L, Rosa L, Pozzi-Mucelli R. Characterization of focal liver lesions with contrast-specific US modes and a sulfur hexafluoride-filled microbubble contrast agent: diagnostic performance and confidence. *Radiology* 2004; **232**: 420-430

14 **von Herbay A**, Vogt C, Willers R, Häussinger D. Real-time imaging with the sonographic contrast agent SonoVue: differentiation between benign and malignant hepatic lesions. *J Ultrasound Med* 2004; **23**: 1557-1568

15 **Hamilton WF**, Moore JW, Kinsman MJ, Spurling RG. Studies on the circulation. IV. Further analysis of the injection method, and of changes in hemodynamics under physiological and pathological conditions. *Am J Physiol* 1932: **99**: 534-551

16 **Kinsman JM**, Moore JW, Hamilton WF. Studies on the circulation. I. Injection method: physical and mathematical considerations. *Am J Physiol* 1929; **89**: 322-330

17 **Mischi M**, Del Prete Z, Korsten HHM. Indicator dilution techniques in cardiovascular quantification. In: Leondes CT, editor. Biomechanical Systems Technology: Cardiovascular Systems. Singapore: World Scientific Publishing Company, 2007: 89-156

18 **Li PC**, Yang MJ. Transfer function analysis of ultrasonic time-intensity measurements. *Ultrasound Med Biol* 2003; **29**: 1493-1500

19 **Lampaskis M**, Averkiou M. Investigation of the relationship of nonlinear backscattered ultrasound intensity with microbubble concentration at low MI. *Ultrasound Med Biol* 2010; **36**: 306-312

20 **Whittingham TA**. Contrast-specific imaging techniques: technical perspective. In: Quaia E, editor. Contrast media in ultrasonography: basic principles and clinical applications. Berlin, Heidelberg, New-York: Springer, 2005: 43-70

21 **Lassau N**, Koscielny S, Chebil M, Chami L, Bendjilali R, Roche. A, Escudier B, Le Cesne A, Soria J () Functional imaging using DCE-US: which parameters for the early evaluation of antiangiogenetic therapies? *J Clin Oncol* 2009; **27** (15 Suppl): 3524

22 **Lassau N**, Koscielny S, Albiges L, Chami L, Benatsou B, Chebil M, Roche A, Escudier BJ. Metastatic renal cell carcinoma treated with sunitinib: early evaluation of treatment response using dynamic contrast-enhanced ultrasonography. *Clin Cancer Res* 2010; **16**: 1216-1225

23 **Lassau N**, Lacroix J, Aziza R, Vilgrain V, Taeb S, Koscielny S. French Multicentric Prospective Evaluation of Dynamic Contrast-enhanced Ultrasound (DCE-US) for the Evaluation of Antiangiogenic Treatments. Radiological Society of North America. 95th Scientific Assembly and Annual Meeting; 2009 No 29-Dec 4; Mc Cormick Place, Chicago

24 **Veltmann C**, Lohmaier S, Schlosser T, Shai S, Ehlgen A, Pohl C, Becher H, Tiemann K. On the design of a capillary flow phantom for the evaluation of ultrasound contrast agents at very low flow velocities. *Ultrasound Med Biol* 2002; **28**: 625-634

25 **Meyer-Wiethe K**, Cangür H, Seidel GU. Comparison of different mathematical models to analyze diminution kinetics of ultrasound contrast enhancement in a flow phantom. *Ultrasound Med Biol* 2005; **31**: 93-98

26 **Lavisse S**, Lejeune P, Rouffiac V, Elie N, Bribes E, Demers B, Vrignaud P, Bissery MC, Brulé A, Koscielny S, Péronneau P, Lassau N. Early quantitative evaluation of a tumor vasculature disruptive agent AVE8062 using dynamic contrast-enhanced ultrasonography. *Invest Radiol* 2008; **43**: 100-111

27 **Verbeek XA**, Willigers JM, Prinzen FW, Peschar M, Ledoux LA, Hoeks AP. High-resolution functional imaging with ultrasound contrast agents based on RF processing in an in vivo kidney experiment. *Ultrasound Med Biol* 2001; **27**: 223-233

28 **Correas JM**, Burns PN, Lai X, Qi X. Infusion versus bolus of an ultrasound contrast agent: in vivo dose-response measurements of BR1. *Invest Radiol* 2000; **35**: 72-79

29 **Gorce JM**, Arditi M, Schneider M. Influence of bubble size distribution on the echogenicity of ultrasound contrast agents: a study of SonoVue. *Invest Radiol* 2000; **35**: 661-671

30 **Vicenzini E**, Delfini R, Magri F, Puccinelli F, Altieri M, Santoro A, Giannoni MF, Bozzao L, Di Piero V, Lenzi GL. Semiquantitative human cerebral perfusion assessment with ultrasound in brain space-occupying lesions: preliminary data. *J Ultrasound Med* 2008; **27**: 685-692

31 **de Marco G**, Dassonvalle P, M.C. H-F, Onen F, Idy-Peretti I. Cerebral perfusion: dynamic suceptibility contrast MR imaging. Part 2: vascular models and data extraction. *Med Nucl* 2004; **28**: 35-48

32 **Kwee JK**, Mitidieri E, Affonso OR. Lowered superoxide dismutase in highly metastatic B16 melanoma cells. *Cancer Lett* 1991; **57**: 199-202

33 **Ohira T**, Ohe Y, Heike Y, Podack ER, Olsen KJ, Nishio K, Nishio M, Miyahara Y, Funayama Y, Ogasawara H. In vitro and in vivo growth of B16F10 melanoma cells transfected with interleukin-4 cDNA and gene therapy with the transfectant. *J Cancer Res Clin Oncol* 1994; **120**: 631-635

34 **Yerlikaya A**, Erin N. Differential sensitivity of breast cancer and melanoma cells to proteasome inhibitor Velcade. *Int J Mol Med* 2008; **22**: 817-823

35 **Gupta LC**, Sahu UC. Diagnostic ultrasound. New Delhi: Jaypee Brothers Publishers, 2007

36 **Hedrick W**, Hykes D, Starchman D. Ultrasound physics and instrumentation. 3rd ed. Saint-Louis, MO: Mosby, 1995

37 **Goldstein A**, Powis RL. Medical ultrasonic diagnostics. In: Papadakis P, editor. Ultrasonic instruments and devices: reference for modern instrumentation, techniques, and technology. San Diego, CA: Academic Press, 1999: 46-193

38 **Casciaro S**, Demitri C, Conversano F, Casciaro E, Distante A. Experimental investigation and theoretical modelling of the nonlinear acoustical behaviour of a liver tissue and comparison with a tissue mimicking hydrogel. *J Mater Sci Mater Med* 2008; **19**: 899-906

39 **Casciaro S**, Conversano F, Musio S, Casciaro E, Demitri C, Sannino A. Full experimental modelling of a liver tissue mimicking phantom for medical ultrasound studies employing different hydrogels. *J Mater Sci Mater Med* 2009; **20**: 983-989

40 **Sarkar K**, Katiyar A, Jain P. Growth and dissolution of an encapsulated contrast microbubble: effects of encapsulation permeability. *Ultrasound Med Biol* 2009; **35**: 1385-1396

41 **Kwan JJ**, Borden MA. Microbubble dissolution in a multigas environment. *Langmuir* 2010; **26**: 6542-6548

42 **Casciaro S**, Errico RP, Conversano F, Demitri C, Distante A. Experimental investigations of nonlinearities and destruction mechanisms of an experimental phospholipid-based ultrasound contrast agent. *Invest Radiol* 2007; **42**: 95-104

43 **Ng CS**, Raunig DL, Jackson EF, Ashton EA, Kelcz F, Kim KB, Kurzrock R, McShane TM. Reproducibility of perfusion parameters in dynamic contrast-enhanced MRI of lung and liver tumors: effect on estimates of patient sample size in clinical trials and on individual patient responses. *AJR Am J Roentgenol* 2010; **194**: W134-W140

44 **Marcus CD**, Ladam-Marcus V, Cucu C, Bouché O, Lucas L, Hoeffel C. Imaging techniques to evaluate the response to treatment in oncology: current standards and perspectives. *Crit Rev Oncol Hematol* 2009; **72**: 217-238

45 **Evelhoch JL**, LoRusso PM, He Z, DelProposto Z, Polin L, Corbett TH, Langmuir P, Wheeler C, Stone A, Leadbetter J, Ryan AJ, Blakey DC, Waterton JC. Magnetic resonance imaging measurements of the response of murine and human tumors to the vascular-targeting agent ZD6126. *Clin Cancer Res* 2004; **10**: 3650-3657

46 **Morgan B**, Utting JF, Higginson A, Thomas AL, Steward WP, Horsfield MA. A simple, reproducible method for monitoring the treatment of tumours using dynamic contrast-enhanced MR imaging. *Br J Cancer* 2006; **94**: 1420-1427

47 **Wells P**, Jones T, Price P. Assessment of inter- and intrapatient variability in C15O2 positron emission tomography measurements of blood flow in patients with intra-abdominal cancers. *Clin Cancer Res* 2003; **9**: 6350-6356

48 **Cenic A**, Nabavi DG, Craen RA, Gelb AW, Lee TY. Dynamic CT measurement of cerebral blood flow: a validation study. *AJNR Am J Neuroradiol* 1999; **20**: 63-73

49 **Groves AM**, Goh V, Rajasekharan S, Kayani I, Endozo R, Dickson JC, Menezes LJ, Shastry M, Habib SB, Ell PJ, Hutton BF. CT coronary angiography: quantitative assessment of myocardial perfusion using test bolus data-initial experience. *Eur Radiol* 2008; **18**: 2155-2163

50 **Miller JC**, Pien HH, Sahani D, Sorensen AG, Thrall JH. Imaging angiogenesis: applications and potential for drug development. *J Natl Cancer Inst* 2005; **97**: 172-187

51 **Thomas AL**, Morgan B, Horsfield MA, Higginson A, Kay A, Lee L, Masson E, Puccio-Pick M, Laurent D, Steward WP. Phase I study of the safety, tolerability, pharmacokinetics, and pharmacodynamics of PTK787/ZK 222584 administered twice daily in patients with advanced cancer. *J Clin Oncol* 2005; **23**: 4162-4171

52 **Willett CG**, Boucher Y, di Tomaso E, Duda DG, Munn LL, Tong RT, Chung DC, Sahani DV, Kalva SP, Kozin SV, Mino M, Cohen KS, Scadden DT, Hartford AC, Fischman AJ, Clark JW, Ryan DP, Zhu AX, Blaszkowsky LS, Chen HX, Shellito PC, Lauwers GY, Jain RK. Direct evidence that the VEGF-specific antibody bevacizumab has antivascular effects in human rectal cancer. *Nat Med* 2004; **10**: 145-147

53 **Meijerink MR**, van Cruijsen H, Hoekman K, Kater M, van Schaik C, van Waesberghe JH, Giaccone G, Manoliu RA. The use of perfusion CT for the evaluation of therapy combining AZD2171 with gefitinib in cancer patients. *Eur Radiol* 2007; **17**: 1700-1713

54 **Lassau N**, Lamuraglia M, Vanel D, Le Cesne A, Chami L, Jaziri S, Terrier P, Roche A, Leclere J, Bonvalot S. Doppler US with perfusion software and contrast medium injection in the early evaluation of isolated limb perfusion of limb sarcomas: prospective study of 49 cases. *Ann Oncol* 2005; **16**: 1054-1060

55 **Miles KA**, Griffiths MR. Perfusion CT: a worthwhile enhancement? *Br J Radiol* 2003; **76**: 220-231

56 **Lassau N**, Chebil M, Koscielny S, Chami L, Bendjilali R, Roche A. Dynamic Contrast-enhanced Ultrasonography (DCE-US) with Quantification for the Early Evaluation of HCC Treated by Bevacizumab: Which Parameters? Radiological Society of North America. 95th Scientific Assembly and Annual Meeting; 2009 Nov 29-Dec 4; Chicago: Mc Cormick Place

57 **Lassau N**, Chebil M, Chami L, Bidault S, Girard E, Roche A. Dynamic contrast-enhanced ultrasonography (DCE-US): a new tool for the early evaluation of antiangiogenic treatment. *Target Oncol* 2010; **5**: 53-58

58 **Quaia E**, D'Onofrio M, Palumbo A, Rossi S, Bruni S, Cova M. Comparison of contrast-enhanced ultrasonography versus baseline ultrasound and contrast-enhanced computed tomography in metastatic disease of the liver: diagnostic performance and confidence. *Eur Radiol* 2006; **16**: 1599-1609

S- Editor Cheng JX **L- Editor** O'Neill M **E- Editor** Zheng XM

World Journal of Radiology

Online Submissions: http://www.wjgnet.com/1949-8470office
wjr@wjgnet.com
doi:10.4329/wjr.v3.i3.82

World J Radiol 2011 March 28; 3(3): 82-84
ISSN 1949-8470 (online)

CASE REPORT

Paraparesis induced by extramedullary haematopoiesis

Paolo Savini, Arianna Lanzi, Giorgio Marano, Chiara Carli Moretti, Giovanni Poletti, Giuseppe Musardo, Francesco Giuseppe Foschi, Giuseppe Francesco Stefanini

Paolo Savini, Arianna Lanzi, Giorgio Marano, Giuseppe Musardo, Francesco Giuseppe Foschi, Giuseppe Francesco Stefanini, Department of Internal Medicine, Faenza Hospital, viale Stradone 9, 48018 Faenza, Italy
Chiara Carli Moretti, Department of Radiology, Faenza Hospital, viale Stradone 9, 48018 Faenza, Italy
Giovanni Poletti, Department of Pathology, Ravenna Hospital, viale Randi 5, 48121 Ravenna, Italy
Author contributions: Savini P refer to physician of the clinical case; Lanzi A and Marano G contributes to writing the manuscript; Carli Moretti C provided radiologic images of the case; Poletti performed laboratory analysis; Musardo G and Foschi FG screened the literature and contributed to writing the first draft of the paper; Stefanini GF was responsible for the final approval of the manuscript.
Correspondence to: Paolo Savini, MD, Department of Internal Medicine, Faenza Hospital, viale Stradone 9, 48018 Faenza, Italy. p.savini@ausl.ra.it
Telephone: +39-546-601111 Fax: +39-546-601517
Received: November 13, 2010 Revised: January 10, 2011
Accepted: January 17, 2011
Published online: March 28, 2011

Abstract

We describe a case of worsening paraparesis induced by spinal cord compression at T6-T7 levels associated with compensatory extramedullary haematopoiesis from a compound heterozygote for haemoglobin E and for β-thalassemia. An emergency T3-T9 laminectomy was performed with excision of the masses and complete rehabilitation of the patient.

Key words: Extramedullary hematopoiesis; Thalassemia; Anemia; Spinal cord compression; Laminectomy

Peer reviewers: Yi-Xiang Wang, MMed, PhD, Associate Professor, Department of Diagnostic Radiology and Organ Imaging, Prince of Wales Hospital, The Chinese University of Hong Kong, Shatin, NT, Hong Kong, China; Kennith F Layton, MD, FAHA, Division of Neuroradiology and Director of Interventional Neuroradiology, Department of Radiology, Baylor University Medical Center, 3500 Gaston Avenue, Dallas, TX 75246, United States

Savini P, Lanzi A, Marano G, Moretti CC, Poletti G, Musardo G, Foschi FG, Stefanini GF. Paraparesis induced by extramedullary haematopoiesis. *World J Radiol* 2011; 3(3): 82-84 Available from: URL: http://www.wjgnet.com/1949-8470/full/v3/i3/82.htm DOI: http://dx.doi.org/10.4329/wjr.v3.i3.82

INTRODUCTION

Extramedullary haematopoiesis (EMH) is a physiologic response to chronic anemia, observed in various hematologic disorders such as thalassemias[1], myelofibrosis and polycythemia. Since the first description by Gatto *et al*[2], several cases of EMH at different sites have been reported.

The EMH, as a tumor-like mass, is commonly seen in the liver, spleen and lymph nodes. Involvement of the epidural space causing spinal cord compression has rarely been reported[3].

Because of its rarity, there are no evidence-based guidelines for the treatment of paraspinal pseudotumors caused by EMH. Management options include hypertransfusion, radiotherapy, surgery or a combination of these modalities. Recently, hydroxyurea or erythropoietin in combination with radiotherapy as treatment was described[4-6], but management still remains controversial.

Decompressive laminectomy, as in our case, has been used in patients with rapid neurological deterioration[7].

We hereby present a case of EMH in a 21-year-old man with thalassemia presenting with paraplegia due to a spinal cord compression that was treated successfully with surgery.

CASE REPORT

A 21-year-old man with a not well defined history of transfusion-dependent microcytic anemia in his native country, Bangladesh, presented to the emergency department with worsening paraparesis.

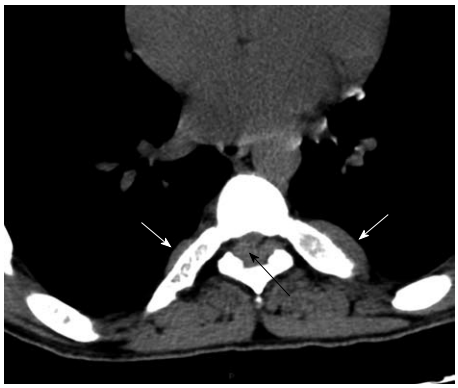

Figure 1 Pre-operative computed tomography scan of the chest without contrast media showing the large bilateral costal masses (white arrows) and an intracanalicular extradural mass (black arrow).

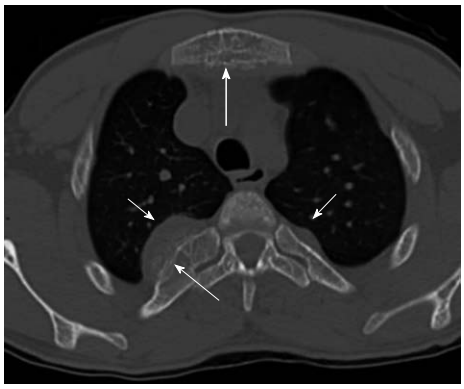

Figure 2 Pre-operative "bone window" computed tomography scan of the chest without contrast media shows large bilateral, well circumscribed lobulated soft tissue masses that cause widening of the ribs (short arrows) and periosteal reaction, without interruption of cortical bone (thin long arrow). Coexisting involvement of the sternum body (thick long arrow).

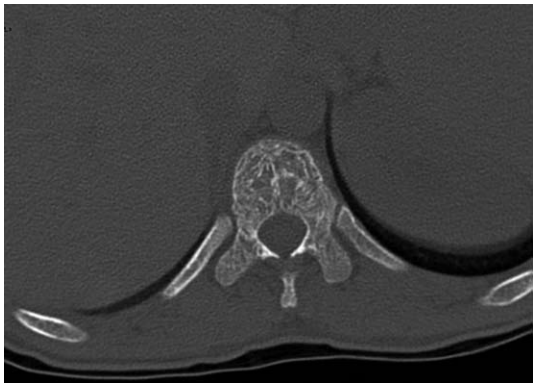

Figure 3 Pre-operative "bone window" computed tomography scan without contrast media: the vertebral body is devoid of bony erosion and has a lacey appearance.

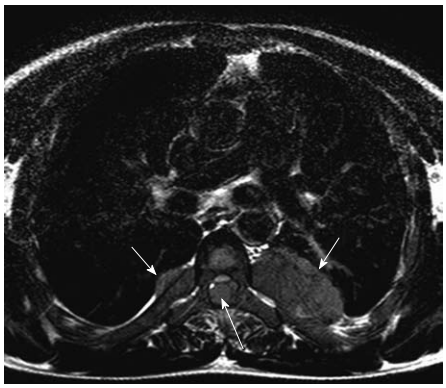

Figure 4 Preoperative axial magnetic resonance imaging, T2 weighted, shows paravertebral and intracanal masses, isointense with the spinal cord, widening the ribs (short arrows) and causing cord compression (long arrow).

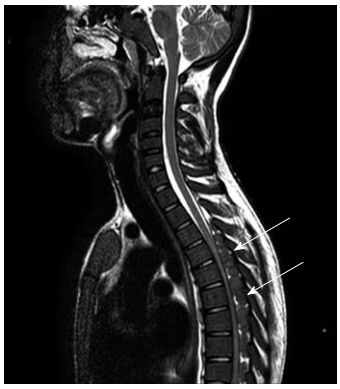

Figure 5 Preoperative sagittal MRI, T2 weighted, shows masses extending from T4 to T9 with cord compression (white arrows), embedded within the epidural fat and isointense with the spinal cord.

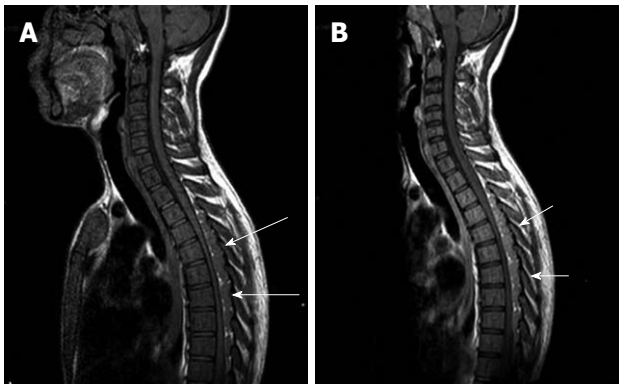

Figure 6 Preoperative sagittal magnetic resonance imaging, T1 weighted, without contrast media (A) (long arrows), and after Gadolinium administration (B) (short arrows) shows poor and homogeneous contrast enhancement of the masses.

Computed tomography (Figures 1-3) and magnetic resonance imaging (MRI, Figures 4-6) revealed bilateral paravertebral soft-tissue masses at T4-L1 levels and a mass with the same features was seen inside the vertebral canal inducing spinal cord compression at T4-T9 levels. Furthermore, a marked medullary expansion of the bony structures was present. Laboratory analyses showed a haemoglobin (Hb) level of 8.5 g/dL and mean corpuscular volume (MCV) of 68 fL. Hb electrophoresis revealed HbE at 45%, HbF at 30% and HbA2 at 20%.

Molecular analysis showed the patient was a compound heterozygote for HbE (β-26 glutamine → lysine)

and for β-thalassemia (β+IVS1-nt5). All these findings appeared to be associated with compensatory extramedullary haematopoiesis.

An emergency T3-T9 laminectomy was performed with a complete excision of the masses. A morphological and immunohistochemical analysis was then carried out. The masses were composed of a heterogeneous cellular population resembling physiological haematopoiesis in all its components.

The patient received a rehabilitation cycle and five months after the surgery, with continuing red blood cell transfusions, remains free of symptoms.

DISCUSSION

HbE (β26Glu → Lys) is the most common Hb variant in Southeast Asia and the second most prevalent worldwide.

HbE, when associated with β thalassemia (HbE/β-thalassemia) in a compound heterozygous state, results in a clinically severe condition. HbE activates a cryptic splice site that produces non-functional mRNAs. Hb IVS1-1 is a Mediterranean mutation that affects mRNA processing giving rise to β (o)-thalassemia. HbE/β thalassemia has a very variable clinical phenotype. HbE/β-thalassemia generally manifests with severe anemia where individuals exhibit β-thalassemia major with regular blood transfusions or β-thalassemia intermedia with periodic blood transfusions. Extramedullary haematopoiesis is a consequence of insufficient bone marrow function that is unable to meet circulatory demands. Thalassemia major or intermedia, congenital spherocytosis, congenital haemolytic anemia and sickle cell anemia account for most cases of EMH. It is rarely seen in myelofibrosis and Gaucher's disease.

Intrathoracic EMH is most often visualized on the chest roentgenogram or the chest computed tomography (CT) scan as single or multiple paravertebral mass lesions. While a paravertebral mass may represent EMH, other disorders of the posterior mediastinum, such as neurogenic tumor, lymphoma, primary and metastatic malignancy, paravertebral abscess, lateral meningocele, and extrapleural cyst, must be considered.

The characteristic features observed in the chest roentgenogram and the chest CT scan were helpful in recognizing intrathoracic EMH. These included the following[8]: (1) Widening of the ribs by expansion of the medullary cavity or by periosteal elevation, without bony erosion; (2) The presence of a unilateral or bilateral well-circumscribed lobulated, paravertebral mass lesion usually located caudal to the sixth thoracic vertebrae; and (3) The absence of calcification and the presence of adipose tissue within the mass.

MRI is currently the technique of choice in evaluating spinal EMH. On MRI, EMH is usually characterized by lobular masses with increased signal intensity compared to that of the red marrow in the adjacent vertebral bodies[7]. The lack of gadolinium enhancement allows its differentiation from other epidural masses such as abscesses or metastases.

REFERENCES

1 **Cappellini MD**, Musallam KM, Taher AT. Insight onto the pathophysiology and clinical complications of thalassemia intermedia. *Hemoglobin* 2009; **33** Suppl 1: S145-S159

2 **Gatto I**, Terrana V, Biondi L. [Compression of the spinal cord due to proliferation of bone marrow in epidural space in a splenectomized person with Cooley's disease]. *Haematologica* 1954; **38**: 61-76

3 **Logothetis J**, Constantoulakis M, Economidou J, Stefanis C, Hakas P, Augoustaki O, Sofroniadou K, Loewenson R, Bilek M. Thalassemia major (homozygous beta-thalassemia). A survey of 138 cases with emphasis on neurologic and muscular aspects. *Neurology* 1972; **22**: 294-304

4 **Cario H**, Wegener M, Debatin KM, Kohne E. Treatment with hydroxyurea in thalassemia intermedia with paravertebral pseudotumors of extramedullary hematopoiesis. *Ann Hematol* 2002; **81**: 478-482

5 **Cianciulli P**, Sorrentino F, Morino L, Massa A, Sergiacomi GL, Donato V, Amadori S. Radiotherapy combined with erythropoietin for the treatment of extramedullary hematopoiesis in an alloimmunized patient with thalassemia intermedia. *Ann Hematol* 1996; **72**: 379-381

6 **Malik M**, Pillai LS, Gogia N, Puri T, Mahapatra M, Sharma DN, Kumar R. Paraplegia due to extramedullary hematopoiesis in thalassemia treated successfully with radiation therapy. *Haematologica* 2007; **92**: e28-e30

7 **Dibbern DA Jr**, Loevner LA, Lieberman AP, Salhany KE, Freese A, Marcotte PJ. MR of thoracic cord compression caused by epidural extramedullary hematopoiesis in myelodysplastic syndrome. *AJNR Am J Neuroradiol* 1997; **18**: 363-366

8 **Alam R**, Padmanabhan K, Rao H. Paravertebral mass in a patient with thalassemia intermedia. *Chest* 1997; **112**: 265-267

S- Editor Cheng JX **L- Editor** Lutze M **E- Editor** Zheng XM

World Journal of Radiology

Online Submissions: http://www.wjgnet.com/1949-8470office
wjr@wjgnet.com
www.wjgnet.com

World J Radiol 2011 March 28; 3(3): I
ISSN 1949-8470 (online)

Acknowledgments to reviewers of *World Journal of Radiology*

Many reviewers have contributed their expertise and time to the peer review, a critical process to ensure the quality of *World Journal of Radiology*. The editors and authors of the articles submitted to the journal are grateful to the following reviewers for evaluating the articles (including those published in this issue and those rejected for this issue) during the last editing time period.

Charles Bellows, MD, Associate Professor, Chief of General Surgery, Tulane University, Department of Surgery SL-22, 1430 Tulane Ave, New Orleans, LA 70112, United States

Filippo Cademartiri, MD, PhD, Departmento of Radiology - c/o Piastra Tecnica - Piano 0, Azienda Ospedaliero-Universitaria di Parma, Via Gramsci, 14 - 43100 Parma, Italy

Sergio Casciaro, PhD, Institute of Clinical Physiology - National Research Council,Campus Universitario Ecotekne, Via Monteroni, 73100 Lecce, Italy

Chan Kyo Kim, MD, Assistant Professor, Department of Radiology, Samsung Medical Center, Sungkyunkwan University School of Medicine, 50 Ilwon-dong, Kangnam-gu, Seoul 135-710, South Korea

Stefania Romano, MD, A. Cardarelli Hospital, Department of Diagnostic Imaging, Section of General and Emergency Radiology, Viale Cardarelli, 9, 80131 Naples, Italy

Francesco Lassandro, MD, Department of Radiology, Monaldi Hospital, via Leonardo Bianchi, Napoli, 80129, Italy

Kennith F Layton, MD, FAHA, Division of Neuroradiology and Director of Interventional Neuroradiology, Department of Radiology, Baylor University Medical Center, 3500 Gaston Avenue, Dallas, TX 75246, United States

Yicheng Ni, MD, PhD, Professor, Biomedical Imaging, Interventional Therapy and Contrast Media Research, Department of Radiology, University Hospitals, K.U. Leuven, Herestraat 49, B-3000, Leuven, Belgium

Yi-Xiang Wang, MMed, PhD, Associate Professor, Department of Diagnostic Radiology and Organ Imaging, Prince of Wales Hospital, The Chinese University of Hong Kong, Shatin, NT, Hong Kong, China

Ying Xiao, PhD, Professor, Director, Medical Physics, Department of Radiation Oncology, Thomas Jefferson University Hospital, Philadelphia, PA 19107-5097, United States

WJR World Journal of Radiology

Online Submissions: http://www.wjgnet.com/1949-8470office
wjr@wjgnet.com
www.wjgnet.com

World J Radiol 2011 March 28; 3(3): I
ISSN 1949-8470 (online)

Meetings

Events Calendar 2011

January 23-27
Radiology at Snowbird
San Diego, Mexico

January 24-28
Neuro/ENT at the Beach
Palm Beach, FL, United States

February 28-29
MIAD 2011 - 2nd International Workshop on Medical Image Analysis and Description for Diagnosis System
Rome, Italy

February 5-6
Washington Neuroradiology Review
Arlington, VA, United States

February 12-17
MI11 - SPIE Medical Imaging 2011
Lake Buena Vista, FL, United States

February 17-18
2nd National Conference Diagnostic and Interventional Radiology 2011
London, United Kingdom

Februrary 17-18
VII National Neuroradiology Course
Lleida, Spain

February 18
Radiology in child protection
Nottingham, United Kingdom

Februrary 19-22
COMPREHENSIVE REVIEW OF MUSCULOSKELETAL MRI
Lake Buena Vista, FL, United States

March 2-5
2011 Abdominal Radiology Course
Carlsbad, CA, United States

March 3-7
European Congress of Radiology Meeting ECR 2011
Vienna, Austria

March 6-9
World Congress Thoracic Imaging - IV
Bonita Springs, FL, United States

March 14-18
9th Annual NYU Radiology Alpine Imaging Symposium at Beaver Creek
Beaver Creek, CO, United States

March 20-25
Abdominal Radiology Course 2011
Carlsbad, CA, United States

March 26-31
2011 SIR Annual Meeting
Chicago, IL, United States

March 28-April 1
University of Utah Neuroradiology 2nd Intensive Interactive Brain & Spine Imaging Conference
Salt Lake City, UT, United States

April 3-8
1st Annual Ottawa Radiology Resident Review
Ottawa, Canada

April 3-8
43rd International Diagnostic Course Davos on Diagnostic Imaging and Interventional Techniques
Davos, Switzerland

April 6-9
Image-Based Neurodiagnosis: Intensive Clinical and Radiologic Review, CAQ Preparation
Cincinnati, OH, United States

April 28-May 1
74th Annual Scientific Meeting of the Canadian Association of Radiologists CAR
Montreal, Canada

May 5-8
EMBL Conference-Sixth International Congress on Electron Tomography
Heidelberg, Germany

May 10-13
27th Iranian Congress of Radiology
Tehran, Iran

May 14-21
Radiology in Marrakech
Marrakech, Morocco

May 21-24
European Society of Gastrointestinal and Abdominal Radiology 2011 Annual Meeting
Venice, Italy

May 23-25
Sports Medicine Imaging State of the Art: A Collaborative Course for Radiologists and Sports Medicine Specialists
New York, NY, United States

May 24-26
Russian Congress of Radiology
Moscow, Russia

May 28-31
International Congress of Pediatric Radiology (IPR)
London, United Kingdom

June 4-8
58th Annual Meeting of the Society of Nuclear Medicine
San Antonio, TX, United States

June 6-8
UKRC 2011 - UK Radiological Congress
Manchester, United Kingdom

June 8-11
CIRA 2011 - Canadian Internventinal Radiology Association Meeting
Montreal, QC, Canada

June 9-10
8th ESGAR Liver Imaging Workshop
Dublin, Ireland

June 17-19
ASCI 2011 - 5th Congress of Asian Society of Cardiovascular Imaging
Hong Kong, China

June 22-25
CARS 2011 - Computer Assisted Radiology and Surgery - 25th International Congress and Exhibition
Berlin, Germany

June 27-July 1
NYU Summer Radiology Symposium at The Sagamore
Lake George, NY, United States

July 18-22
Clinical Case-Based Radiology Update in Iceland
Reykjavik, Iceland

August 1-5
NYU Clinical Imaging Symposium in Santa Fe
Santa Fe, NM, United States

September 22-25
European Society of Neuroradiology (ESNR) XXXV Congress and 19th Advanced Course
Antwerp, Belgium

October 12-14
International Conference Vipimage 2011 - Computational Vision and Medical Image Processing
Algarve, Portugal

October 15-16
Essentials of Emergency and Trauma Radiology
Ottawa, Canada

October 23-29
2011 IEEE NSS - 2011 IEEE Nuclear Science Symposium and Medical Imaging Conference
Valencia, Spain

October 25-28
NYU Radiology in Scottsdale - Fall Radiology Symposium in Scottsdale
Scottsdale, AZ, United States

October 28-30
Fourth National Congress of Professionals of Radiological Techniques
Florianópolis, Brazil

October 28-30
Multi-Modality Gynecological & Obstetric Imaging
Ottawa, Canada

November 3-4
9th ESGAR Liver Imaging Workshop
Taormina, Italy

November 15-19
EANM 2011 - Annual Congress of the European Association of Nuclear Medicine
Birmingham, United Kingdom

November 22-29
NSS/MIC - Nuclear Science Symposium and Medical Imaging Conference 2011
Valencia, Spain

November 26-28
8th Asia Oceaninan Congress of Neuro-Radiology
Bangkok, Thailand

WJR World Journal of Radiology

Online Submissions: http://www.wjgnet.com/1949-8470office
wjr@wjgnet.com
www.wjgnet.com

World J Radiol 2011 March 28; 3(3): I-V
ISSN 1949-8470 (online)

Instructions to authors

GENERAL INFORMATION

World Journal of Radiology (*World J Radiol*, *WJR*, online ISSN 1949-8470, DOI: 10.4329), is a monthly, open-access (OA), peer-reviewed journal supported by an editorial board of 319 experts in Radiology from 40 countries.

The biggest advantage of the OA model is that it provides free, full-text articles in PDF and other formats for experts and the public without registration, which eliminates the obstacle that traditional journals possess and usually delays the speed of the propagation and communication of scientific research results. The open access model has been proven to be a true approach that may achieve the ultimate goal of the journals, i.e. the maximization of the value to the readers, authors and society.

Maximization of personal benefits

The role of academic journals is to exhibit the scientific levels of a country, a university, a center, a department, and even a scientist, and build an important bridge for communication between scientists and the public. As we all know, the significance of the publication of scientific articles lies not only in disseminating and communicating innovative scientific achievements and academic views, as well as promoting the application of scientific achievements, but also in formally recognizing the "priority" and "copyright" of innovative achievements published, as well as evaluating research performance and academic levels. So, to realize these desired attributes of *WJR* and create a well-recognized journal, the following four types of personal benefits should be maximized. The maximization of personal benefits refers to the pursuit of the maximum personal benefits in a well-considered optimal manner without violation of the laws, ethical rules and the benefits of others. (1) Maximization of the benefits of editorial board members: The primary task of editorial board members is to give a peer review of an unpublished scientific article via online office system to evaluate its innovativeness, scientific and practical values and determine whether it should be published or not. During peer review, editorial board members can also obtain cutting-edge information in that field at first hand. As leaders in their field, they have priority to be invited to write articles and publish commentary articles. We will put peer reviewers' names and affiliations along with the article they reviewed in the journal to acknowledge their contribution; (2) Maximization of the benefits of authors: Since *WJR* is an open-access journal, readers around the world can immediately download and read, free of charge, high-quality, peer-reviewed articles from *WJR* official website, thereby realizing the goals and significance of the communication between authors and peers as well as public reading; (3) Maximization of the benefits of readers: Readers can read or use, free of charge, high-quality peer-reviewed articles without any limits, and cite the arguments, viewpoints, concepts, theories, methods, results, conclusion or facts and data of pertinent literature so as to validate the innovativeness, scientific and practical values of their own research achievements, thus ensuring that their articles have novel arguments or viewpoints, solid evidence and correct conclusion; and (4) Maximization of the benefits of employees: It is an iron law that a first-class journal is unable to exist without first-class editors, and only first-class editors can create a first-class academic journal. We insist on strengthening our team cultivation and construction so that every employee, in an open, fair and transparent environment, could contribute their wisdom to edit and publish high-quality articles, thereby realizing the maximization of the personal benefits of editorial board members, authors and readers, and yielding the greatest social and economic benefits.

Aims and scope

The major task of *WJR* is to rapidly report the most recent improvement in the research of medical imaging and radiation therapy by the radiologists. *WJR* accepts papers on the following aspects related to radiology: Abdominal radiology, women health radiology, cardiovascular radiology, chest radiology, genitourinary radiology, neuroradiology, head and neck radiology, interventional radiology, musculoskeletal radiology, molecular imaging, pediatric radiology, experimental radiology, radiological technology, nuclear medicine, PACS and radiology informatics, and ultrasound. We also encourage papers that cover all other areas of radiology as well as basic research.

Columns

The columns in the issues of *WJR* will include: (1) Editorial: To introduce and comment on major advances and developments in the field; (2) Frontier: To review representative achievements, comment on the state of current research, and propose directions for future research; (3) Topic Highlight: This column consists of three formats, including (A) 10 invited review articles on a hot topic, (B) a commentary on common issues of this hot topic, and (C) a commentary on the 10 individual articles; (4) Observation: To update the development of old and new questions, highlight unsolved problems, and provide strategies on how to solve the questions; (5) Guidelines for Basic Research: To provide guidelines for basic research; (6) Guidelines for Clinical Practice: To provide guidelines for clinical diagnosis and treatment; (7) Review: To review systemically progress and unresolved problems in the field, comment on the state of current research, and make suggestions for future work; (8) Original Articles: To report innovative and original findings in radiology; (9) Brief Articles: To briefly report the novel and innovative findings in radiology; (10) Case Report: To report a rare or typical case; (11) Letters to the Editor: To discuss and make reply to the contributions published in *WJR*, or to introduce and comment on a controversial issue of general interest; (12) Book Reviews: To introduce and comment on quality monographs of radiology; and (13) Guidelines: To introduce consensuses and guidelines reached by international and national academic authorities worldwide on the research in radiology.

Name of journal

World Journal of Radiology

Serial publication number

ISSN 1949-8470 (online)

Indexed and Abstracted in

PubMed Central, PubMed.

Published by

PubMed Central, PubMed, Digital Object Identifer, and Directory of Open Access Journals.

SPECIAL STATEMENT

All articles published in this journal represent the viewpoints of the authors except where indicated otherwise.

Biostatistical editing

Statisital review is performed after peer review. We invite an expert in Biomedical Statistics from to evaluate the statistical method used

in the paper, including *t*-test (group or paired comparisons), chi-squared test, Ridit, probit, logit, regression (linear, curvilinear, or stepwise), correlation, analysis of variance, analysis of covariance, *etc*. The reviewing points include: (1) Statistical methods should be described when they are used to verify the results; (2) Whether the statistical techniques are suitable or correct; (3) Only homogeneous data can be averaged. Standard deviations are preferred to standard errors. Give the number of observations and subjects (*n*). Losses in observations, such as drop-outs from the study should be reported; (4) Values such as ED50, LD50, IC50 should have their 95% confidence limits calculated and compared by weighted probit analysis (Bliss and Finney); and (5) The word 'significantly' should be replaced by its synonyms (if it indicates extent) or the *P* value (if it indicates statistical significance).

Conflict-of-interest statement

In the interests of transparency and to help reviewers assess any potential bias, *WJR* requires authors of all papers to declare any competing commercial, personal, political, intellectual, or religious interests in relation to the submitted work. Referees are also asked to indicate any potential conflict they might have reviewing a particular paper. Before submitting, authors are suggested to read "Uniform Requirements for Manuscripts Submitted to Biomedical Journals: Ethical Considerations in the Conduct and Reporting of Research: Conflicts of Interest" from International Committee of Medical Journal Editors (ICMJE), which is available at: http://www.icmje.org/ethical_4conflicts.html.

Sample wording: [Name of individual] has received fees for serving as a speaker, a consultant and an advisory board member for [names of organizations], and has received research funding from [names of organization]. [Name of individual] is an employee of [name of organization]. [Name of individual] owns stocks and shares in [name of organization]. [Name of individual] owns patent [patent identification and brief description].

Statement of informed consent

Manuscripts should contain a statement to the effect that all human studies have been reviewed by the appropriate ethics committee or it should be stated clearly in the text that all persons gave their informed consent prior to their inclusion in the study. Details that might disclose the identity of the subjects under study should be omitted. Authors should also draw attention to the Code of Ethics of the World Medical Association (Declaration of Helsinki, 1964, as revised in 2004).

Statement of human and animal rights

When reporting the results from experiments, authors should follow the highest standards and the trial should conform to Good Clinical Practice (for example, US Food and Drug Administration Good Clinical Practice in FDA-Regulated Clinical Trials; UK Medicines Research Council Guidelines for Good Clinical Practice in Clinical Trials) and/or the World Medical Association Declaration of Helsinki. Generally, we suggest authors follow the lead investigator's national standard. If doubt exists whether the research was conducted in accordance with the above standards, the authors must explain the rationale for their approach and demonstrate that the institutional review body explicitly approved the doubtful aspects of the study.

Before submitting, authors should make their study approved by the relevant research ethics committee or institutional review board. If human participants were involved, manuscripts must be accompanied by a statement that the experiments were undertaken with the understanding and appropriate informed consent of each. Any personal item or information will not be published without explicit consents from the involved patients. If experimental animals were used, the materials and methods (experimental procedures) section must clearly indicate that appropriate measures were taken to minimize pain or discomfort, and details of animal care should be provided.

SUBMISSION OF MANUSCRIPTS

Manuscripts should be typed in 1.5 line spacing and 12 pt. Book Antiqua with ample margins. Number all pages consecutively, and start each of the following sections on a new page: Title Page, Abstract, Introduction, Materials and Methods, Results, Discussion, Acknowledgements, References, Tables, Figures, and Figure Legends. Neither the editors nor the publisher are responsible for the opinions expressed by contributors. Manuscripts formally accepted for publication become the permanent property of Baishideng Publishing Group Co., Limited, and may not be reproduced by any means, in whole or in part, without the written permission of both the authors and the publisher. We reserve the right to copy-edit and put onto our website accepted manuscripts. Authors should follow the relevant guidelines for the care and use of laboratory animals of their institution or national animal welfare committee. For the sake of transparency in regard to the performance and reporting of clinical trials, we endorse the policy of the ICMJE to refuse to publish papers on clinical trial results if the trial was not recorded in a publicly-accessible registry at its outset. The only register now available, to our knowledge, is http://www.clinicaltrials.gov sponsored by the United States National Library of Medicine and we encourage all potential contributors to register with it. However, in the case that other registers become available you will be duly notified. A letter of recommendation from each author's organization should be provided with the contributed article to ensure the privacy and secrecy of research is protected.

Authors should retain one copy of the text, tables, photographs and illustrations because rejected manuscripts will not be returned to the author(s) and the editors will not be responsible for loss or damage to photographs and illustrations sustained during mailing.

Online submissions

Manuscripts should be submitted through the Online Submission System at: http://www.wjgnet.com/1949-8470office. Authors are highly recommended to consult the ONLINE INSTRUCTIONS TO AUTHORS (http://www.wjgnet.com/1949-8470/g_info_20100316162358.htm) before attempting to submit online. For assistance, authors encountering problems with the Online Submission System may send an email describing the problem to wjr@wjgnet.com, or by telephone: +86-10-85381892. If you submit your manuscript online, do not make a postal contribution. Repeated online submission for the same manuscript is strictly prohibited.

MANUSCRIPT PREPARATION

All contributions should be written in English. All articles must be submitted using word-processing software. All submissions must be typed in 1.5 line spacing and 12 pt. Book Antiqua with ample margins. Style should conform to our house format. Required information for each of the manuscript sections is as follows:

Title page

Title: Title should be less than 12 words.

Running title: A short running title of less than 6 words should be provided.

Authorship: Authorship credit should be in accordance with the standard proposed by International Committee of Medical Journal Editors, based on (1) substantial contributions to conception and design, acquisition of data, or analysis and interpretation of data; (2) drafting the article or revising it critically for important intellectual content; and (3) final approval of the version to be published. Authors should meet conditions 1, 2, and 3.

Institution: Author names should be given first, then the complete name of institution, city, province and postcode. For example, Xu-Chen Zhang, Li-Xin Mei, Department of Pathology, Chengde Medical College, Chengde 067000, Hebei Province, China. One author may be represented from two institutions, for example, George Sgourakis, Department of General, Visceral, and Transplantation Surgery, Essen 45122, Germany; George Sgourakis, 2nd Surgical

Department, Korgialenio-Benakio Red Cross Hospital, Athens 15451, Greece

Author contributions: The format of this section should be: Author contributions: Wang CL and Liang L contributed equally to this work; Wang CL, Liang L, Fu JF, Zou CC, Hong F and Wu XM designed the research; Wang CL, Zou CC, Hong F and Wu XM performed the research; Xue JZ and Lu JR contributed new reagents/analytic tools; Wang CL, Liang L and Fu JF analyzed the data; and Wang CL, Liang L and Fu JF wrote the paper.

Supportive foundations: The complete name and number of supportive foundations should be provided, e.g., Supported by National Natural Science Foundation of China, No. 30224801

Correspondence to: Only one corresponding address should be provided. Author names should be given first, then author title, affiliation, the complete name of institution, city, postcode, province, country, and email. All the letters in the email should be in lower case. A space interval should be inserted between country name and email address. For example, Montgomery Bissell, MD, Professor of Medicine, Chief, Liver Center, Gastroenterology Division, University of California, Box 0538, San Francisco, CA 94143, United States. montgomery.bissell@ucsf.edu

Telephone and fax: Telephone and fax should consist of +, country number, district number and telephone or fax number, e.g., Telephone: +86-10-85381892 Fax: +86-10-85381893

Peer reviewers: All articles received are subject to peer review. Normally, three experts are invited for each article. Decision for acceptance is made only when at least two experts recommend an article for publication. Reviewers for accepted manuscripts are acknowledged in each manuscript, and reviewers of articles which were not accepted will be acknowledged at the end of each issue. To ensure the quality of the articles published in *WJR*, reviewers of accepted manuscripts will be announced by publishing the name, title/position and institution of the reviewer in the footnote accompanying the printed article. For example, reviewers: Professor Jing-Yuan Fang, Shanghai Institute of Digestive Disease, Shanghai, Affiliated Renji Hospital, Medical Faculty, Shanghai Jiaotong University, Shanghai, China; Professor Xin-Wei Han, Department of Radiology, The First Affiliated Hospital, Zhengzhou University, Zhengzhou, Henan Province, China; and Professor Anren Kuang, Department of Nuclear Medicine, Huaxi Hospital, Sichuan University, Chengdu, Sichuan Province, China.

Abstract

There are unstructured abstracts (no more than 256 words) and structured abstracts (no more than 480). The specific requirements for structured abstracts are as follows:

An informative, structured abstracts of no more than 480 words should accompany each manuscript. Abstracts for original contributions should be structured into the following sections. AIM (no more than 20 words): Only the purpose should be included. Please write the aim as the form of "To investigate/study/…; MATERIALS AND METHODS (no more than 140 words); RESULTS (no more than 294 words): You should present *P* values where appropriate and must provide relevant data to illustrate how they were obtained, e.g. 6.92 ± 3.86 *vs* 3.61 ± 1.67, $P < 0.001$; CONCLUSION (no more than 26 words).

Key words

Please list 5-10 key words, selected mainly from *Index Medicus*, which reflect the content of the study.

Text

For articles of these sections, original articles and brief articles, the main text should be structured into the following sections: INTRODUCTION, MATERIALS AND METHODS, RESULTS and DISCUSSION, and should include appropriate Figures and Tables. Data should be presented in the main text or in Figures and Tables, but not in both. The main text format of these sections, editorial, topic highlight, case report, letters to the editors, can be found at: http://www.wjgnet.com/1949-8470/g_info_20100313183720.htm.

Illustrations

Figures should be numbered as 1, 2, 3, *etc.*, and mentioned clearly in the main text. Provide a brief title for each figure on a separate page. Detailed legends should not be provided under the figures. This part should be added into the text where the figures are applicable. Figures should be either Photoshop or Illustrator files (in tiff, eps, jpeg formats) at high-resolution. Examples can be found at: http://www.wjgnet.com/1007-9327/13/4520.pdf; http://www.wjgnet.com/1007-9327/13/4554.pdf; http://www.wjgnet.com/1007-9327/13/4891.pdf; http://www.wjgnet.com/1007-9327/13/4986.pdf; http://www.wjgnet.com/1007-9327/13/4498.pdf. Keeping all elements compiled is necessary in line-art image. Scale bars should be used rather than magnification factors, with the length of the bar defined in the legend rather than on the bar itself. File names should identify the figure and panel. Avoid layering type directly over shaded or textured areas. Please use uniform legends for the same subjects. For example: Figure 1 Pathological changes in atrophic gastritis after treatment. A: ...; B: ...; C: ...; D: ...; E: ...; F: ...; G: …*etc.* It is our principle to publish high resolution-figures for the printed and E-versions.

Tables

Three-line tables should be numbered 1, 2, 3, *etc.*, and mentioned clearly in the main text. Provide a brief title for each table. Detailed legends should not be included under tables, but rather added into the text where applicable. The information should complement, but not duplicate the text. Use one horizontal line under the title, a second under column heads, and a third below the Table, above any footnotes. Vertical and italic lines should be omitted.

Notes in tables and illustrations

Data that are not statistically significant should not be noted. $^{a}P < 0.05$, $^{b}P < 0.01$ should be noted ($P > 0.05$ should not be noted). If there are other series of *P* values, $^{c}P < 0.05$ and $^{d}P < 0.01$ are used. A third series of *P* values can be expressed as $^{e}P < 0.05$ and $^{f}P < 0.01$. Other notes in tables or under illustrations should be expressed as ^{1}F, ^{2}F, ^{3}F; or sometimes as other symbols with a superscript (Arabic numerals) in the upper left corner. In a multi-curve illustration, each curve should be labeled with ●, ○, ■, □, ▲, △, *etc.*, in a certain sequence.

Acknowledgments

Brief acknowledgments of persons who have made genuine contributions to the manuscript and who endorse the data and conclusions should be included. Authors are responsible for obtaining written permission to use any copyrighted text and/or illustrations.

REFERENCES

Coding system

The author should number the references in Arabic numerals according to the citation order in the text. Put reference numbers in square brackets in superscript at the end of citation content or after the cited author's name. For citation content which is part of the narration, the coding number and square brackets should be typeset normally. For example, "Crohn's disease (CD) is associated with increased intestinal permeability[1,2]". If references are cited directly in the text, they should be put together within the text, for example, "From references[19,22-24], we know that..."

When the authors write the references, please ensure that the order in text is the same as in the references section, and also ensure the spelling accuracy of the first author's name. Do not list the same citation twice.

PMID and DOI

Pleased provide PubMed citation numbers to the reference list, e.g. PMID and DOI, which can be found at http://www.ncbi.nlm.nih.gov/sites/entrez?db=pubmed and http://www.crossref.org/SimpleTextQuery/, respectively. The numbers will be used in E-version of this journal.

Style for journal references

Authors: the name of the first author should be typed in bold-faced letters. The family name of all authors should be typed with the initial letter capitalized, followed by their abbreviated first and middle initials. (For example, Lian-Sheng Ma is abbreviated as Ma LS, Bo-Rong Pan as Pan BR). The title of the cited article and italicized journal title (journal title should be in its abbreviated form as shown in PubMed), publication date, volume number (in black), start page, and end page [PMID: 11819634 DOI: 10.3748/wjg.13.5396].

Style for book references

Authors: the name of the first author should be typed in bold-faced letters. The surname of all authors should be typed with the initial letter capitalized, followed by their abbreviated middle and first initials. (For example, Lian-Sheng Ma is abbreviated as Ma LS, Bo-Rong Pan as Pan BR) Book title. Publication number. Publication place: Publication press, Year: start page and end page.

Format

Journals

English journal article (list all authors and include the PMID where applicable)

1 **Jung EM**, Clevert DA, Schreyer AG, Schmitt S, Rennert J, Kubale R, Feuerbach S, Jung F. Evaluation of quantitative contrast harmonic imaging to assess malignancy of liver tumors: A prospective controlled two-center study. *World J Gastroenterol* 2007; **13**: 6356-6364 [PMID: 18081224 DOI: 10.3748/wjg.13.6356]

Chinese journal article (list all authors and include the PMID where applicable)

2 **Lin GZ**, Wang XZ, Wang P, Lin J, Yang FD. Immunologic effect of Jianpi Yishen decoction in treatment of Pixu-diarrhoea. *Shijie Huaren Xiaohua Zazhi* 1999; **7**: 285-287

In press

3 **Tian D**, Araki H, Stahl E, Bergelson J, Kreitman M. Signature of balancing selection in Arabidopsis. *Proc Natl Acad Sci USA* 2006; In press

Organization as author

4 **Diabetes Prevention Program Research Group**. Hypertension, insulin, and proinsulin in participants with impaired glucose tolerance. *Hypertension* 2002; **40**: 679-686 [PMID: 12411462 PMCID:2516377 DOI:10.1161/01.HYP.0000035706.28494.09]

Both personal authors and an organization as author

5 **Vallancien G**, Emberton M, Harving N, van Moorselaar RJ; Alf-One Study Group. Sexual dysfunction in 1, 274 European men suffering from lower urinary tract symptoms. *J Urol* 2003; **169**: 2257-2261 [PMID: 12771764 DOI:10.1097/01.ju.0000067940.76090.73]

No author given

6 21st century heart solution may have a sting in the tail. *BMJ* 2002; **325**: 184 [PMID: 12142303 DOI:10.1136/bmj.325.7357.184]

Volume with supplement

7 **Geraud G**, Spierings EL, Keywood C. Tolerability and safety of frovatriptan with short- and long-term use for treatment of migraine and in comparison with sumatriptan. *Headache* 2002; **42** Suppl 2: S93-99 [PMID: 12028325 DOI:10.1046/j.1526-4610.42.s2.7.x]

Issue with no volume

8 **Banit DM**, Kaufer H, Hartford JM. Intraoperative frozen section analysis in revision total joint arthroplasty. *Clin Orthop Relat Res* 2002; (**401**): 230-238 [PMID: 12151900 DOI:10.1097/00003086-200208000-00026]

No volume or issue

9 Outreach: Bringing HIV-positive individuals into care. *HRSA Careaction* 2002; 1-6 [PMID: 12154804]

Books

Personal author(s)

10 **Sherlock S**, Dooley J. Diseases of the liver and billiary system. 9th ed. Oxford: Blackwell Sci Pub, 1993: 258-296

Chapter in a book (list all authors)

11 **Lam SK**. Academic investigator's perspectives of medical treatment for peptic ulcer. In: Swabb EA, Azabo S. Ulcer disease: investigation and basis for therapy. New York: Marcel Dekker, 1991: 431-450

Author(s) and editor(s)

12 **Breedlove GK**, Schorfheide AM. Adolescent pregnancy. 2nd ed. Wieczorek RR, editor. White Plains (NY): March of Dimes Education Services, 2001: 20-34

Conference proceedings

13 **Harnden P**, Joffe JK, Jones WG, editors. Germ cell tumours V. Proceedings of the 5th Germ cell tumours Conference; 2001 Sep 13-15; Leeds, UK. New York: Springer, 2002: 30-56

Conference paper

14 **Christensen S**, Oppacher F. An analysis of Koza's computational effort statistic for genetic programming. In: Foster JA, Lutton E, Miller J, Ryan C, Tettamanzi AG, editors. Genetic programming. EuroGP 2002: Proceedings of the 5th European Conference on Genetic Programming; 2002 Apr 3-5; Kinsdale, Ireland. Berlin: Springer, 2002: 182-191

Electronic journal (list all authors)

15 Morse SS. Factors in the emergence of infectious diseases. Emerg Infect Dis serial online, 1995-01-03, cited 1996-06-05; 1(1): 24 screens. Available from: URL: http://www.cdc.gov/ncidod/eid/index.htm

Patent (list all authors)

16 **Pagedas AC**, inventor; Ancel Surgical R&D Inc., assignee. Flexible endoscopic grasping and cutting device and positioning tool assembly. United States patent US 20020103498. 2002 Aug 1

Statistical data

Write as mean ± SD or mean ± SE.

Statistical expression

Express *t* test as *t* (in italics), *F* test as *F* (in italics), chi square test as χ^2 (in Greek), related coefficient as *r* (in italics), degree of freedom as υ (in Greek), sample number as *n* (in italics), and probability as *P* (in italics).

Units

Use SI units. For example: body mass, m (B) = 78 kg; blood pressure, p (B) = 16.2/12.3 kPa; incubation time, t (incubation) = 96 h, blood glucose concentration, c (glucose) 6.4 ± 2.1 mmol/L; blood CEA mass concentration, p (CEA) = 8.6 24.5 μg/L; CO_2 volume fraction, 50 mL/L CO_2, not 5% CO_2; likewise for 40 g/L formaldehyde, not 10% formalin; and mass fraction, 8 ng/g, *etc.* Arabic numerals such as 23, 243, 641 should be read 23 243 641.

The format for how to accurately write common units and quantums can be found at: http://www.wjgnet.com/1949-8470/g_info_20100313185816.htm.

Abbreviations

Standard abbreviations should be defined in the abstract and on first mention in the text. In general, terms should not be abbreviated unless they are used repeatedly and the abbreviation is helpful to the reader. Permissible abbreviations are listed in Units, Symbols and Abbreviations: A Guide for Biological and Medical Editors and Authors (Ed. Baron DN, 1988) published by The Royal Society of Medicine, London. Certain commonly used abbreviations, such as DNA, RNA, HIV, LD50, PCR, HBV, ECG, WBC, RBC, CT, ESR, CSF, IgG, ELISA, PBS, ATP, EDTA, mAb, can be used directly without further explanation.

Italics
Quantities: *t* time or temperature, *c* concentration, *A* area, *l* length, *m* mass, *V* volume.
Genotypes: *gyrA*, *arg* 1, *c myc*, *c fos*, *etc.*
Restriction enzymes: *Eco*RI, *Hin*dI, *Bam*HI, *Kbo* I, *Kpn* I, *etc.*
Biology: *H. pylori*, *E coli*, *etc.*

Examples for paper writing
Editorial: http://www.wjgnet.com/1949-8470/g_info_20100313182341.htm

Frontier: http://www.wjgnet.com/1949-8470/g_info_20100313182448.htm

Topic highlight: http://www.wjgnet.com/1949-8470/g_info_20100313182639.htm

Observation: http://www.wjgnet.com/1949-8470/g_info_20100313182834.htm

Guidelines for basic research: http://www.wjgnet.com/1949-8470/g_info_20100313183057.htm

Guidelines for clinical practice: http://www.wjgnet.com/1949-8470/g_info_20100313183238.htm

Review: http://www.wjgnet.com/1949-8470/g_info_20100313183433.htm

Original articles: http://www.wjgnet.com/1949-8470/g_info_20100313183720.htm

Brief articles: http://www.wjgnet.com/1949-8470/g_info_20100313184005.htm

Case report: http://www.wjgnet.com/1949-8470/g_info_20100313184149.htm

Letters to the editor: http://www.wjgnet.com/1949-8470/g_info_20100313184410.htm

Book reviews: http://www.wjgnet.com/1949-8470/g_info_20100313184803.htm

Guidelines: http://www.wjgnet.com/1949-8470/g_info_20100313185047.htm

SUBMISSION OF THE REVISED MANUSCRIPTS AFTER ACCEPTED

Please revise your article according to the revision policies of *WJR*. The revised version including manuscript and high-resolution image figures (if any) should be re-submitted or uploaded online. The author should send copyright transfer letter, and responses to the reviewers and science news to us *via* email.

Editorial Office

World Journal of Radiology
Editorial Department: Room 903, Building D,
Ocean International Center, No. 62 Dongsihuan Zhonglu,
Chaoyang District, Beijing 100025, China
E-mail: wjr@wjgnet.com
http://www.wjgnet.com
Telephone: +86-10-85381892
Fax: +86-10-85381893

Language evaluation
The language of a manuscript will be graded before it is sent for revision. (1) Grade A: priority publishing; (2) Grade B: minor language polishing; (3) Grade C: a great deal of language polishing needed; and (4) Grade D: rejected. Revised articles should reach Grade A or B.

Copyright assignment form
Please download a Copyright assignment form from http://www.wjgnet.com/1949-8470/g_info_20100313185522.htm.

Responses to reviewers
Please revise your article according to the comments/suggestions provided by the reviewers. The format for responses to the reviewers' comments can be found at: http://www.wjgnet.com/1949-8470/g_info_20100313185358.htm.

Proof of financial support
For paper supported by a foundation, authors should provide a copy of the document and serial number of the foundation.

Links to documents related to the manuscript
WJR will be initiating a platform to promote dynamic interactions between the editors, peer reviewers, readers and authors. After a manuscript is published online, links to the PDF version of the submitted manuscript, the peer-reviewers' report and the revised manuscript will be put on-line. Readers can make comments on the peer reviewer's report, authors' responses to peer reviewers, and the revised manuscript. We hope that authors will benefit from this feedback and be able to revise the manuscript accordingly in a timely manner.

Science news releases
Authors of accepted manuscripts are suggested to write a science news item to promote their articles. The news will be released rapidly at EurekAlert/AAAS (http://www.eurekalert.org). The title for news items should be less than 90 characters; the summary should be less than 75 words; and main body less than 500 words. Science news items should be lawful, ethical, and strictly based on your original content with an attractive title and interesting pictures.

Publication fee
WJR is an international, peer-reviewed, Open-Access, online journal. Articles published by this journal are distributed under the terms of the Creative Commons Attribution Non-commercial License, which permits use, distribution, and reproduction in any medium, provided the original work is properly cited, the use is non commercial and is otherwise in compliance with the license. Authors of accepted articles must pay a publication fee. The related standards are as follows. Publication fee: 1300 USD per article; Reprints fee: 350 USD per 100 reprints, including postage cost. Editorial, topic highlights, book reviews and letters to the editor are published free of charge.